

UNIVERSITY OF NAPLES FEDERICO II

School of Polytechnic and Basic Sciences



DEPARTMENT OF CHEMICAL, MATERIALS AND INDUSTRIAL PRODUCTION

XXXI PhD PROGRAMME IN

INDUSTRIAL PRODUCTS AND PROCESSES ENGINEERING

CURRICULUM ON PRODUCTION TECHNOLOGY AND SYSTEMS

PHD PROGRAMME COORDINATOR: PROF. ING. GIUSEPPE MENSITIERI

***Biaxial test on composite and polymeric
materials***

PhD PROJECT SUPERVISOR

PROF. ING. Antonio Langella

PhD CANDIDATE

ING. Tania Langella

List of contents	
<i>List of Figures</i>	<i>i</i>
<i>List of Tables</i>	<i>iv</i>
<i>Abstract</i>	<i>v</i>
Chapter1.State of art.....	1
1.1 Monoaxial and biaxial tests for characterization of materials.....	1
1.2 Machine and devices for biaxial mechanical tests.....	3
1.2.1 Stand alone machine.....	3
1.2.2 Test rig connected to pre-existing single-axis machines.....	11
1.2.3 Test devices for composite and polymeric materials.....	14
1.3 Shape for biaxial test specimen.....	18
1.3.1 Shape for composite materials.....	18
1.3.2 Shape for polymeric materials.....	26
<i>References</i>	33
Chapter2.Study of a new equipment for biaxial tests.....	35
2.1 Technical characteristics and components of the equipment.....	35
2.1.1 Loading group.....	36
2.1.2 The frame assembly.....	40
2.2.3 Group for the transmission of motion.....	41
2.2 Multibody analysis: MSC Adams.....	43
2.2.1 Model construction in Adams.....	43
2.2.2 Simulation results.....	53
2.2.3 Choice of bearings.....	55
2.3 Creation of the model for finite element analysis.....	57
2.3.1 Linear static analysis.....	62
2.3.2 Flex analysis in Adams/Nastran environment.....	67

<i>References</i>	72
Chapter 3. Study of specimen shape for biaxial tests on composite and polymer materials.....	73
3.1 Optimization of shape for composite materials.....	73
3.2 Optimization of shape for polymeric materials.....	81
<i>References</i>	85
Chapter 4. Experimental activity.....	86
4.1 Introduction.....	86
4.2 Materials and method.....	86
4.2.1 Materials.....	86
4.2.2 Test setup.....	88
4.2.3 Specimen preparation for DIC.....	90
4.2.4 Biaxial tests and digital correlation of images.....	91
4.3 Results and fem validation.....	93
4.4 Conclusions.....	98
<i>References</i>	104

List of figures

- Figure 1.1** Biaxial testing machine for cruciform specimens (Makinde et al.)
- Figure 1.2** Non-uniformity degree estimation of the strain within the useful length of three cruciform specimens
- Figure 1.3** Specimen shape of Boheler et al.
- Figure 1.4** The isostress lines within the test section of the optimized specimen
- Figure 1.5** Horizontal test rig of Kuwabara et al.
- Figure 1.6** σ - ε curve for a SPECEN steel (Kuwabara and Ikeda, 2002a, b)
- Figure 1.7** Relationship between load and strain during uniaxial and biaxial tests. (Shimamoto et al., 2003)
- Figure 1.8** Failure of the specimen after the biaxial dynamic test (Shimamoto et al., 2003)
- Figure 1.9** σ - ε curve in uniaxial and biaxial test (Shimamoto et al., 2003)
- Figure 1.10** σ - ε curve for high-strength steel
- Figure 1.11** Test rig (Fraunhofer, 2005)
- Figure 1.12** Pantograph mechanism for the biaxial test (Ferron and Makinde, 1988)
- Figure 1.13** Equipment for the biaxial test (Smits et al. 2006)
- Figure 1.14** Types of Arcan systems: (a) classic type, (b) modified type
- Figure 1.15** Photographs of the Arcan plant and instrumental assembly
- Figure 1.16** Biaxial test machine (Brieu et al.)
- Figure 1.17** Cross-shaped specimen with a circular and reduced central section
- Figure 1.18** Cruciform specimen with notches
- Figure 1.19** Schematic drawing of a specimen for biaxial tests used by Welsh et al.
- Figure 1.20** Schematic drawing of a modified specimen for biaxial tests used by Welsh et al.
- Figure 1.21** Detail of the round and square measuring section for a cross-shaped specimen with a tapered thickness
- Figure 1.22** Strain along the main direction in the four cruciform geometries [11]
- Figure 1.23** Shear strains in the four cruciform geometries[11]
- Figure 1.24** Types of specimens for the biaxial tests of Arnaud. 3D CAD model and axisymmetric 2D model: (a) straight edge, (b) cleaned edge, (c) pecking with a cleaned edge, (d) chamfered edge with polished edge, (e) bevelling with a cleaned edge and pecking
- Figure 1.25** Typologies A, B and C of specimens analyzed by Chwdhury
- Figure 1.26** Comparison between numerical results and experimental observations of Zarouchas and Nijssen
- Figure 1.27** Schematic diagram of a biaxial specimen according to Duncan. The dotted part shows how the corners have been removed for some analysis
- Figure 1.28** Specimen dimensions of Brieu et al.
- Figure 1.29** Hollenstein et al. specimen
- Figure 1.30** Boundary conditions of Hollenstein specimen
- Figure 1.31** Test machine and specimen of Smidt et al. [18]
- Figure 2.1** New equipment
- Figure 2.2** Clamps properties
- Figure 2.3** CAD model Hydraulic Wedge Grip MTS 647
- Figure 2.4** CAD model of connection between Hydraulic Wedge Grip MTS 647, spiral washers and relative slider
- Figure 2.5** CAD model SPIRAL WASHERS model 601
- Figure 2.6** CAD model of the slider
- Figure 2.7** CAD model of box
- Figure 2.8** CAD model of the Support Arm coupled to the Axles

Figure 2.9 CAD model of a crank
Figure 2.10 CAD model of a connecting rod
Figure 2.11 Units settings in Adams
Figure 2.12 File import setting
Figure 2.13 Part name setting
Figure 2.14 Detail of slider with clamp imported into Adams
Figure 2.14 Setting of the material characteristics
Figure 2.15 Complete model in Adams
Figure 2.16 Degrees of freedom
Figure 2.17 “Fixed” constraint assignment
Figure 2.18 Assignment of fixed constraint to the box
Figure 2.19 Revolute constraint between crank and axle
Figure 2.20 Spherical constraint between cranks and connecting rods
Figure 2.21 Hooke constraint
Figure 2.22 Translational constraint between slider and box
Figure 2.23 Motion constraint assignment
Figure 2.24 Motion constraint assignment of parameters
Figure 2.25 Force assignment
Figure 2.26 Model check
Figure 2.27 Time and step integration parameters
Figure 2.28 Displacement law of sliders
Figure 2.29 Forces between cranks and axles
Figure 2.30 Forces between cranks and connecting rods
Figure 2.31 Bearing data sheet
Figure 2.32 New model assignment
Figure 2.33 Surfaces for the creation of connecting rod model
Figure 2.34 Mesh of connecting rod
Figure 2.35 Complete mesh of the connecting rod
Figure 2.36 RBE2 constraints
Figure 2.37 Material parameters
Figure 2.38 Slider fem model
Figure 2.39 Support structure fem model
Figure 2.40 V-shaped crank fem model
Figure 2.41 Box fem model
Figure 2.42 Connecting rod strains
Figure 2.43 Connecting rod stresses
Figure 2.44 Crank strains
Figure 2.45 Crank stresses
Figure 2.46 Slider strains
Figure 2.47 Slider stresses
Figure 2.48 Support arm strains
Figure 2.49 Support arm stresses
Figure 2.50 Axle strains
Figure 2.51 Axle stresses
Figure 2.52 Box strains in case of thickness 50 mm
Figure 2.53 Box strains in case of thickness 80 mm
Figure 2.54 Box stresses in case of thickness 80 mm
Figure 2.55 Rationale behind the deformability analysis
Figure 2.56 Importation of a flex component in Adams
Figure 2.57 Setting of flex component properties

Figure 2.58 Detail of flexible cranks
Figure 2.59 Equipment with all flexible components during the analysis
Figure 2.60 Comparison of the law of motions in both cases: rigid and flexible components
Figure 3.1 Stacking sequence
Figure 3.2 Investigated shapes
Figure 3.3 Guelho et al. specimen shape and dimensions [2]
Figure 3.4 Modified shape
Figure 3.5 Solid shell element [3]
Figure 3.6 Solid shell mesh
Figure 3.7 Boundary conditions
Figure 3.8 Deformed of the fem model
Figure 3.9 Main strains a) I and b) II for layer₁; main strains c) I and d) II for the layer₂
Figure 3.10 Stresses in the direction a) x and b) y in the CSYS11 reference system for Layer₁; Stresses in direction c) x and d) y in the CSYS11 reference system for Layer₂
Figure 3.11 2D shell mesh
Figure 3.12 Boundary conditions and loads
Figure 3.13 Von Mises strains
Figure 3.14 New shape proposed for polymeric materials
Figure 3.15 Chexa element
Figure 3.16 Main stresses on Versilok specimen
Figure 3.17 Main stresses on Sikasil specimen
Figure 4.1 Fibre Data Sheet
Figure 4.2 σ - ϵ curve
Figure 4.3 CAD model of definitive equipment
Figure 4.4 New equipment for biaxial tests
Figure 4.5 Details of cranks and clamps
Figure 4.6 Speckle pattern on specimen
Figure 4.7 Detail of speckle pattern in the biaxial zone
Figure 4.8 Camera positioning
Figure 4.9 Biaxial test performing
Figure 4.10 Image calibration
Figure 4.11 Area of interest
Figure 4.12 DIC analysis settings
Figure 4.13 Distribution of maximum strain in the main direction with DIC
Figure 4.14 Distribution of maximum strain in the main direction with fem
Figure 4.15 Values for identified element on Patran model
Figure 4.16 Maximum strain distribution in the main direction
Figure 4.17 Strain in y direction
Figure 4.18 Strain in x direction
Figure 4.19 Slider inclination
Figure 4.20 Flexion of the arms
Figure 4.21 Detail of cranks
Figure 4.22 Areas of possible crank contact
Figure 4.23 Position of the springs
Figure 4.24 New plate

List of tables

Table 2.1 Grip specifications

Table 2.2 Possible constraints

Table 2.3 Mechanical properties of 39NiCrMo3

Table 2.4 Comparison between rigid and flex analysis results

Table 4.5 Comparison between DIC and fem values

Abstract

The development of the aircraft with the use of composite materials involves the mechanical characterization of these materials that have the suitable properties to be used in the design phases. The characterization of these materials is made in the mono axial field. However, research activities in recent years are focusing the attention on the study of biaxial tests to get more information to use during the design for the best use of materials.

My thesis has been mainly focused on the development of a new biaxial equipment about composite and polymeric materials. It will try to show that the equipment is able to correctly load the specimens in two perpendicular directions. Then the selected test setup was applied experimentally for biaxial tests on a general aviation carbon resin. The thesis is divided into four sections.

In the first one, the machines and equipment for biaxial tests present in the literature are only presented. Then the forms of biaxial test specimens most used by researchers in the last years for both metallic, composite and polymeric materials have been described.

In the second section, the agreement that led to the creation of a new test rig, with which the tests have been described, are in the fourth section. The third part deals with the choice and optimization of a specimen shape through the use of finite element analysis. In the fourth section, the new equipment and the shape of the specimen chosen in the previous section have been used to carry out tests on a composite material in carbon resin. Here, the materials and the methods used to perform the experimental exercise are described.

The used material is provided within the Tabasco project promoted by the Campania DAC. This project concerns the technologies and the production processes of low-cost components for general aviation.

Conclusive remarks, where the main results are summarized, close this work.

Chapter 1

State of art

1.1 Monoaxial and biaxial tests for characterization of materials

When we select a material to make a component of a structure, a machine or any product, the main objective is to ensure that its properties are suitable for the operating conditions of the component.

Through the evaluation of physical and mechanical properties, it is possible to distinguish different types of materials.

Among the properties that characterize a material, it can be found: density, melting point, optical properties, thermal conductivity, electrical conductivity, and magnetic properties.

Some of these could be of primary importance, but very often the properties that describe how a material reacts when led, have a fundamental role in the choice of the same.

In particular, these are: the elastic modulus, the ductility, the hardness.

The mechanical properties are very important because the function and the performance of a product depend on its ability to withstand the stresses that it must face during this operation.

When the selection of the material is required, the engineer must not only look at its properties but also understand what values and limits are relevant. Mostly, how they are measured.

For these reasons, the engineer must have familiarity with the different procedures used during the tests on materials, and, at the same time, it must consider that the mechanical tests are carried out on specimens. But, these, although, the laboratory conditions are respected, rarely, correspond to the real life application.

When the load is applied to a component, the material deforms, and, in particular, it can be subject to three types of load: traction, compression and cutting.

The tensile load tends to stretch the material; the compression tends to crush it

while the cutting causes the sliding of the surfaces.

These three types of loads are described through the stress-strain curves.

The most used in mechanical tests are the monoaxial ones.

The mechanical properties of materials under single-axle loading are used to estimate the strength and the strain of components during the design of a machine, a structure or a product.

Knowing that loads only act in one direction, it is a simplification that is acceptable for analysing a single point or common materials, like metals.

It must be remembered that during the operation, the conditions the loads are applied simultaneously in different directions, produce a stress that is not directed in a particular direction.

For example, during the operation, the mechanical components obtained by forming, are loaded in different directions at the same time, and, in particular, they are loaded into two axes.

Many aeronautic and aerospace components are also often subject to multi-axial loads.

In general, multiaxial stresses and strains in components that work at high temperatures cannot be described by monoaxial data.

It has been recognized that evaluating the characteristics of a material through a monoaxial test, we can have a wrong evaluation of the material behaviour.

The monoaxial tensile test is used to classify the workability of several metallic alloys.

However, the actual strain of the breaking zone, observed in the monoaxial case, is much lower than the corresponding value found in the biaxial case. For this reason, into the monoaxial tensile test, the deformability, during the real training process, can be underestimated.

By using more realistic loads, and, in particular, introducing biaxial loading conditions, a more accurate representation of the operating behaviour of a structure is obtained.

In general, the stresses acting on a component are multiaxial. For the mentioned reasons, it is necessary to identify the mechanical properties not only under

monoaxial load states but also under multiaxial ones.

Nowadays, the tests are designed in order to reproduce forces that strongly reflect those that act on the material during the training process with specific instructions.

Biaxial tensile tests can be used to simulate forces acting in two directions at the same time. Thanks to this type of test, the σ - ε curves can be obtained from different load directions. There are numerous methods to produce a biaxial stress state in the material made up of many types of specimens: for example, the test with combined torsion-stress. The first one with flexion and flat stress and the swelling test [1].

Furthermore, the ever-increasing use of polymeric materials, fiber-reinforced composites and metal laminates have underlined the importance of carrying out tests through multiaxial loading conditions, unless they are biaxially or multiaxially stressed during the operation.

Biaxial tests, ready to use different types of cruciform specimens, represent the most suitable method to evaluate several biaxial stress conditions by reversing the value of the load or displacement along the two axes.

Furthermore, the single-axis standard test is accurate only for isotropic materials, while thin sheets, composite materials and polymeric materials show anisotropic properties.

1.2 Machine and devices for biaxial mechanical tests

To perform biaxial mechanical tests in order to characterize composite and polymeric materials, machines and devices have been developed to be able to reproduce multiaxial loads.

In particular, they have some features:

- "Stand alone" biaxial test machines
- Test rig that connects to pre-existing single-axis machines to produce biaxial loads.

1.2.1 Stand alone machines

An example about this topic is the biaxial testing machine designed by Makinde et al. (1992) shown in figure 2.1. The device consists of two main parts: the loading system and the control system. The loading system is

configured as shown in the figure. The frame has been oversized to reduce strains, as it is subject to great stress. On the chassis, along with the two axles, two hydraulic actuators have been constructed with a nominal capacity of 250 kN. The presence of the actuators on both axes ensures that the centre of the specimen does not move during the test, anyway, they are constructed in opposite ways and connected to the same hydraulic circuit to reproduce equal and opposite forces.

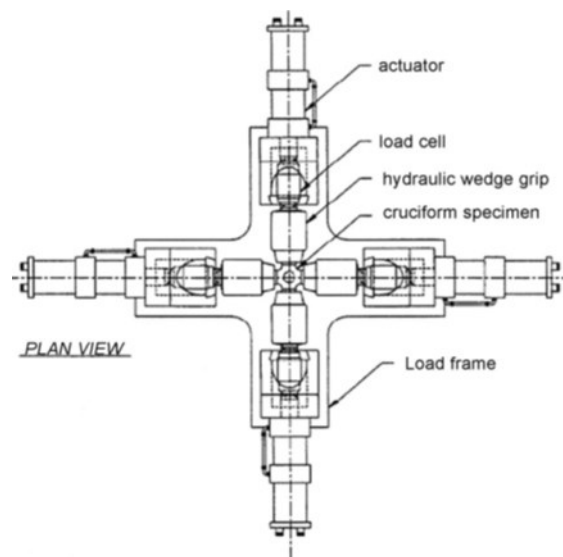


Figure 1.1 Biaxial testing machine for cruciform specimens (Makinde et al.)

The load cells constructed on each actuator are used to measure the force in both directions. Once grabs have been designed, they can be preloaded and can block the specimen before the start of the test. This machine was used to test many types of cruciform specimens. The results of these tests were used to develop a specific specimen for low strains [3].

The researchers used the machine to evaluate the degree of non-uniformity of the strain within the useful part of different cruciform specimens proposed by other researchers as shown in figure 2.2.

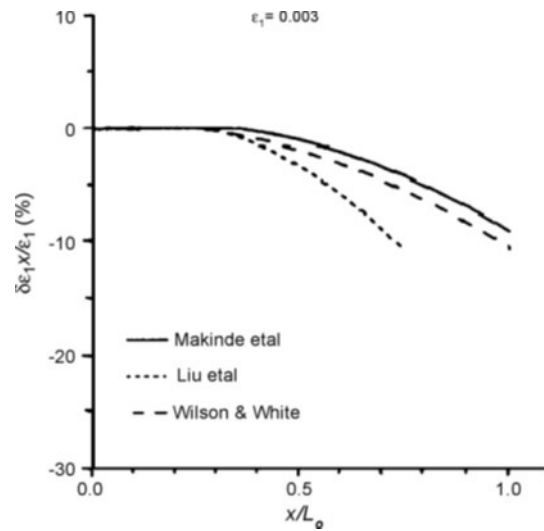


Figure 1.2 Non-uniformity degree estimation of the strain within the useful length of three cruciform specimens

Another type of biaxial machine was made by Boehler et al. (1994). It was composed of four double action screw-driven pistons constructed on an octagonal vertical frame. The four double action pistons assured the locking of the specimen centre during the tests; the screws were activated by two engines. For the tests, a variable DC motor was used, while for the initial positioning an AC motor was used for large displacements. Both engines had a clutch to prevent simultaneous joints. The speedy test could be varied between 0.003 and 0.3 [mm / min]. The maximum load that could be reached is 100 [kN] in both directions. The advantage of using a vertical frame is to have easy access from both sides to construct the specimen, and, it is, also, possible to have a good photographic analysis to analyze the strain field with the laser or other video methods.

This configuration, however, involves a disadvantage. In fact, the weight of each pincer and of the assembly devices must be kept under control to minimize bending on thin specimens.

This machine was used to test a lot of types of cruciform specimens in order to develop an optimal shape of the specimen.

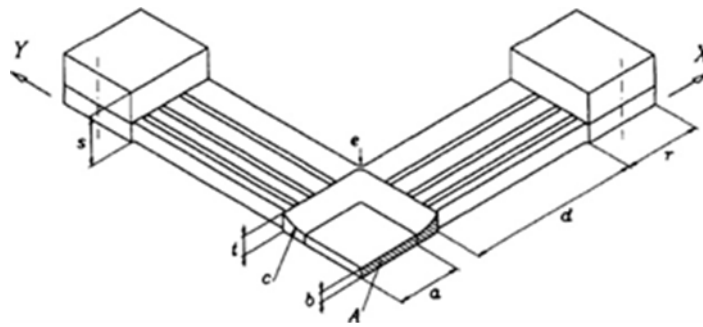


Figure 1.3 Specimen shape of Boheler et al.

The form of the specimen considered by Boheler et al is shown in Fig. 1.3. Researchers used the analysis of finite elements to optimize and comparing the specimen with previously designed specimens. Both rigid grippers and the axes were calibrated on the specimen optimized for an anisotropic elastic material. The numerical model was used to detect the field of shear stresses in the useful area of the specimen. An example of the isostress lines within the test section of the optimized specimen is shown in figure 1.4.

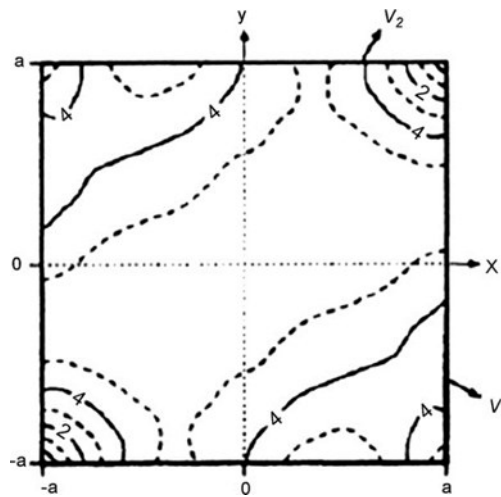


Figure 1.4 The isostress lines within the test section of the optimized specimen

The value at the centre of the section is $\sigma_{xy} \approx 5.8$ [MPa].

For this reason, it was concluded that when the test was focused on anisotropic materials with rigid clamps, the information obtained could not be used to derive the constitutive bond because the main axes of the biaxial stress field obtained could not be determined.

Kuwabara et al (1998) completed a study to clarify the behaviour of elastic and plastic strain of a low-carbon cold-rolled steel under biaxial load.

To complete this experiment a new device for biaxial tests was built. The configuration of this servomechanism is shown in figure 1.5.

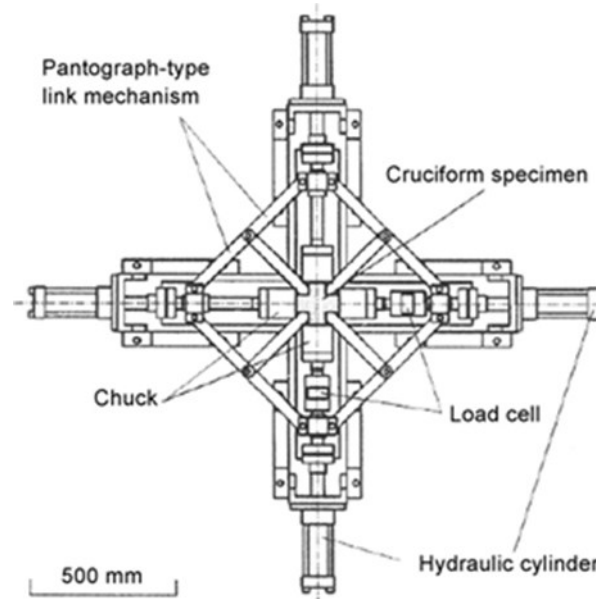


Figure 1.5 Horizontal test rig of Kuwabara et al.

The opposing hydraulic cylinders were connected to a single hydraulic circuit in a way that the same pressure was applied to both. Each hydraulic circuit was controlled independently using a server control. As for the two previous devices, it was essential to keep the centre of the specimen locked during the test. This was achieved using a type of articulated pantograph like the one shown in figure 1.5.

This method was very effective and reduced, with relevance, the costs of the apparatus. In each direction, a load cell was used to calculate the load acting on the specimen. The strain was measured using a strain gauges, which was positioned at the specified section of the specimen. The output of both cells and the strain gauges were analyzed using a calculator. This device was used to test a cruciform specimen of very low carbon steel (SPECEN) and, then, to compare the results obtained with other existing yield criteria as shown in fig. 1.6 (Kuwabara and Ikeda, 2002 a, b).

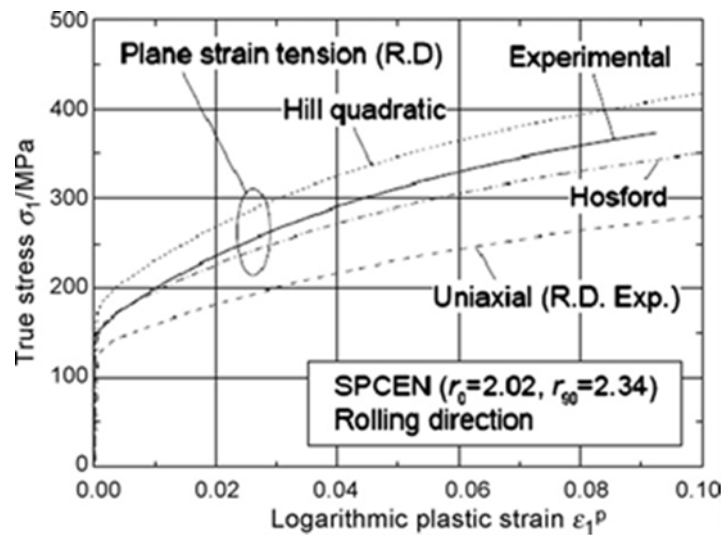


Figure 1.6 σ - ϵ curve for a SPECEN steel (Kuwabara and Ikeda, 2002a, b)

It was observed that the curve detected corresponded to the Hosford yield criterion.

Shimamoto et al. in 2003 developed and validated a bench device for the realization of lots of types of biaxial tests. This device had the ability to perform both static and dynamic tests at controlled temperatures. This biaxial machine presented a vertical configuration.

The applied load was measured with a load cell in each direction and strain gauges were used to measure the strain. Hydraulic actuators were used to perform the test, which meant that the hydraulic circuit included both a static and a dynamic part. The hydraulic actuators were used to provide both the pressure for static tests and that pressure for dynamic tests. A programmed controller was used to monitor the circuit. This device had characteristics that exceeded the limits of the previous devices: a) The test device had a vertical configuration. The developed biaxial machine consisted of 4 actuators, which were oriented at 90 °. The four cylinders operated independently and the centre of gravity was always held in its initial position. (b) Different types of tests, uniaxial traction and compression tests, biaxial traction and compression tests, static and dynamic, biaxial tests under the same biaxial load of bars or plates, changing only the type of grip. (c) It was possible to compare tests under different loads (load ratios from 1: 1 to 1:4) biaxial, static and dynamic under combined loads, biaxial dynamics cutting tests and other load combinations. In addition, the machine was equipped with a cooling liquid (Argon) and an electric heating system, which allowed to perform the dynamic test at a controlled temperature. With this machine, different aluminium specimens were tested at the rate of 0.02 [mm / s] for each axis.

It was confirmed that there was a relationship of proportionality between load and strain “ $\epsilon = 1.7\%$ ” as shown in figure 1.7.

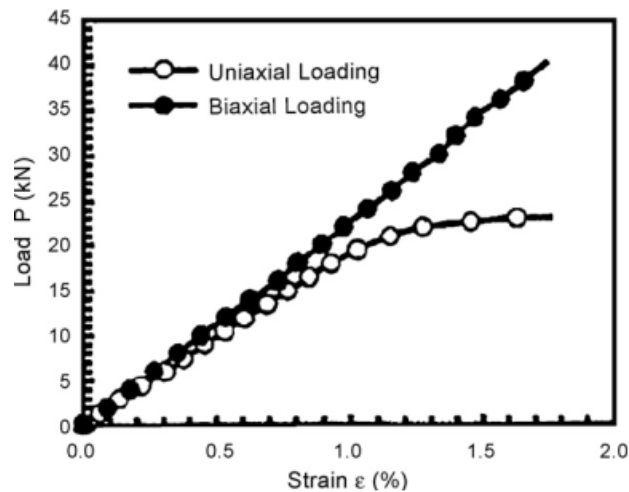


Figure 1.7 Relationship between load and strain during uniaxial and biaxial tests. (Shimamoto et al., 2003).

Shimamoto et al. also used the device to perform dynamic tests useful for studying the propagation of a crack.

In particular, a cruciform aluminium alloy test took place (A7075-T6) at a speed of 1000 [mm / s]. It contained a 30 [mm] long crack put at 45° from the centre. The failure of the above specimen after the biaxial dynamic test is shown in fig. 1.8.

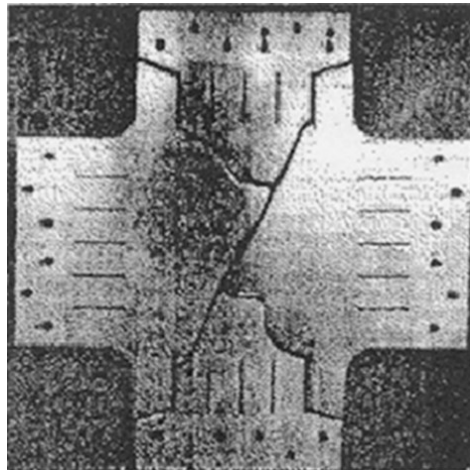


Figure 1.8 Failure of the specimen after the biaxial dynamic test (Shimamoto et al., 2003)

It is evident that the crack propagation has a bilateral symmetry.

The researchers concluded that the device was suitable for both monoaxial and biaxial tests. Test specimen broke after the dynamic biaxial test (Shimamoto et al., 2003).

Another machine was designed by Gozzi et al. to study the behaviour of a high-strength steel under biaxial load. It consisted of two actuators constructed

perpendicularly to each other and four arms hinged to the lower end of the device. The two actuators were self-aligning, while the main disadvantage, deriving from the use of articulated arms, was that the grippers moved along an arched profile. The actuators were controlled by an Instron control unit that could control two actuators independently.

All tests were examined under load control, with a nominal load of 2.7 [MPa / s].

The results from the monoaxial and the biaxial tests were compared, as shown in figure 1.9.

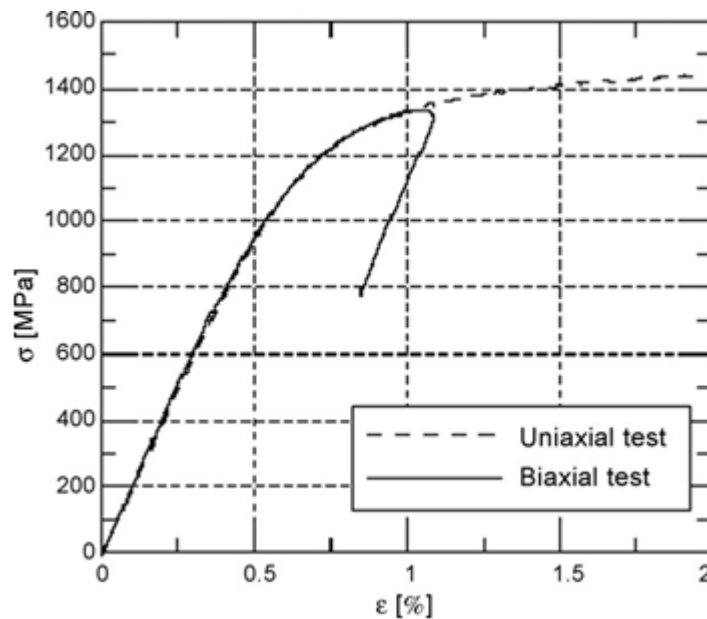


Figure 1.9 σ - ϵ curve in uniaxial and biaxial test (Shimamoto et al., 2003)

From figure 1.9 it can be concluded that the stress in the biaxial specimen during the initial stress can be determined by an accurate monoaxial test.

Granlund studied the effect of a bending force on a cruciform specimen during a biaxial test and found that when a bending force was introduced, it was very small and could also be neglected. (Granlund, 1995, Granlund and Olsson, 1998). These researchers also designed a lateral support plate to prevent buckling during compression tests. The support plates were clamped around the specimen and the clamping force was measured to keep friction losses under control. Furthermore, particular attention was paid to the design of a cross-shaped specimen that allowed the stress in the specific area determined by the external load. Two different grades of steel were tested, one with high and yield strength of 690 [MPa] and one structural mild steel with a yield strength of 275 [MPa].

The results showed that the initial yield criterion between the criterion of Von

Mises and that of Tresca corresponded to previous observations. The following yield criterion was characterized by the Bauschinger effect and a more gradual transition into plastic. So, a new constitutive model was proposed; as shown in figure 1.10, which took into the gradual change under loading conditions [1].

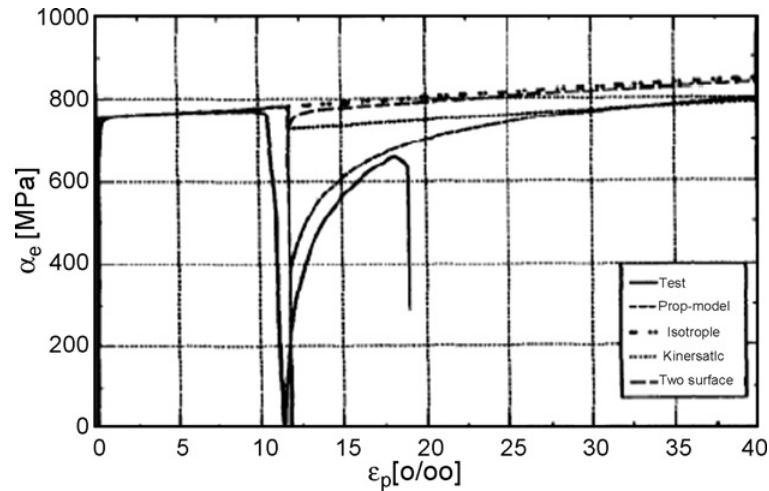


Figure 1.10 σ - ε curve for high-strength steel

1.2.2 Test rig connected to pre-existing single-axis machines

In order to reduce the costs of manufacturing stand-alone test machines, an alternative way to run double-axes tests is the use of auxiliary devices designed for existing machines used for tensile and compressive tests.

Usually, to perform a biaxial test, the operation consists in the conversion into a standard machine for traction. This is achieved by adding a further actuator to the pre-existing system. For example, an horizontal piston can be connected to the vertical traction machine. The existing machine is used to apply the load in the vertical direction, while the removable mechanism is used to put on the load in the horizontal direction. The device was designed by Hoferline et al (2000). It consisted of a removable hydraulic actuator linked to a standard traction machine.

Both horizontal and vertical directions had a load cell and an alignment device. The horizontal device was constructed on a low-friction bearing to ensure that the horizontal structure stayed aligned to the centre of the specimen during the test.

Another biaxial device test was developed at the Fraunhofer Institute in Germany, converting in a compressing machine, through a series of links. (Fraunhofer, 2005). This device is shown in figure 1.11.



Figure 1.11 Test rig (Fraunhofer, 2005)

As we can see from the above figure, the operation of this system is based on the use of four elements added to the load across the compressing machine. When the loading element of the machine moves downwards, the four rods convert the vertical movement into a bidirectional horizontal movement. This movement was used to apply the biaxial force into the cruciform specimen.

As in the cases previously seen, a load cell was used in each direction to measure the applied force, while a camera was used to detect the lengthening of the specimen.

Mohr and Mulalo (2004) used a test on the compressing machine to verify the honeycomb structure under a multi-axial load.

This universal testing device (UBTD) was employed to join large compression displacements combined with those of shear at the edges of the specimen.

A further approach to transform a tensile testing machine into a biaxial testing machine is the method that exploits connecting parts. It was studied and developed by Ferron and Makinde (1998). Through the use of eight parts connected to each other, there was the possibility to convert the vertical movement of the machine crosshead into a bidirectional movement of the grippers. This mechanism is shown in figure 1.12.

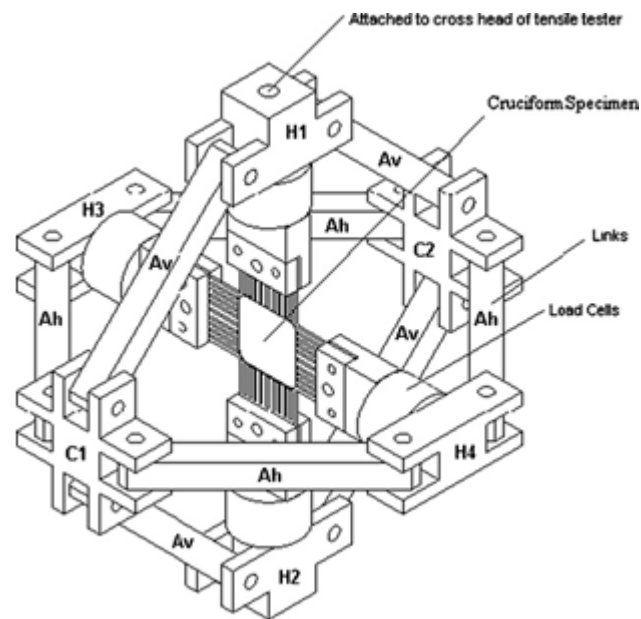


Figure 1.12 Pantograph mechanism for the biaxial test (Ferron and Makinde, 1988)

After constructing the specimen on the device, the complete system is linked up to the testing machine through the head crosspieces H1 and H2, through which the specimen is stressed. During the test, the displacement of the vertical frame, consisting of four arms Av, has ensured a decrease in terms of distance between the connected elements C1 and C2, which have produced an adequate displacement of the horizontal frame made by the four arms Ah. For this reason, there is a greater distance between the two heads H3 and H4. Studying this configuration, we can say that this distance between H3 and H4 was equal than the distance between H1 and H2. The specimen, connected to the four heads H1, H2, H3 and H4, was subject to an equi-biaxial strain through the main connecting plates. When a tensile load was applied to the two heads H1 and H2, the vertical arms were subject to a tensile load whereas the horizontal ones were subject to a compressing load. It can be said that the balance of the specimen strain is true if the elastic strain of the mechanism is negligible. The load on the specimen was measured by two load cells, which were positioned on the H1 and H4 heads.

This mechanism was also used by Terriault et al (2003) to test different alloys at different degrees of temperature. The main difference with this apparatus was that the device used a compressing machine. Here, a compressing force was applied to head C1 and C2, which applied the same movement to the grips as in the previous configuration. The pantograph apparatus converted a

compressing load applied to two cruciform membranes into a biaxial traction across eight articulated arms. The strain was measured using a video extensometer. In this process of study, the aim was to examine whether the beginning of the transformation could be described by the Von Mises' criterion. To achieve this, a test was performed on a Ti-Ni alloy at different degrees of temperature. During the experiment at high temperatures, it was observed that the thickness of a portion of the specimen caused the breakage outside the section. Subsequently, the minimal plastic strain was observed in the section of the specimen which resulted an incomplete stress-strain curve. Makinde et al. (1992b) developed a biaxial strain gauge to measure the strain in the cruciform specimen. The strain gauge allowed both control and strain measurement along two orthogonal directions. The measure of strain in one direction was completely independent from the others. Tests were carried out using the strain gauge on metal sheets and it was delivered to be an excellent method to measure medium-low strains [1].

1.2.3 Test devices for composite and polymeric materials

Unlike metals, only recently, scholars have begun to understand the breakdown of composites under multi-axial loads.

Because of the anisotropic structure of the material, the resistance under biaxial load strongly depends on the direction of the fibers of the material during the test, addressed to the conduct of the load. If the load and the fibers are correctly oriented, the biaxial strength can exceed the value that could be found by a simple uniaxial tensile or compressing test. Otherwise, the resistance can be even much lower. Some researchers believe that the only way to overcome many of these problems is to carry out long-term studies aimed to confirm numerical results through reliable experimental information.

Among these, the biaxial tests, which allow to have results in the space σ_1 - σ_2 and give essential design parameters for the breakdown of the composites, are the most difficult and expensive to realize.

To produce a biaxial stress state, several experimental techniques and types of specimens were used.

These techniques can be classified into two categories:

(i) Tests using a single loading system

(ii) Tests using two or more independent loading systems.

In the first category, the value of the biaxial stress depends on the geometry of the specimen or on the configuration of the loading device, instead of, in the second category it depends on the value of the applied load.

An example of the tests belonging to the first category are the bending tests on cantilever beams and tests using special devices.

Especially, for composites, single-axis specimen tests that have fibers oriented on different axes produce a complex state of stress in the material reference system, also consisting of two or three components in the stress tensor plane.

The respective stress values, however, depends on the angle of orientation of the fibers.

Examples of the second category are a torsion-twisted round bar, thin-walled tubes subjected to a combination of tensile / compression and torsion or internal/external pressure and cruciform specimens under planar biaxial loads.

The most realistic technique, then, is to create a biaxial stress state by applying loads in the same plane along the two arms of a cruciform specimen. Nowadays, it is trying to establish a procedure for biaxial tests and to develop an accurate failure criterion.

The biaxial planar test device by Smits et al. (2006), as shown in fig. 1.13, is a machine that uses four independent hydraulic servo actuators with a special control unit and load cells. This is a very expensive equipment.



Figure 1.13 Equipment for the biaxial test (Smits et al. 2006)

The use of polymeric adhesives like a replacement to traditional riveted structures allows the construction of joints in which there are great

advantages compared to mechanical clamping. In fact, they allow the development of larger structures and more uniform load distributions, unless the gluing area is larger. In addition, the glued structures are more rigid, given the continuity of the gluing itself, and do not show variations on the surface and on the structure of the combined materials. So, the need arises to perform biaxial characterizations also on this type of material.

The types of adhesives can be divided into two categories:

- Structural adhesives
- Flexible adhesives

The former has an elastic behaviour up to break with low strain volumes. The latter is characterized by a high breaking strain and low elastic modules.

Structural adhesives are used to make rigid joints. The base material is generally a resin with a fairly high modulus of elasticity (3-4 GPa). The material, thanks to its cure process at particular temperatures, creates chemical bonds between molecules, generating a high density and therefore a high rigidity.

Very often the structural adhesives are made by adding to the base resin rubber particles that allow to increase their stiffness and consequently the amount of strain before breaking.

The behaviour of structural adhesives with low strains can be modelled through a linear elastic function that in FEM software is extremely simple to implement as a material of this kind. It is completely described by an elastic modulus and Poisson coefficient, obtained through experimental methods, such as, by tensile test.

In 2004 Cognard, Davies et al. [5] developed a system useful to study the behaviour of an adhesive joint subject to tensile and compressive stresses combined with shear stresses. The study started with a machine developed by Arcan in 1987 to understand the fracture behaviour of composite materials. Cognard and al. hypothesized that, with the appropriate modifications, the machine was ideal to generate a load in several directions aimed at the study of adhesives.

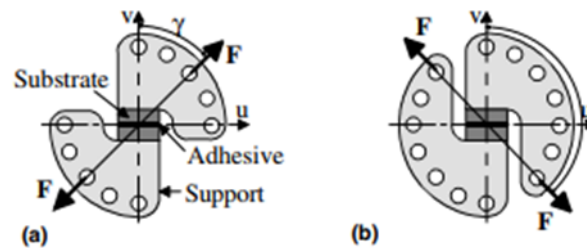


Figure 1.14 Types of Arcan systems: (a) classic type, (b) modified type

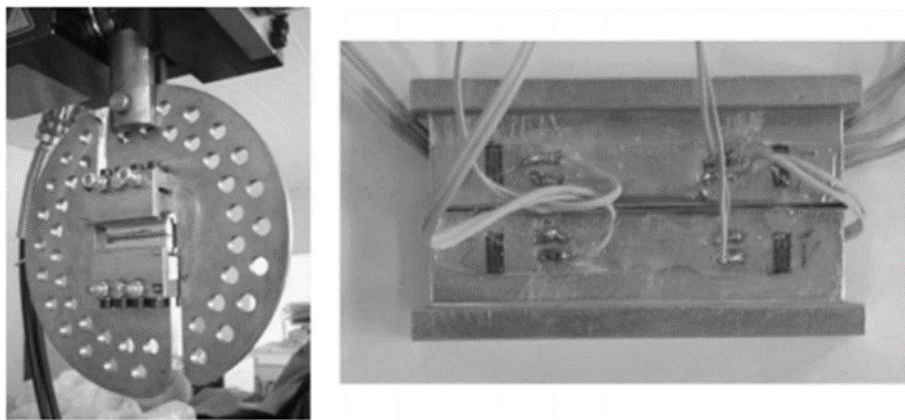


Figure 1.15 Photographs of the Arcan plant and instrumental assembly

For hyperelastic materials, such as adhesives and rubbers, the biaxial load test is performed in order to validate the analytical model used to represent the behaviour of the material.

In the literature, there are a lot of examples of biaxial testing systems or conversion of monoaxial traction machines in biaxial machines to perform tests on hyperelastic materials and composite materials

In general, these machines are classified into two large families:

- Separate Load
- Single load

The systems that provide as many load cells as the actuators are available in the first family and are all independently manageable. These machines can be used to reproduce different multi-axial tension states with extreme precision, with the disadvantage that investment costs are very high.

The second family includes the machines and conversion systems of a single-axis test machine that use only one actuator and only one load cell. The cost of such device is lower than that with multiple load cells. Moreover, a machine of this kind can also be used for single-axis tests.

Brieu, Diani and Bhatnagar in 2007 [12] proposed a new type of machine capable of producing equi-biaxial and non-equibiaxial stresses on each plane of the specimen.

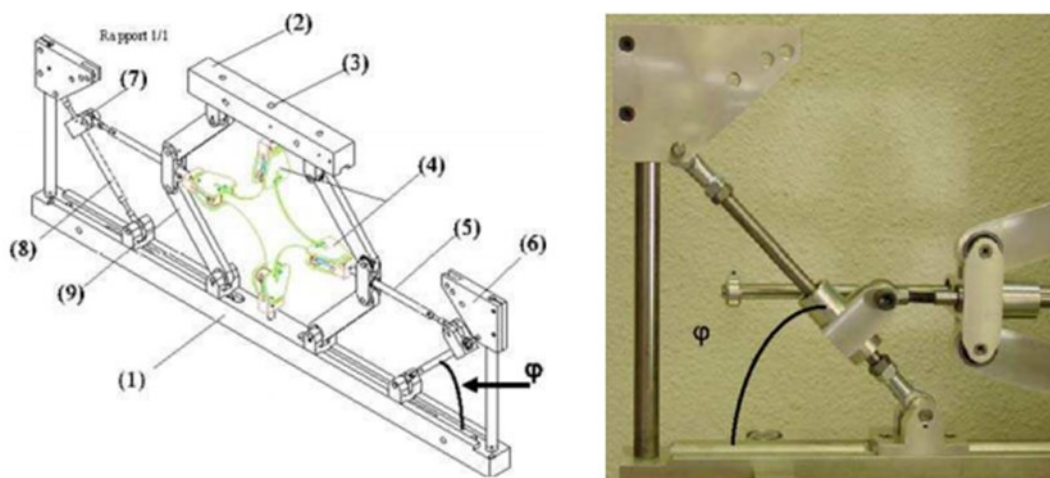


Figure 1.16 Biaxial test machine (Brieu et al.)

The system has been designed to perform cyclic biaxial stress tests with wide strains, with an elongation in the two tension directions and with different load ratio values. The authors Brieu, Diani and Bhatnagar have demonstrated, through their new test machine, that the unit of measure will not be a pure biaxial measurement, but the result of a biaxial traction with an "r" ratio between the variable elongations during the test.

1.3 Types of shape specimen for biaxial test

1.3.1 Shape for composite materials

The characterization of composite materials subjected to uniaxial loads is not able to evaluate the actual behaviour of an engineering component. In fact, many structural components are subject to multiaxial loads [4].

Therefore, biaxial and multiaxial tests were made to perfect the mechanical behaviour of these complex materials, necessarily. Recent years many different set-up tests have been used to produce biaxial stress state, for example, cruciform specimens under in-plane biaxial loading; torsion and internal/external pressure; bending tests on rhomboidal composite plates and tubes subject to a combination of axial loading. Although in theory these tests should have given an advance of composite knowledge, practically, they did not give reliable results [5].

In particular, in the field of composite materials different shapes of cruciform specimens subject to biaxial load were studied with FEM. analysis and tested, but not successfully completed according to the following requirements:

- maximisation of the region of strain uniformity into the biaxial loaded zone;
- minimization of the global shear strains in the biaxial loaded test zone;
- minimization of the strain concentration/failure outside the test zone of interest;
- specimen failure in the biaxial loaded test zone;
- repeatable results. [4-8].

In 1992 Makinde, Thibodeau and Neale [2], referring to the previous studies by Monch et al. [9] have begun to lay the groundwork for carrying out biaxial tests on carbon resin laminated, as precisely as possible. The study dealt with the search for a better geometry that allowed the birth of a larger biaxial stress state in the centre of the specimen. There are two different geometries to consider thanks to their study:

- 1) specimens for tests subject to small strains which have a circular section in the centre where the thickness is reduced (fig. 1.17)
- 2) specimens for large strains that have a central rectangular section with notches in the arms (fig. 1.18)

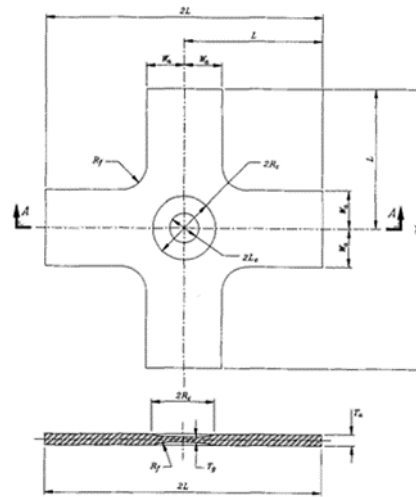


Figure 1.17 Cross-shaped specimen with a circular and reduced central section

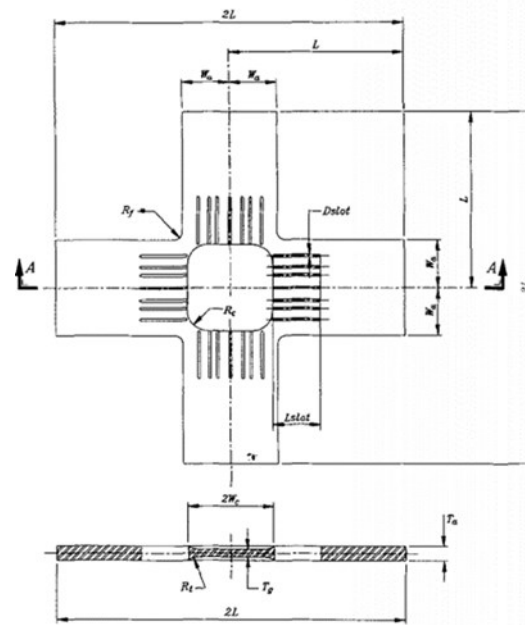


Figure 1.18 Cruciform specimen with notches

From a study by Monch of 1963 [9] it was understood that removing the disturbances produced by the lateral stress of the edges of the specimen it was necessary to insert the notches on the arms of the same. Moreover, it was possible, thanks to them, to produce any two-dimensional load by moving the biaxially specimen.

The notches also allow reducing the rigidity of the arms which could reduce the maximum strains obtained at the centre of the specimen and also restricting the homogeneous stress region.

Among the problems that the authors have found, we can understand that

there is the concentration of the stress between the arms and the central section, in the transition zones, as well as, the concentration of stress in the notches near the measurement area that leads to premature breaking of the specimen.

As we have seen, there are several geometric parameters that cause the variation of the results from test to test. Makinde et al. they have studied a series of geometric variables that influence the distribution of stress and strain.

A specimen used for low strains has seven geometric variables that most influence the test:

- 1) Width of the arms ($2W_a$)
- 2) Length of the specimen outside the grips ($2L$)
- 3) Connecting radius between the arms (R_f)
- 4) Radius of the circular measuring region (R_c)
- 5) Passing radius (R_t)
- 6) Arm thickness (T_a)
- 7) Ratio between the thickness of the arm and that of the measuring section (T_a / T_g)

For a specimen used for large strains, with the notches, there are five other variables to consider:

- 8) Width of the central section ($2W_c$)
- 9) Diameter of the carvings (D_{slot})
- 10) Number of carvings (N_{slot})
- 11) Length of the carvings (L_{slot})
- 12) Location of the carvings (X_{slot}).

The problem is how to determine an optimal combination of the variables to obtain the desired results, as a uniform distribution of stresses and strains for both geometries. The traditional method of changing one variable on time could not work because of the interactions between two or more of them. Makinde has decided to adopt a design on a statistical basis able to combine the change of several variables. For each combination, the measured effects were the width of the measurement area, where stress and strain did not have to be moved more than 5% away from the central values of the specimen, nor that maximum elongation obtained in the centre of the specimen before breaking.

In 2002 Welsh and Adams [10], starting from previous works and previous

forms of specimens (fig.1.19), focused the attention on the improvement of the same (especially about the measurement area that is made with a smaller thickness), they carried out tests on a laminate AS4 / 3501- 6 cross-ply carbon/epoxy.

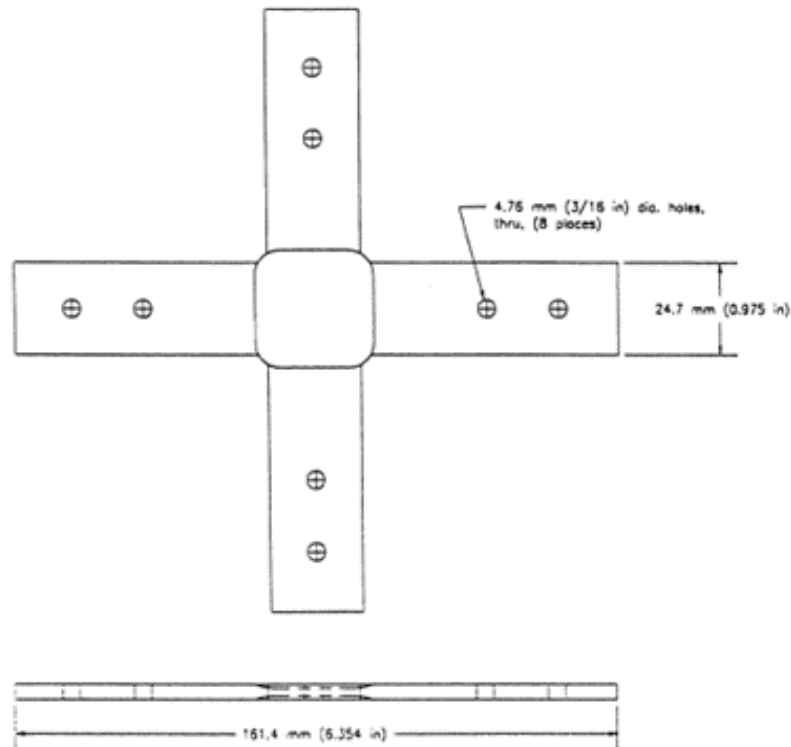


Figure 1.19 Schematic drawing of a specimen for biaxial tests used by Welsh et al.

The first improvement consisted of removing the internal hole, to align the specimen with the grips, from each arm. This is because the position near the edge of the arm is the one with the lowest stress and therefore, the concentration of stresses near the holes is greater. Eliminating the zone with greater stress, on the arms of the specimen, there will remain only a low concentration of themselves. This prevents possible unwanted breakage of the arms.

Another change involves the variability of the geometry of the loaded arm. In fact, it is possible to increase the thickness of the arms in such a way that the uniaxial stress state is lower in each arm and this can avoid undesired breakages. In addition, the reduction of the width of each arm could be gradual in the region between the end of the wedge handle and the unit of measure(fig.1.20). This variation has different consequences including the fact that depending on the amount of the reduction of the measured size could be significant. Among the advantages, of course, there is the fact that

the maximum amount of force required to break the specimen is shut down.

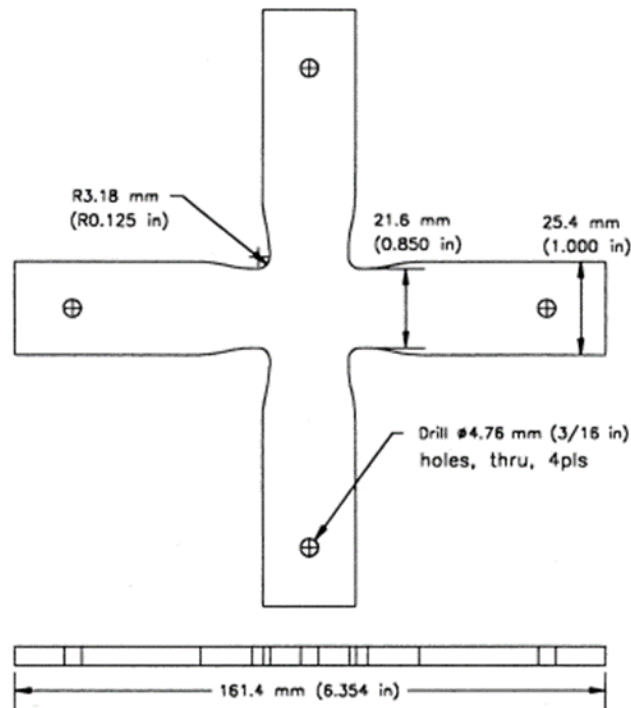


Figure 1.20 Schematic drawing of a modified specimen for biaxial tests used by Welsh et al.

In addition to these changes, Welsh and Adams investigated two other essential aspects of the form of an audition:

- The radius of connection at the intersection of two arms
- The shape of the measuring process.

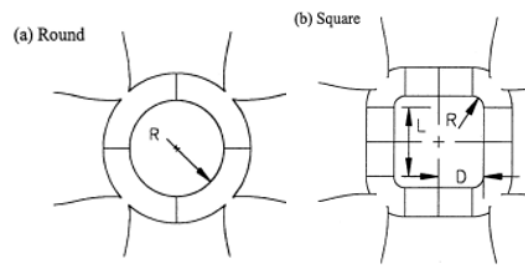


Figure 1.21 Detail of the round and square measuring section for a cross-shaped specimen with a tapered thickness

A series of tests with different tension ratios between the x-axis and the y-axis have shown that the difference, when the connecting radius varies, is very low. It was, therefore, arbitrarily deduced that, the largest fitting can be used

to carry out a series of characterizing tests.

According to the shape of the measurement area, the two authors have considered two types of sections: square and circular (fig. 1.21).

To understand which one was the best, they confronted the tests on both types and compared the experimental results. The tests were performed at three different load ratios and at the same connection the radius between the arms and the unit of measure.

It is inferred that the shape of the measure influences the biaxial force and it has been observed, moreover, that the applied load can be increasingly transferred through the section if the latter has a wide and round shape (about 98% of the load). The use of a small and square geometry, instead, indicates that 30% of the applied load circumvents the unit of measure during the biaxial test.

So, the primary objective of the different tests is to investigate the effects of stress concentration. The highest measure of biaxial efforts is generally considered as indicator of the best geometry. Considering, therefore, that at high concentration of the tensions near the measurement area, always corresponds a lower value of the measured resistance, it is deduced that, there must be in this case, a low concentration of the tensions. These evaluations lead to define the best geometry for the specimen, for example, the one with the small and square measured required and the other, with a large radius of connection between the arms.

Later Smits, Van Hemelrijck, Philippidis and Cardon in 2005 [11] analyzed the previous work by Welsh and Adams. Carrying out the analysis about a finite element that consisted of different types of specimens and comparing the results with experimental tests where the strains were acquired with an extensometer and an optical system, they defined a stacking sequence $[(\pm 45/0)_4/\pm 45]_A$ used as the standard for all samples.

In the figures 1.22-1.23 there are the results of the analysis for the main strains and the shear strains.

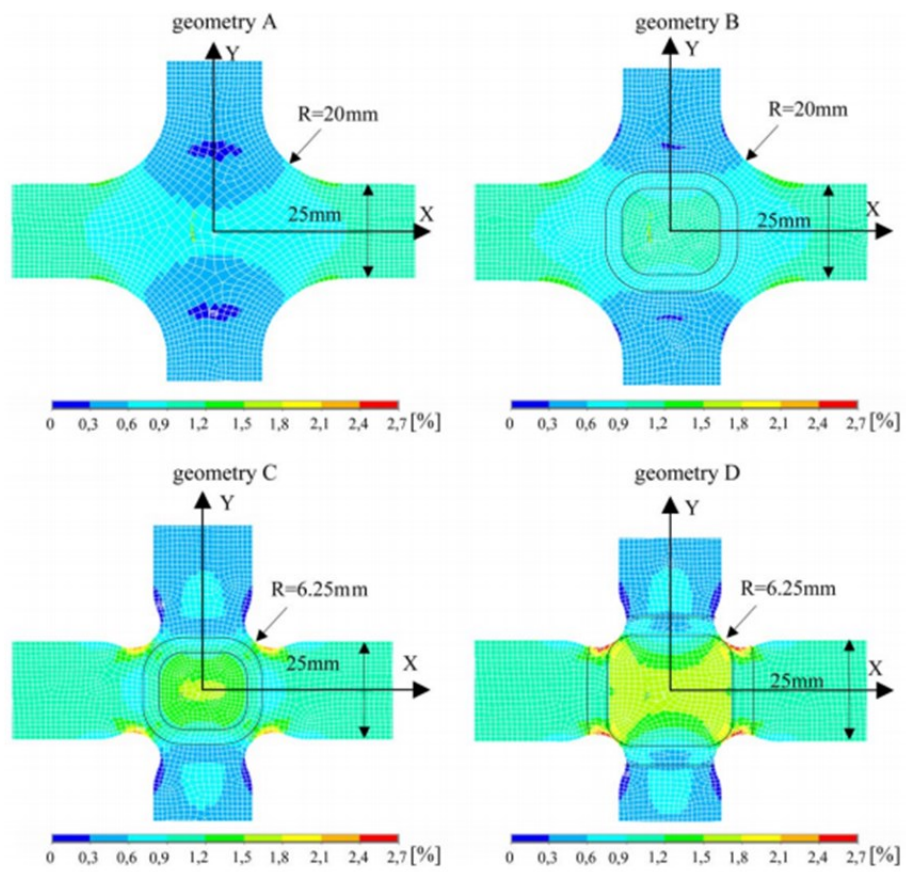


Figure 1.22 Strain along the main direction in the four cruciform geometries [11]

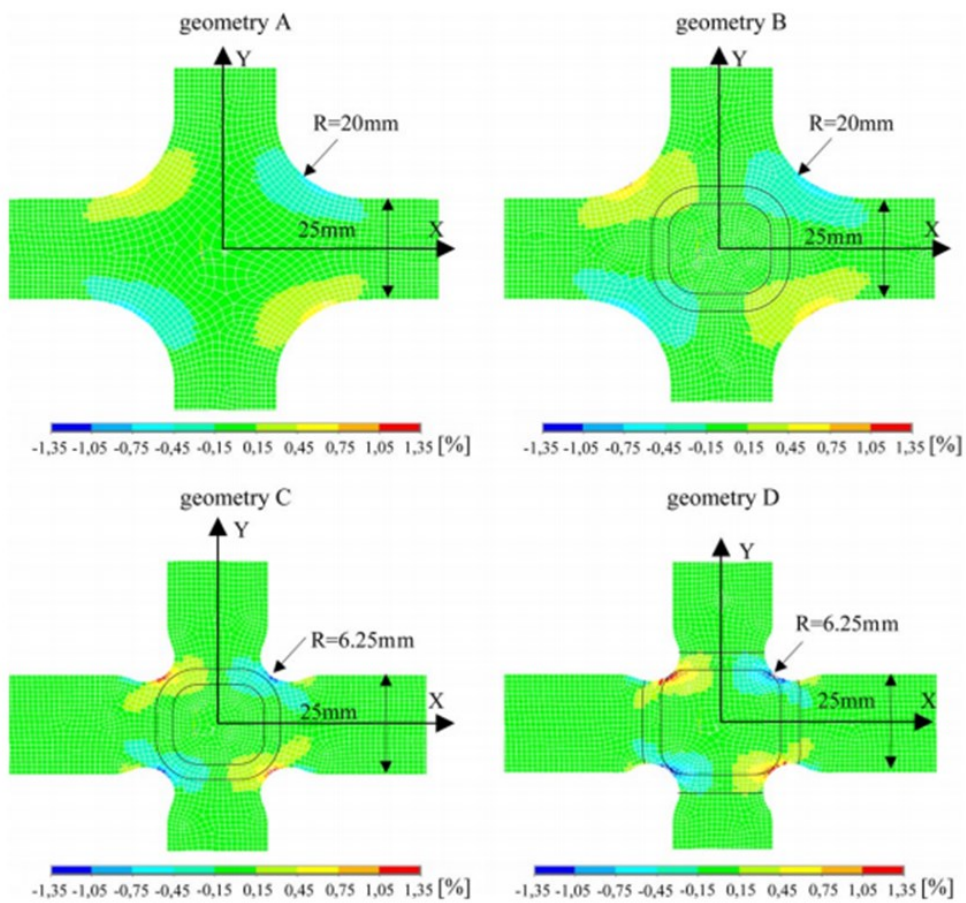


Figure 1.23 Shear strains in the four cruciform geometries[11]

The geometry test piece A is the constant thickness and has a connection between the arms. For this reason, the main strains are lower in the centre area than in the arms, with consequent breaking in the latter. This is because the area that absorbs the load is greater in the centre. Scholars have thus reshaped both the thickness of the central area and the connecting rays at the intersection of the arms. In this figure C, we see these leads to the geometry where the strains are high in the biaxial loading zone and the breakage will occur in the centre of the specimen. Also the geometry D like that C has a presence of strains in the biaxial loading zone and will ensure a break into the centre of the specimen, but the second has more constant strains and a lower decrease of the same. In addition, we can say that because of the lower shear strain, therefore, this kind of phenomenon it is chosen as the best geometry. This confirms the hypothesis that for fibre-reinforced laminates the best solution is to reduce the central thickness.

1.3.2 Shape for polymeric materials

Using the Arcan machine, the number of loading directions is given by the number of holes on the device, but the loading domain is discrete. So the researchers N. Arnaud et al. in 2014 [13], starting from this device have studied a way to apply, continuously, load spectra on specimens. To carry out this, they used a tubular specimen.

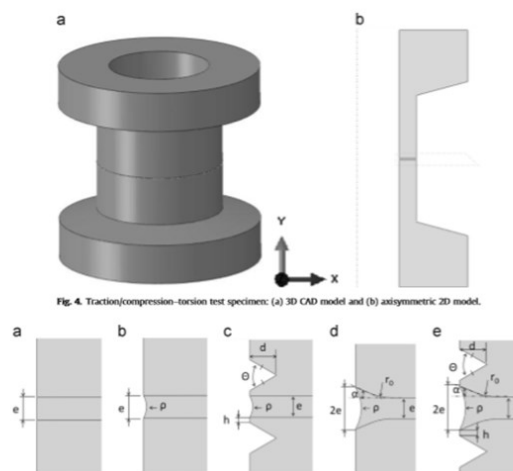


Figure 1.24 Types of specimens for the biaxial tests of Arnaud. 3D CAD model and axisymmetric 2D model: (a) straight edge, (b) cleaned edge, (c) pecking with a cleaned edge, (d) chamfered edge with polished edge, (e) bevelling with a cleaned edge and pecking

The study was based on 5 different geometries, all related to the tubular specimen (fig. 1.24). FEM tests have shown that the geometries C and E prove to be the best to determine a biaxial stress state.

In 2015 Chowdhury and Wang [14] studied the effects of biaxial stresses on a specimen in adhesive material, specifically FM355 (a particular type of epoxy adhesive). The aim was to find a particular geometry of the specimen that respected the criteria of the biaxial tests. The researchers did experimental tests on three different sample configurations, comparing the results with those obtained from FEM tests.

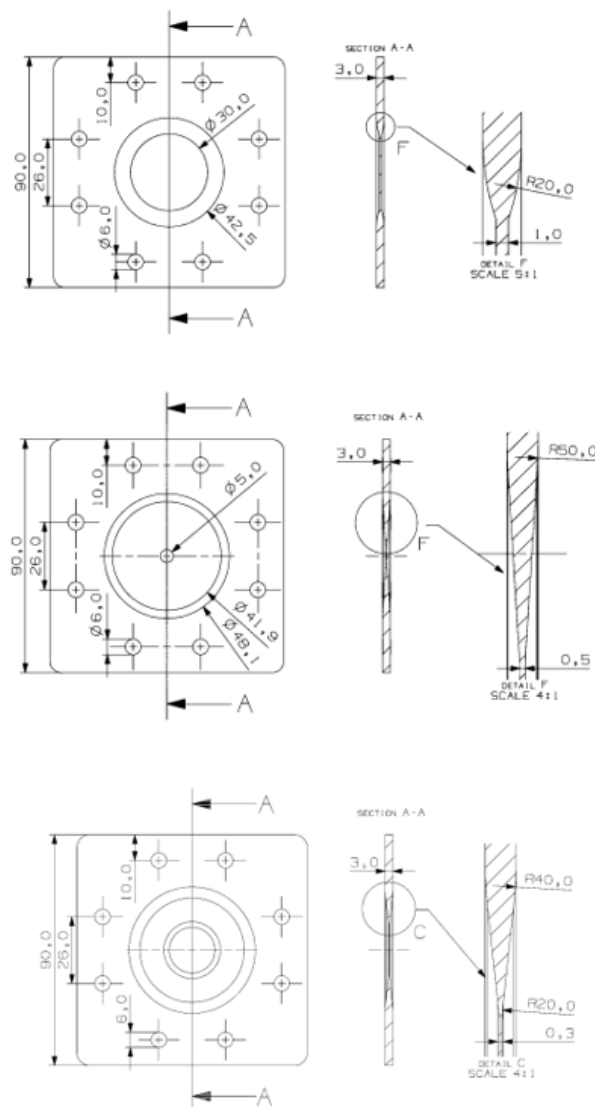


Figure 1.25 Typologies A, B and C of specimens analyzed by Chowdhury

In 2016 Zarouchas and Nijssen [15] performed biaxial tests on a new specimen geometry, made of EPIKPTE MGS Paste 135 / G adhesive, in order to understand how best to adapt the adhesive material to create junctions on the leading edge of the turbine blade.

The geometric configuration was a tubular type with a reduced measured thickness.

The tests were carried out at controlled load and at biaxial tension ratio (ratio between normal tension and cutting tension in the measure indicated) constant for each individual test.

Measurements of the strains were made with strain gauges oriented at 0° , 45° and 90° respect to the longitudinal axis of the specimen.

The comparison obtained between experimental data and the FEM model shows that the latter provides a very precise point of the break. In fact, it can be seen from figure 1.26 the position of the break obtained experimenting through numerical forecasts.

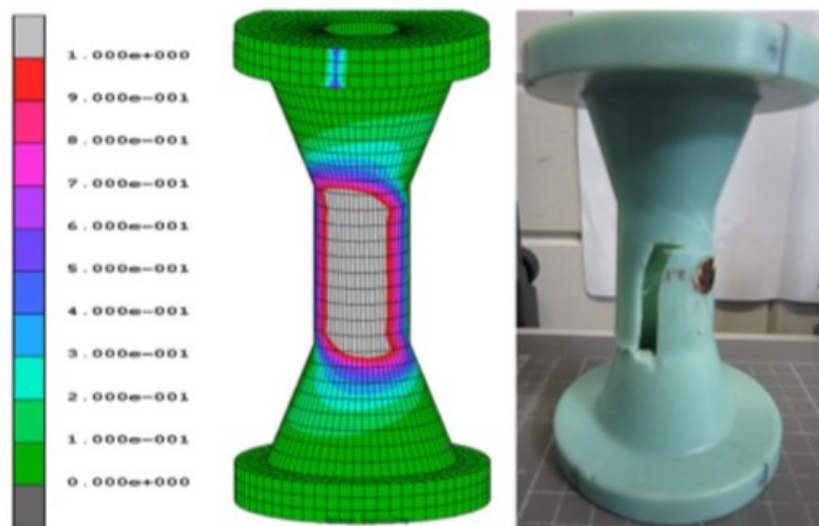


Figure 1.26 Comparison between numerical results and experimental observations of Zarouchas and Nijssen

As for the hyperelastic adhesives, the specimen used in 1999 Duncan has defined a specimen of HKL material, with each square of 45mm and a thickness of 1.6mm. Once that it was put on his test machine, the measure became 28mm.

Two types of tests were experimented: one consisted of the square-shaped specimen and the other of the same shape, but with the corners removed in order to alleviate any concentration of stress.

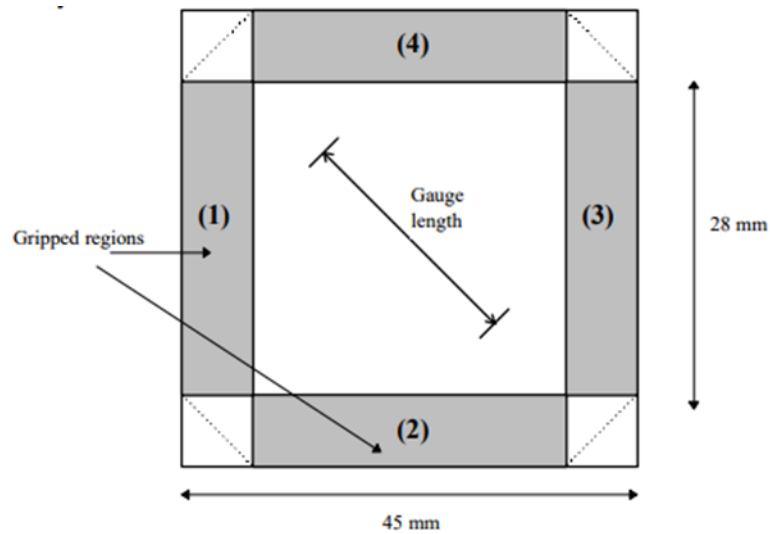


Figure 1.27 Schematic diagram of a biaxial specimen according to Duncan. The dotted part shows how the corners have been removed for some analysis

During this experiment of Brieu and Diani [12], the specimen, in order to validate the biaxial test, must be uniformly grasped during the test. The dimensions of the specimen, in this case, are related to the radius of connection between the arm and the measured area, which must be provided in such a way to guarantee the biaxial load in the centre of the specimen (fig. 1.28). Obviously, it can be noted that the variation of R will also vary the behaviour of the specimen submitted to the test.

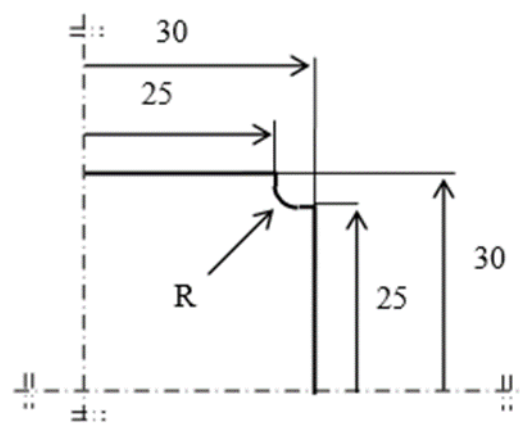


Figure 1.28 Specimen dimensions of Brieu et al.

Hollenstein, Helfenstein, and Mazza in 2009 [17] tested a cruciform specimen, with 5 notches on each arm (see fig. 1.29).

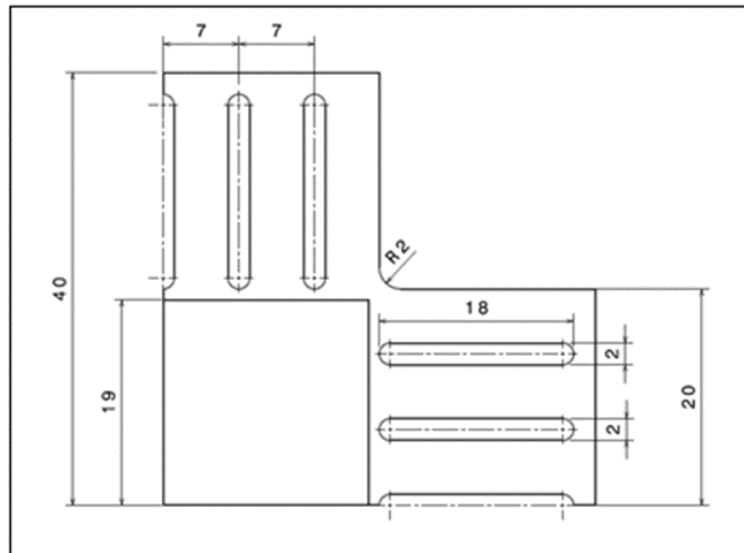


Figure 1.29 Hollenstein et al. specimen

Thanks to the notches, the influence of the transition from uniaxial stress in the arms to the biaxial ones in the measured area is reduced.

The objective of the FEM analysis has reached. In fact, to maximize the area in which a biaxial load acts homogeneously, a series of deductions are made and parameterized in this way :

- Width w
- Length l
- Distance from the loaded edge u
- Distance between the centre of two consecutive notches d

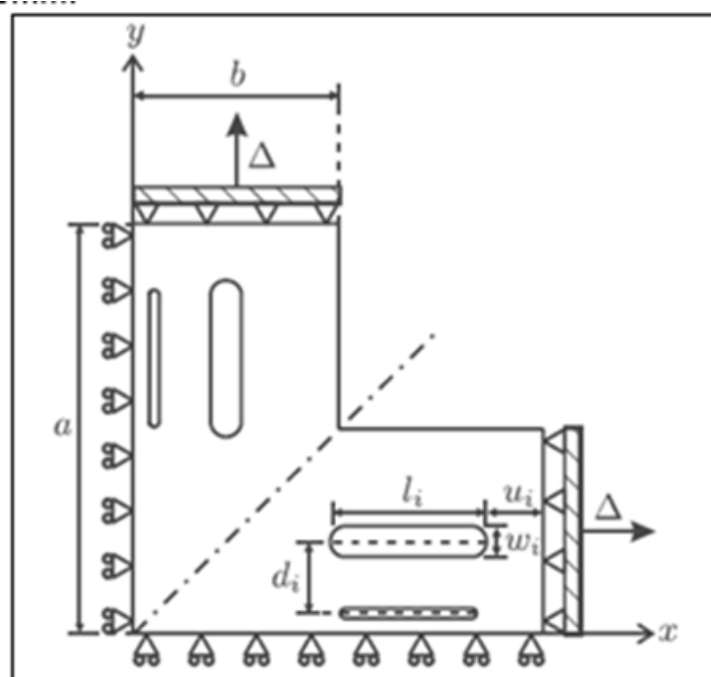


Figure 1.30 Boundary conditions of Hollenstein specimen

Hollenstein, Helfenstein, and Mazza [17] used these parameters as variables of an optimization algorithm. So, starting from the results of a FEM code, to maximizes the size of the square region in which a uniform stress state acts.

This is based on two conditions:

- the main stresses acting at each point must differ from each other by 5%
- the main stress acting at each point must not differ more than 1% from that acting in the centre of the specimen.

The study, thanks to the symmetry, was performed on a quarter of the specimen and the stress state was considered plane. The final solution envisaged the area of the test specimen by comparing a geometry with 4 notches on the specimen arms with the one previously studied by Mazza.

The tests about Finite Elements were aimed at finding which model was the most extended into the biaxial area. The numerical models have been discretized Quad elements, whose membranous type of freedom, is the translational one in the plane. Making sure that the only thing to vary in the two models was the geometry, you could make a comparison between the two types of specimens.

When carrying out studies at the FEM, it is always necessary to define the constitutive models of the material that define their laws. For this kind of material the laws of the stress-strain curve are always based on elastic models, but with a high non-linear behaviour.

There are different patterns of hyperelastic behaviour and they are all linked to coefficients that are defined by experimental tests.

The model assumed prevalently in all the studies seen previously takes the model name of Mooney-Rivlin and assumes the trend of the curve with the help of coefficients whose values were found by Chevalier and Marco in a work of 2002 [16], through a series of experimental data collected on uniaxial and biaxial tests. The same scholars have validated a second behaviour model that takes the name of Ogdeon and that was used in the study by Hollenstein, Helfenstein and Mazza in order to understand what statistical results are correct for the two geometric models and for the two material models. We are closer to the limits imposed for biaxial behaviour.

In 2011 Schmidt, Bergamini, Kovacs and Mazza [18], starting from Helfenstein's study on the form of the specimen, developed a series of biaxial tests on an elastomer material for the study of Elastomeric Dielectric Actuators.

These actuators are nothing more than a combination of polymer membranes coated with layers of conductive material which act as electrodes and, if subject to voltage, contract in the thickness direction and expand into the plane generating a biaxial stress state.

Nonlinear dependence allows modelling this type of materials with hyperelastic trend.

The author's study is aimed at carrying out a series of biaxial tests in order to find the best function to define the strain energy density.

The instrumentation used for the tests is that of the ETH Zurich and allows a separated control of forces and displacements on the four actuators. It has been widely demonstrated that the specimen must be used for the presence of five notches on each side to reduce the influence of the transition from the uniaxial stress state in the arms into the equibiaxial zone in the centre.

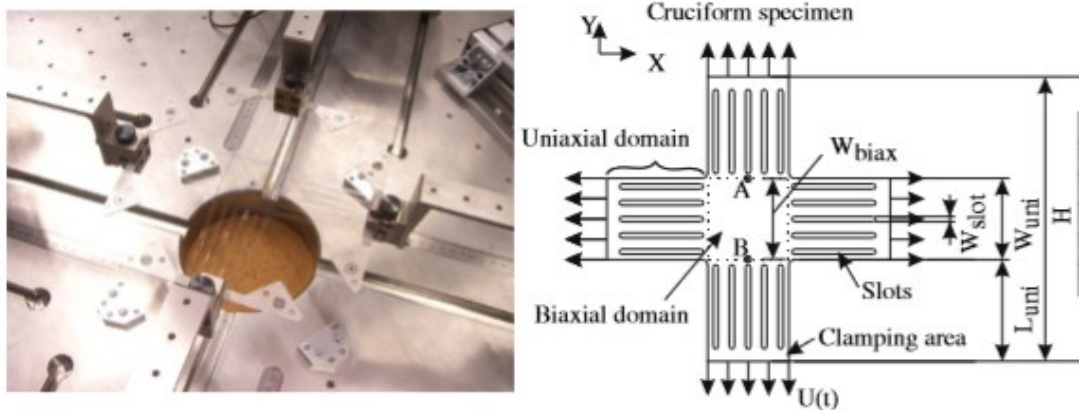


Figure 1.31 Test machine and specimen of Smidt et al. [18]

References

- [1] Alan Hannon, Peter Tiernan, “A review of a planar biaxial tensile test system for sheet metal”, *Journal of material processing technology* 198 (2008) 1-13.
- [2] A. Makinde, L. Thibodeau, KW. Neale, Development of an apparatus for biaxial testing using cruciform specimens, *Exp. Mech.* 1992, 32(2):138-44
- [3] N. Bathnagar, R. Bhardwaj, P. Selvakumar, M. Brieu, “Development of a biaxial tensile test fixture for reinforced, Polymer Testing”, *Journal of material processing technology* 26 (2007) 154–161
- [4] A. Smits, D. Van Hemelrijck , T.P. Philippidisand, A. Cardon, Design of a cruciform specimen for biaxial testing of fiber reinforced composite laminates, *Composites Science and Technology* 66(2006)964-975
- [5] - J.Y. Cognard, P. Davies, B. Gineste, L. Sohier (2004). Development of an improved adhesive test method for composite assembly design. *Composites Science and Technology* Volume 65, Issues 3–4, Pages 359-368
- [6] E. Lamkanfi, W. Van Paepegem, J. Degrieck, C. Ramault, A. Makris, D. Van Hemelrijck, Strain distribution in cruciform specimens subject to biaxial loading conditions. Part 1: Two dimensional versus three-dimensional finite element model, *Polymer Testing* 29(2010)7-13
- [7] A. Makris, T. Vandenberg, C. Ramault, D. Van Hemelrijck, E. Lamkanfi, W. Van Paepegem, Shape optimization of a biaxially loaded cruciform specimen, *Polymer Testing* 29(2010)216-223
- [8] I. Guelho, L. Reis, M. Freitas, B. Li, J.F.A. Madeira, R.A. Cláudio, Optimization of cruciform specimen for low capacity biaxial testing machine, (2013)
- [9] - E Mönch, D Galster (1963). A method for producing a defined uniform biaxial tensile stress field. *British Journal of Applied Physics*, Volume 14, Number 11
- [10] J. S.Welsh, D. F.Adams (2002). An experimental investigation of the biaxial strength of IM6/3501-6 carbon/epoxy cross-ply laminates using cruciform

specimens. Composites Part A: Applied Science and Manufacturing, Volume 33, Issue 6, Pages 829-839

[11] A.Smits, D.Van Hemelrijck, T.P.Philippidis, A.Cardon (2006). Design of a cruciform specimen for biaxial testing of fiber reinforced composite laminates. Composites Science and Technology. Volume 66, Issues 7–8, Pages 964-975

[12] - M. Brieu, J. Diani, N. Bhatnagar, “A new fixture for uniaxial testing machine –A validation for hyperelastic behaviour rubber-like materials”, I. J. of Testing and Evaluation, Vol. 35, N. 4

[13] - N. Arnaud, R. Créacohcade, J.Y. Cognard (2014). A stress/compression–torsion test suited to analyze the mechanical behaviour of adhesives under non-proportional loadings. International Journal of Adhesion and Adhesives Volume 53, Pages 3-14

[14] - N. T. Chowdhury, J. Wang, W. K. Chiu (2015). Design of a Flat Plate Specimen Suitable for Biaxial Tensile Tests on Polymer Materials

[15] – D. Zarouchas, R. Nijssen (2016). Mechanical behaviour of thick structural adhesives in wind turbine blades under multi-axial loading. Journal of Adhesion Science and Technology, 30:13, 1413-1429

[16] - L. Chevalier, Y.Marco, 2002. Tools for Multiaxial Validation of Behaviour Laws Chosen for Modeling Hyper-elasticity of Rubber-like Materials. Polymer Engineering And Science, vol.42, 280-298..

[17] - Helfenstein J, Hollenstein M, Mazza E (2009). Investigation on the optimal specimen design for planar-biaxial materials testing of soft materials. Proc. 6th Eur. Conf. Cost. Models for Rubber, 371-376.

[18] - A. Schmidt, A. Bergamini, G. Kovacs, E. Mazza (2011). Multiaxial Mechanical Characterization of Interpenetrating Polymer Network Reinforced Acrylic Elastomer. Experimental Mechanics, Volume 51, Issue 8, pp.1421–1433

Chapter 2

The study of a new equipment for biaxial tests

2.1 Technical characteristics and components of the equipment

All the equipments described in the state of the art are not able to pursue the main objective of the thesis that is to create equipment that can be mounted on a universal test machine, so with vertical positioning, and which allows to modify the force between the two traction axles simply by changing some mechanical elements.

This work concerns the realization of capable equipment to transmit the input from a single direction along both the X and Y axes, in order to characterize composite or polymeric materials (figure 2.1) according to a biaxial scheme.



Figure 2.1 New equipment

The equipment is designed in order to distribute the force in both directions symmetrically.

The technical design specifications of the biaxial testing equipment are:

- Maximum tensile load capacity for each specimen arm 10,000 [N]
- Frequency not lower than 5 [Hz]

The main components of the equipment are:

- Load group consisting of:

- Hydraulic clamps
- Spiral washers
- Locking slider for grippers

- Chassis group consisting of:

- Support box
- Eight support arms
- Connection axes

- Group for the transmission of movement consisting of:

- Connecting rods
- V-shaped cranks

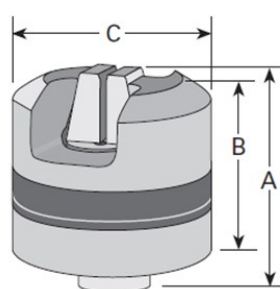
The individual components that reach the equipment through their CAD drawings will be illustrated below.

2.1.1 Loading group

The load group refers to the system of components (hydraulic clamps, spiral washers and sliders) useful to grasp the specimen and to apply it to biaxial load.

- Hydraulic clamps (MTS model 647) [1]

The hydraulic clamps have the function of locking and holding the specimen in the same way in the test area, so that the tests have more precision and repetitiveness. Thanks to their large clamping and alignment ability, deflection strains are reduced. Specimen slippage can invalidate test, especially during tensile and compression cycles. In addition, the hydraulic pressure of the external circuit allows testing on several types of materials.



Specifications

Force Rating

► See tables.

Dimensions & Weight

► See tables.

Wedge Width

► See tables for standard width. Wider wedges available. See 647 Wedges pages.

Required Grip Supply Pressure

► 21 MPa (3000 psi)

► 70 MPa (10,000 psi) for 647.25, 647.50, 647.100 and 647.200

Temperature Range

► -18 to +65°C (0 to 150°F) with standard grip supply.

► -40 to +175°C (-40 to +350°F) with high-temperature grip supply.

Figure 2.2 Clamps properties

Axial Grip Specifications									
Model Number	Force Rating		Weight (each)	Wedge Width*	Grip Dimensions			Stud Size	Part Number
	Dynamic	Monotonic			A (max)	B	C		
647.02B	5.5 kip	7.0 kip	10 lb	1.0 in	5.2 in	4.4 in	4.5 in	1/2-20	056-078-605
647.02B	25 kN	31 kN	5 kg	25 mm	131 mm	112 mm	114 mm	M12 x 1.25	056-078-605
647.10A	22 kip	27 kip	67 lb	1.75 in	7.4 in	6.3 in	8.0 in	1-14	047-080-605
647.10A	100 kN	120 kN	30 kg	45 mm	188 mm	159 mm	203 mm	M27 x 2	047-080-605
647.25A	55 kip	75 kip	170 lb	2.0 in	9.8 in	8.9 in	10.5 in	1-1/2-12	047-080-905
647.25A	250 kN	333 kN	77 kg	50 mm	249 mm	225 mm	267 mm	M36 x 2	047-080-905
647.50A	110 kip	120 kip	325 lb	4.0 in	11.5 in	9.8 in	13.0 in	2-12	047-595-505
647.50A	500 kN	550 N	148 kg	101 mm	291 mm	248 mm	330 mm	M52 x 2	047-595-505
647.100A-01	220 kip	264 kip	850 lb	5.0 in	16.4 in	12.35 in	17.5 in	3-12	053-137-202

Table 2.1 Grip specifications



Figure 2.3 CAD model Hydraulic Wedge Grip MTS 647

The used wedges have the useful saw teeth surfaces. It makes possible the clamping capacity of the specimens' increase during the tests.

The grippers are linked to the slider through the spiral washers as shown in the following figure 2.4.

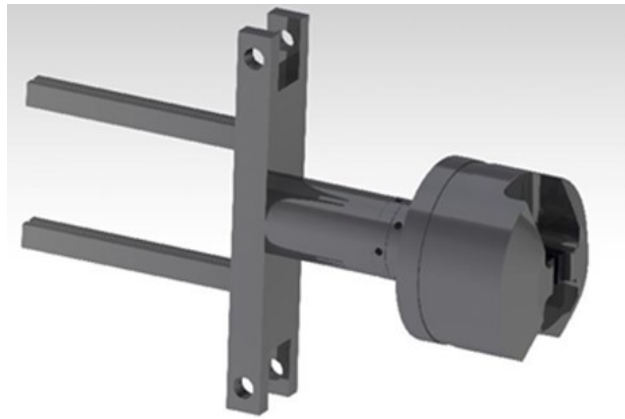


Figure 32.4 CAD model of connection between Hydraulic Wedge Grip MTS 647, spiral washers and relative slider

o Spiral washers (MTS model 601) [2]

These accessories are used to connect the different elements of the thrust to compensate the possible presence of clearance.

If the preload between the elements of the assembly has to be changed the spiral washers can be fixed up.

They are placed on the top of connection pins called connector studs.

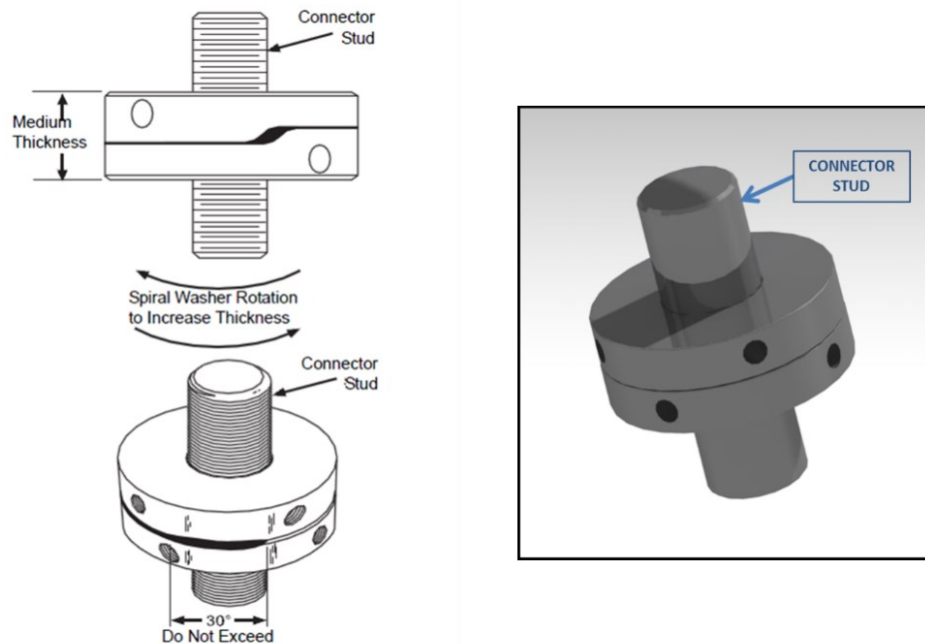


Figure 2.5 CAD model SPIRAL WASHERS model 601

o Sliders

The slider is the element that allows the gripper to be fixed in the right position by the spiral washer through a special threaded central hole.

During the test, these sliders are transported into the box where there are holes.

Along the slider, there are channels that have the function of housing metal spheres, which allow obtaining the rolling friction rather than the sliding friction, with a consequential increase in accuracy and lower friction losses.

At the end, there are some seats where the basic arms will be added to the movement of the equipment through the pins.



Figure 2.6 CAD model of the slider

2.1.2 The frame assembly

The frame assembly is the set of all the components of the machine. These elements are supported so that the deviation of the movement can be carried out into two orthogonal directions, X and Y.

This is illustrated below by according to the CAD representation.

○ Box

It is the real support of the structure on which all the components are constructed. It has the important function to resist the weight of the components, and, the forces that are discharged by kinematics.

It is provided with holes that allow both movement of the slider, and the locking, by the special threaded element related to the monoaxial traction machine chosen to perform the tests.

Made of aluminium, it has the important feature of combining requirements and lightness of the material required.



Figure 2.7 CAD model of box

- Support arms and axles

The support arms are those structural elements used to connect the kinematic support axles to the body. They have minimized rigid strains of hundredths of millimeters.

They are locked to the box with M10 x 1,25 snapped screws.

The axles are constructed by rolling bearings. Thanks to their form they can obtain the rotation required.



Figure 2.8 CAD model of the Support Arm coupled to the Axles

2.1.3 Group for the transmission of motion

This group is the main element of the whole equipment, because it contains the parts that actually allow the transmission of the movement from the input to four hydraulic clamps.

- V-shaped cranks

The cranks are the elements that are constructed on the axles by bearings.

Thanks to their rotation, it is possible to obtain the translation required of the grippers and the success of the test, consequently. Their shape was designed to realize the same displacements to all four sliders. For this reason, there are the seats through which rods will be linked to suitable pins.



Figure 2.9 CAD model of a crank

- Connecting rods

The connection rods are the elements that allow the connection, through special pins, located between the sliders and the cranks.

Their dimensions and shapes have been designed according to their size. They can correct the cruciform and the success of the test.

These dimensions were then verified with the consequential dynamic analysis performed through the Msc_Adams simulation software.



Figure 2.10 CAD model of a connecting rod

The dimensions of these rods and cranks are constructed to get a 25mm stroke for each slide, according to the known formula which regulates the displacements in a centred thrust crank:

$$s = r(1 - \cos \alpha + \frac{L}{r} - \frac{L}{r} \cos \beta)$$

With $r=62\text{mm}$, $\alpha=45^\circ$, $L=141\text{mm}$, $\beta=20^\circ$.

2.2 Multibody analysis: MSC_Adams

Msc_Adams is one of the most widespread multibody analysis software known in the world for the study of body dynamics and movements.

Thanks to this software it is possible to study the dynamics of all parts of the body; and how the loads and the acting forces are distributed in the body through the connecting joints.

Depending on the type of the relative movement that the parts of the body can have, we can understand the best kind of specific connecting joint to choose for the purpose.

The biggest advantage of using such software lies in the possibility of avoiding the traditional "build and head" process.

This type of approach, especially during experimentation, inevitably leads to a waste of time and money.

On the contrary, thanks to the use of a software of this type, starting from the CAD model of assembly it is possible to simulate the movement of the whole mechanism and check if it responds to expectations or not.

These virtual prototypes allow to consider all the aspects of the interaction between the parts, such as frictions or possible interpenetrations.

2.2.1 Model construction in Adams

Once the complete CAD model is generated, it is possible to create the model in Msc_Adams.

The first operation that needs to be done is to correctly set the global parameters of the system and in particular the reference units for the fundamental quantities:

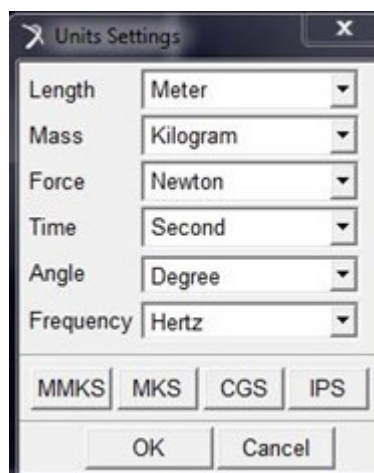


Figure 2.11 Units settings in Adams

The next step is to import to the Adams environment every single part from the CAD assembly, made, for example by CATIA V5, but paying great attention to respect the mutual positions that every single part has within the assembly itself.

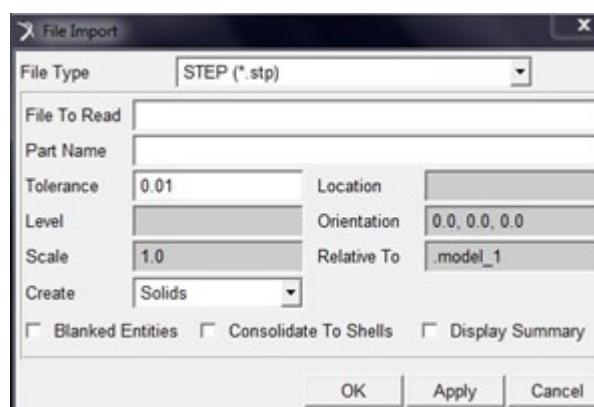


Figure 2.12 File import setting

Among the options to import CAD files, there are all the type of file. In our case, we chose to use a neutral file format, such as STEP, in order to allow the best possible communication between the software reducing the risk of losing information during the translation.

The program in order to correctly import the part requires the user to specify the names of the parts and the orientation they must have according to the coordinated system.

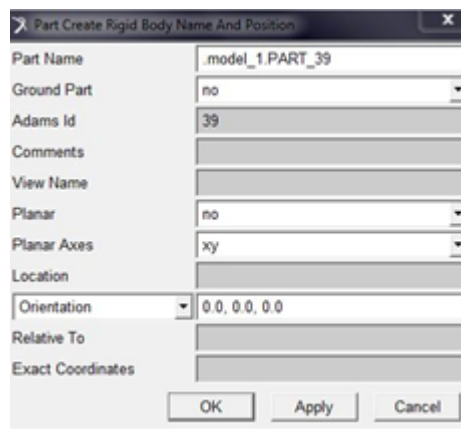


Figure 2.13 Part name setting

In this way, the program proceeds to correctly import the parts in the assembly.

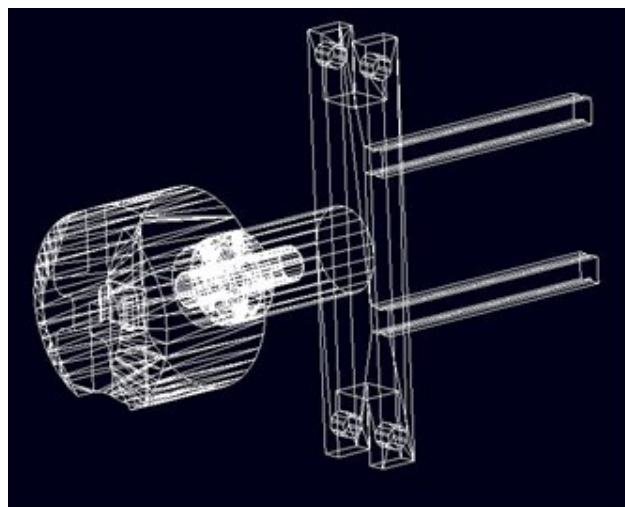


Figure 2.14 Detail of slider with clamp imported into Adams

Once a part has been imported, it is necessary to specify the material of the component.

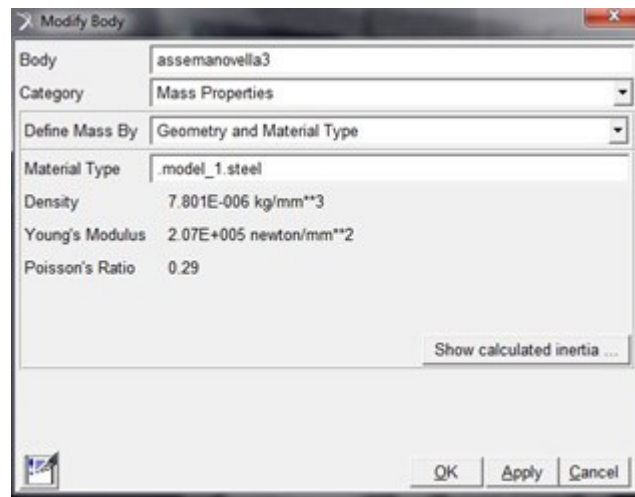


Figure 2.14 Setting of the material characteristics

This operation must be done with all the different components of the assembly. Once the important of all the parts is completed, the model in the Adams environment can be created.

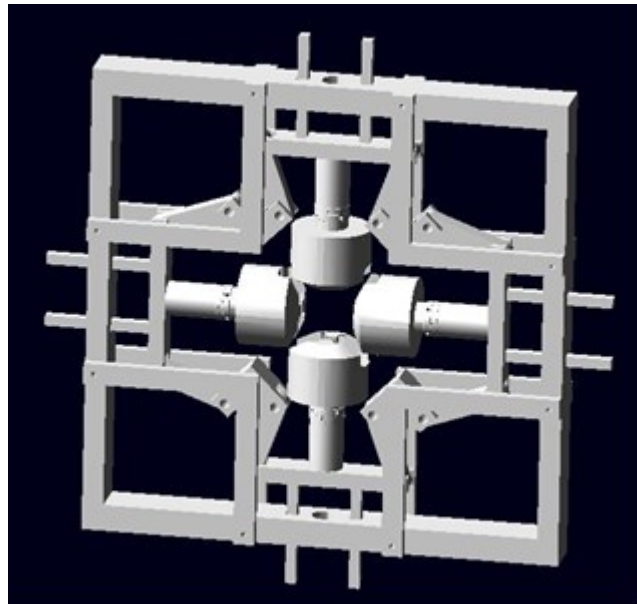


Figure 2.15 Complete model in Adams

After that, it is necessary to connect the several parts of the equipment by assigning the constraints chosen to describe the movement of the mechanism and then calculate the forces applied within the body.

The possible constraints that can be assigned are listed in table 2.1. There, the degrees of freedom, also, will be subtracted from the single specified part.

	Translation along x	Translation along y	Translation along z	Rotation about x	Rotation about y	Rotation about z	TOTAL
FIXED	✓	✓	✓	✓	✓	✓	6
REVOLUTE	✓	✓	✓	✓	✓		5
TRANSLATIONAL	✓	✓		✓	✓	✓	5
CYLINDRICAL	✓	✓		✓	✓		4
UNIVERSAL/HOOKE	✓	✓	✓			✓	4
SPHERICAL	✓	✓	✓				3
PLANAR			✓	✓	✓		3

Table 2.2 Possible constraints

Each part is treated as a rigid body, provided with 6 degrees of freedom.

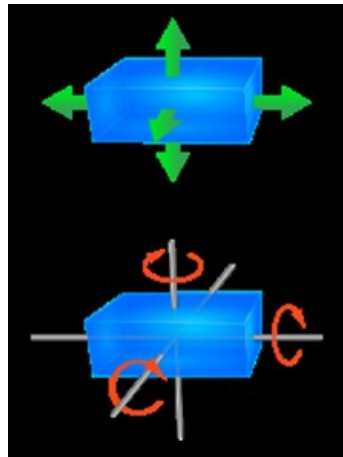


Figure 2.1336 Degrees of freedom

As said, the constraints must be assigned considering the real movement of the part within the mechanism and in compliance with the Gruebler formula that provides the number of degrees of freedom of a mechanism placed in the plane.

This formula can be expressed as follows:

$$gdl = 3(m - 1) - 2C_1 - C_2$$

Where :

- 3 is the maximum number of degrees of freedom that the mechanism has in the plane: two translations and one rotation.
- m: number of members into the mechanism.
- C₁: number of elementary kinematic pairs of the mechanism.
- C₂: number of II degree upper kinematic pairs.

The constraints assigned to the components are therefore fundamental for the

analysis related to the program to get positive results. In the first instance, the "FIXED" constraint has been given to the box, based on the assumption that the Box is a load-bearing element of the structure and will be the element that will be constructed on the traction machine. The "FIXED" assigned constraint requires the specific bodies according to this type of constraint. It has to be valid.

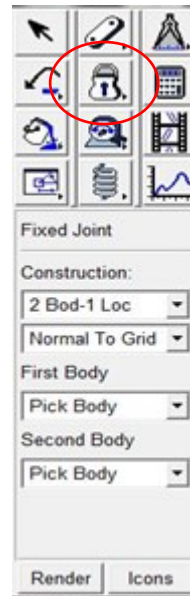


Figure 2.17 "Fixed" constraint assignment

Consequently, the same type of constraint is linked to the support arms and the axles stationary during this movement.

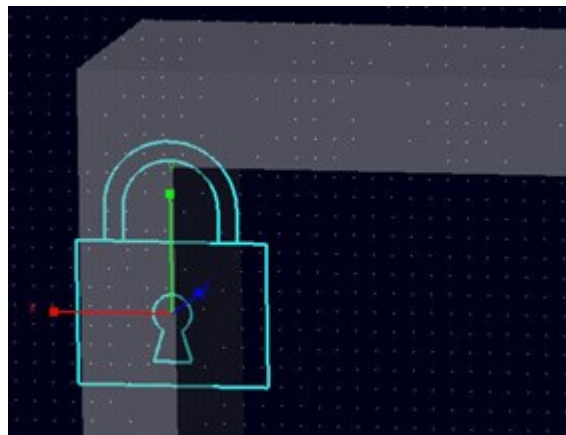


Figure 2.18 Assignment of fixed constraint to the box

In the case of the box, the constraint is referred to the "Ground". In the case of the support arms, this type of constraint is referred to the box; while in the case of the axles it is referred to the support arms.

The cranks have been given the "REVOLUTE" constraint with the same

principle before expressed.

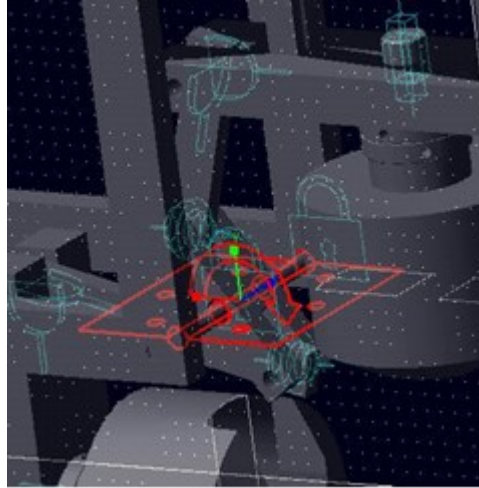


Figure 2.19 Revolute constraint between crank and axle

This type of constraint was given between the cranks and the axles. This constraint was considered the most suitable to rotate around its z-axis. Once the degrees of freedom guaranteed for the crank have been defined, it is necessary to give a constraint that allows the connecting rods to rotate around the axis of the pins that links them to the cranks. But at the same time there is the transitory movement of the slider. Because of this, a "SPHERICAL" constraint was chosen.

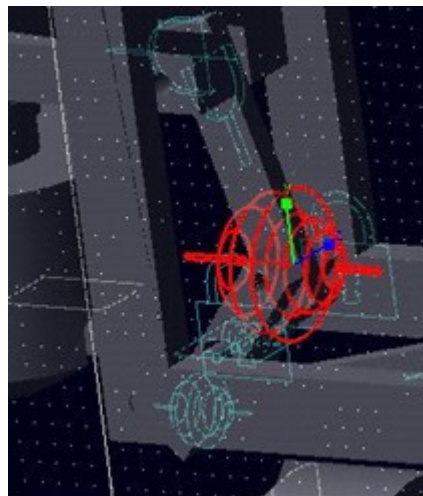


Figure 2.20 Spherical constraint between cranks and connecting rods

The constraints that are in Adams, in addition to the effective movement that

the parts will have inside the mechanism, it does not have to be redundancy with those already assigned.

Considering what it has just been said, a "HOOKE" constraint has been added between the connecting rods and the sliders.

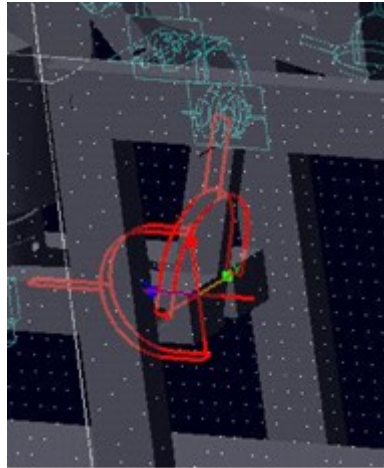


Figure 2.21 Hooke constraint

In the final analysis, "TRANSLATIONAL" type constraints were linked to 3 of the 4 sliders, while the last of these was related to a "CYLINDRICAL" constraint.

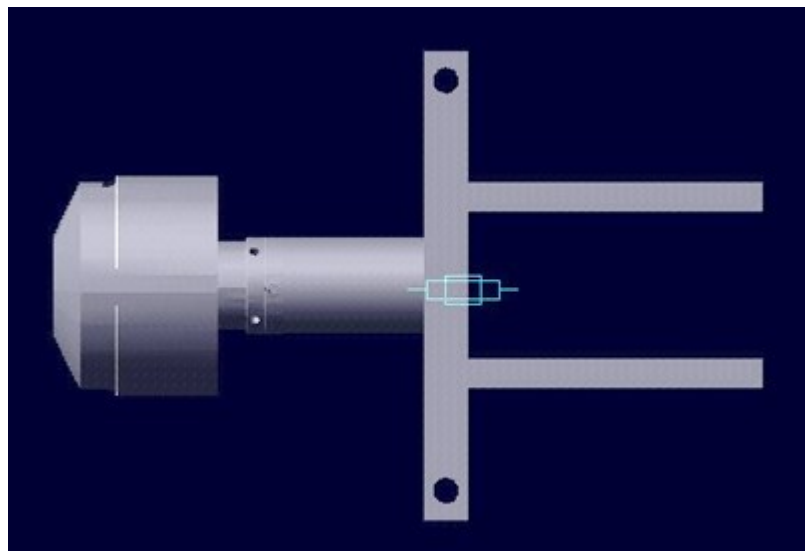


Figure 2.22 Translational constraint between slider and box

Compared to the "Translational" constraint which allows only the movement of translation between two bodies along an appropriately predetermined direction; the "Cylindrical" constraint allows, in addition to the before mentioned translation, also a rotation around a predetermined axis.

This type of choice was made because, in the mechanism to be studied, it is also necessary to give a "MOVEMENT CONSTRAINT".

This "movement constraint" will also be able to "eliminate" this further degree of freedom that we have left free and to avoid that there are redundancies or movements in the model that do not occur, really.

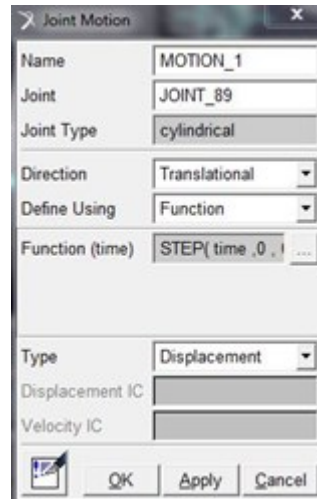


Figure 2.23 Motion constraint assignment

In order to correctly simulate the movement that is thought to be occurred during a traction test of this type, a "STEP" type has been set, whose parameters of interest are the time and the displacement of the sliders.

The time has been chosen in four seconds and the slat displacement in 25 mm.

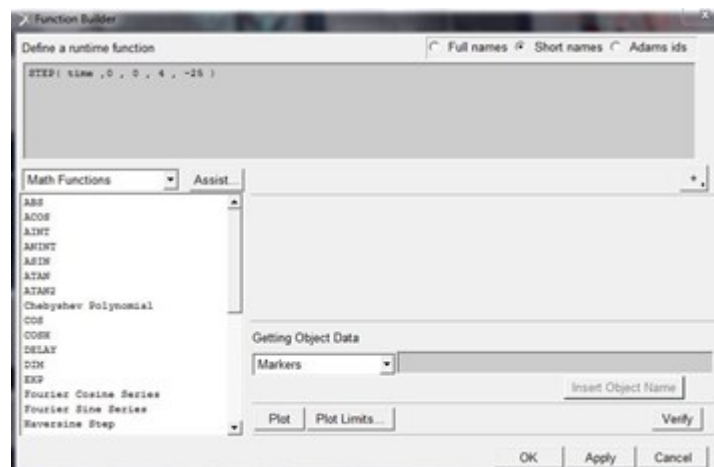


Figure 2.24 Motion constraint assignment of parameters

During the test, it is important to be able to simulate also the limits that the equipment must get through during the progress of this test.

Therefore, it is important to consider at the ends of the four clamps, the force that opposes the movement, same as the previous defined, or higher than 10000 N, in the equipment specifications.

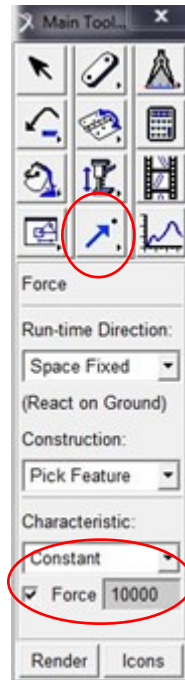


Figure 2.25 Force assignment

Before the simulation test, it is necessary to check if the model has been correctly created and if the software identifies degrees of redundancy or anomalies that prevent the success of the test.

```
VERIFY MODEL: .model_1

  0 Gruebler Count (approximate degrees of freedom)
 29 Moving Parts (not including ground)
  1 Cylindrical Joints
  4 Revolute Joints
  8 Spherical Joints
  3 Translational Joints
 13 Fixed Joints
  8 Hooke Joints
  1 Motions

There are no redundant constraint equations.

Model verified successfully
```

Figure 2.26 Model check

The check of the model shows how the model has been successfully created and how the feedback has been provided on the presence of redundant constraints. Gruebler's formula results in a 0 output. This was desirable in the same way as the "Movement constraint" is counted as a degree of freedom.

To start the analysis, it is necessary to set the timer of the simulation and the number of integrated steps.



Figure 2.27 Time and step integration parameters

Practical experience suggests that reliable results can be obtained when the ratio between the duration of the simulation and the number of integration steps. So, this result is 1:100

2.2.2 Simulation results

The results of the simulation were important for the consequential structural check with the FEM Patran / Nastran analysis software. Thanks to the simulation it was possible to evaluate the actual displacement of each slider; the pliers that tighten the specimen, and in addition to this, it was possible to evaluate the forces that the elements of the equipment exchange with each other by the connecting pins.

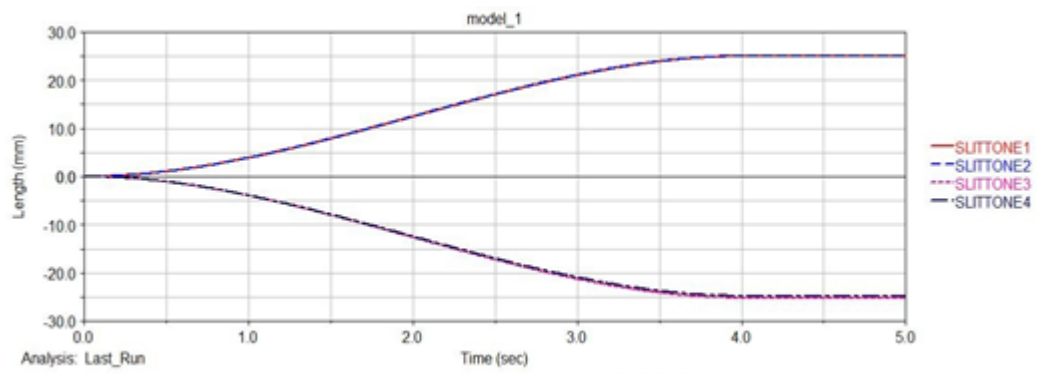


Figure 2.28 Displacement law of sliders

This result highlighted that all the traverses have the same magnitude of displacement and this is very important. It means that the test is carried out in the right way, and, during the test the centre of the cruciform is locked.

The following image (fig. 2.29) allows evaluating the forces that the cranks transfer to the machine axles by bearings.

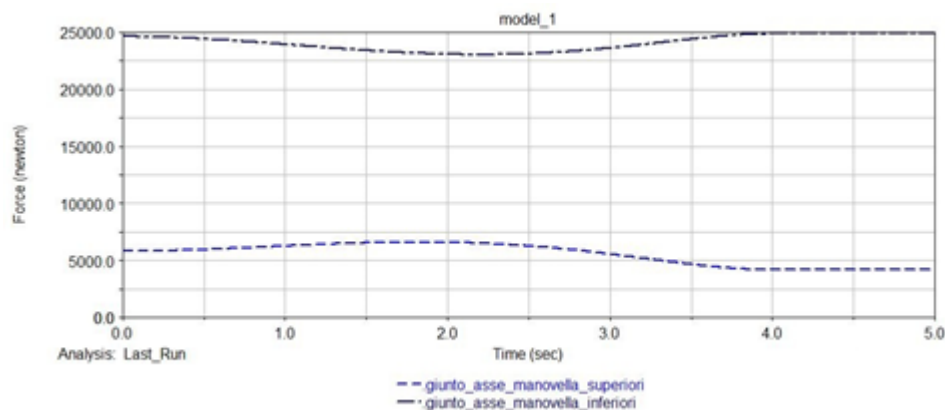


Figure 2.29 Forces between cranks and axles

In particular, it is possible to highlight the double symmetry that exists in the movements of the forces that can be explained by the fact that there are not four "Translational" constraints into the "Movement constraint".

Through the consequential check with the FEM software, we can see that the largest forces will be transmitted to the module.

From the same principle, it is also possible to evaluate the forces exchanged between the crank and the connecting rods linked to it (fig. 2.30).

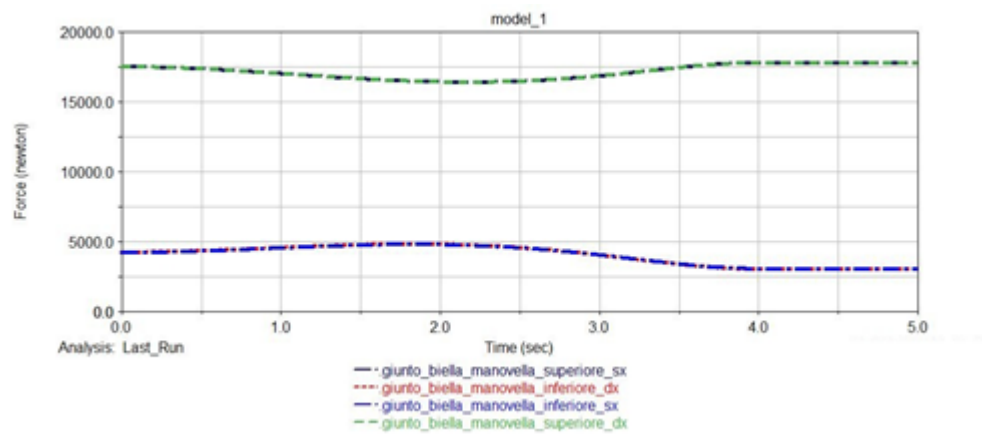


Figure 2.30 Forces between cranks and connecting rods

These forces are also very important for the choice that has been made for the most suitable rolling bearings. In this way, the forces are downloaded during the movement.

As soon as the bodies are rigid, the forces are transmitted through the body to the sliders connected to them by the pins.

Based on the same principle, the forces previously seen between the cranks and the axles are transferred to the support arms.

These forces will be divided equally between the two arms that support the single axles and so the same forces will be discharged on the body.

2.2.3. Choice of the bearings

The results obtained through the simulation carried out with the Msc_Adams Software it has been possible to identify and select the most suitable bearings for the equipment.

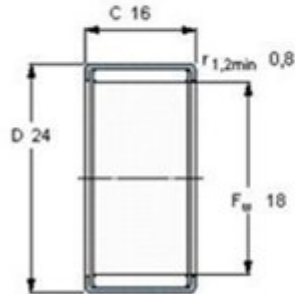
The choice of a bearing depends on the type of application for which the equipment is used, but at the same time a series of further parameters must be considered according to:

- Free space
- Project loads
- System stiffness
- Accuracy

The characteristics listed above are fundamental for the equipment which has to be able to perform biaxial traction tests.

One of the characteristics required to our equipment is the compactness and the smallest bulk. Because of this, it was considered suitable to choose the type of radial bearing with little rolls and without inner ring, in particular, we know that the initials of the Skf bearing are HN1816 [4].

Dimensioni d'ingombro			Coeff. di carico dinamico statico		Carico limite di fatica	Velocità di base	Velocità di riferimento	Massa	Appellativo
F_w	D	C	C	C_0	P_u				
mm			kN		kN	giri/min		kg	-
18	24	16	16,1	33,5	3,8	14000	11000	0,020	HN 1816

**Accessori adatti**

Anello interno IR
 anello interno LR
 Tenuta G
 Guarnizione SD

IR 15x18x16.5
 LR 15x18x16.5
 G 18x24x3
 SD 18x24x3

Figure 2.31 Bearing data sheet

Their small footprint makes it possible to withstand the loads that have been evaluated in the Adams Software and which stimulate the junctions of the different parts of the equipment.

The magnitude of the load is one of the factors that usually determine the size of the bearing to be used. Generally, roll bearings are able to withstand substantial loads and the size that increases with the diameter of the shaft. The loads are considered really radial.

For this reason, especially in the case of equipment, for testing machines, the main issue of everything is the misalignment between the shaft and the bearing housing.

This misalignment is due, for example, to the deflection of the shaft due to the load or to incorrect machining of the bearing seats. This misalignment is to be avoided or made with modesty.

The precision required to the bearing, in this particular type of application, and its stiffness are both key factors. The type of bearing chosen ensures high rotation accuracy and low friction

In order to guarantee the correct axial locking and in particular to put the bearing in the condition to stop and to work correctly, the use of internal Seeger stop rings have been foreseen.

For the type of use expected for this type of equipment, the criterion used for choosing the type and size of the bearing is the load capacity rather than duration. This type of approach is possible according to the following conditions :

- the loads are an example of an intermittent type, they can be considered not applied continuously over the time.
- the bearing rotates under load at a very low speed ($n < 10$ rpm)

When it is found, as in the case discussed here, in one of these conditions, the admissible load is not determined by the work of the material as much as by the number of permanent strains on the races caused by the load. Loads acting on a stationary bearing, produce facets on the rolling elements and imprints on the races. If the magnitude of such strains is considerable, they can lead to vibrations, noise, greater friction and loss of the precision. These characteristics chosen are guaranteed. The parameter of interest, in this case, is the static load factor. The static load factor is evaluated starting from a static safety factor and the equivalent static load.

The equivalent static load can be evaluated by the general formula:

$$P_0 = X_o F_r + Y_o F_a$$

Here, the effects of radial and axial loads acting on the bearing are weighed.

In this case $P_0 = 30000$ N

These values can be found in the literature, at a room temperature conditions. A safety factor of 1 has been chosen for the static safety factor. For the most applications operating under normal conditions, grease lubrication is certainly the best. Compared to an oil lubrication, grease does not have problems to go away from the system and at the same time helps to protect from moisture.

These lubricating greases consist of mineral oils combined with thickeners, and have a fundamental variable from 1 to 3 according to the NLGI scale, in the case of rolling bearings. For applications like this, it seemed advisable to use a grease normal solidity, that has the value of two.

2.3 Creation of the model for finite element analysis

It has been chosen to perform Pre-Processing and Post-Processing with one of the most common software on the market, called Msc_Patran; while for the Processing phase the software of the same manufacturer was chosen Msc_Nastrum. This software can easily compared with the MSC Adams software that was introduced into the dynamic study of the system. In particular, they allow performing the dynamic simulation of the whole mechanism by introducing the deformability of some components, and correct the law of movement provided by the rigid-body analysis with the implementation of the strains generated into those components.

This type of analysis is of particular interest because it allows a more realistic view of the behaviour of the equipment when working.

The first step is to create a geometric model that is as much representative as possible of the object to be analyzed. When the program is started, it is necessary to set the type of analysis to be carried out, the code chosen for the analysis, the approximate dimensions of the component or of the assembly that will be modelled. In this case, it was decided to carry out a structural analysis with the MD Nastran code. The dimensions are variable and depending on the type of component.

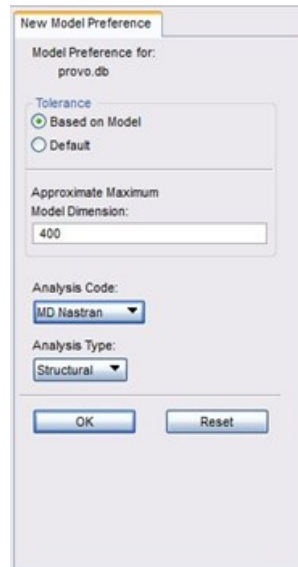


Figure 2.32 New model assignment

The geometry of each component can be created in the Patran environment or imported into a neutral file format such as the Step file from a CAD software. The Patran environment offers many types of geometries (based on points, curves, surfaces, solids) thanks to these combinations it is also possible to create models of high complexity. Here it was decided to import a suitable flat geometry modified in Step format by the CATIA V5 software. This choice was essentially dictated by the need to be able to exercise higher control during discretization of the structural dominance in the most stressed areas in which the mesh would have had to be denser. Also, in this case, it is very important to keep consistence between the units of measures used in the CAD modelling phase and those of the model in Patran.

When we talk about suitable modified geometry plane, we mean a geometry made up of a set of lines connected to each other, also internally, which will be used in the Patran environment to create Surfaces. For the creation of these surfaces, the Patran software offers several tools; in this case, the "Edge" method was used to create a surface by choosing the lines that delimit it. Repeating the operation for each trait of interest we obtain the outcome as in figure 2.33.

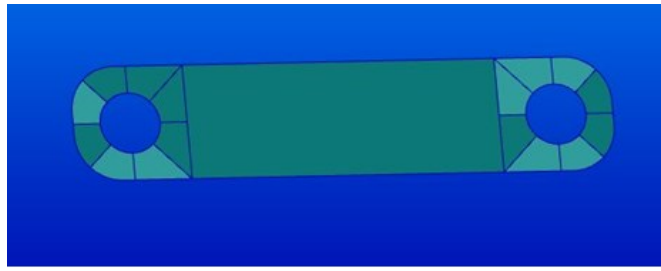


Figure 2.33 Surfaces for the creation of connecting rod model

Then, we move on to creating the Mesh. To create a Mesh that is thick at the points of greatest interest, it is necessary to use the so-called “Mesh Seed”, which represents the "guide points" to which the program refers when the mesh will be created afterwards.

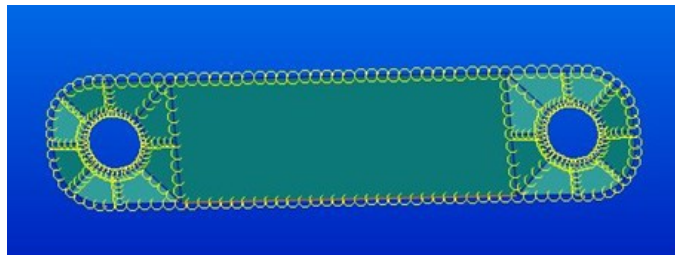


Figure 2.34 Mesh of connecting rod

The “Mesh seed” should be chosen in a way to have the same ratio of the length in several parts of the element. In this way, the elements are not excessively deformed. The next step is to realize the Mesh.

To do this, the program provides a special menu within which you can choose the type of algorithm to be used and the type of elements that best suits the analysis. In this case, the Isomesh algorithm and the Quad4 elements have been chosen. Once the plane Mesh has been created, it has been put inside a perpendicular direction through the reference plane, from which the solid Hexa8 elements [5] Mesh is obtained.

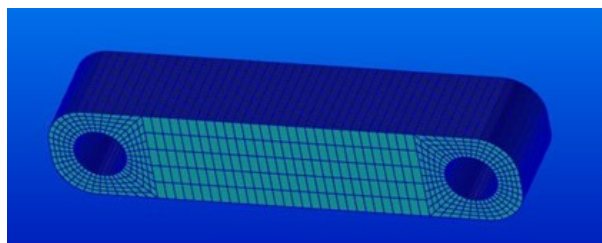


Figure 2.35 Complete mesh of the connecting rod

Following the elimination of the flat elements, the model is composed of 32400 solid elements. Once the discretization of the structural domain has been completed it is necessary to set the boundary conditions : external loads and constraints.

The values of the loads, through which the individual parts of the equipment will be

checked, are those outgoing from the dynamic analysis directed to Adams.

A very useful technique to simulate the pressure of the indoor connecting pins, of the connecting rods and other components of the equipment is to use the Multipoint Constraint (MPCs). The Multipoint Constraint is a constraint condition that relates the degrees of freedom of one or more nodes, called “independent”, to the degrees of freedom of the nodes called “dependent”. In this case, was chosen RBE2. The RBE2 are characterized by having 1 independent node and several dependent nodes that are constrained to move in the same way than independent nodes.

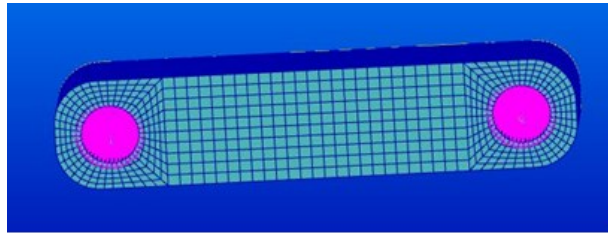


Figure 2.36 RBE2 constraints

In particular, as an independent node, a dummy node has been created in the centre of the hole, where the pin will be positioned and all those nodes in contact with the plug itself will be selected. Once these RBE2 have been created for both the connecting rod holes, previously, assessed loads can be applied. These forces will be applied to the independent nodes of the Constraint Multipoint which will coincide with the central node located on the pin axis.

In order to simulate the behaviour of the element, it is necessary to constrain the component in the space. For this component, a joint and a support constraint were assigned to the independent nodes used for the Multipoint Constraint. In this way, the component is allowed to be constrained and at the same time be able to simulate its movement inside the equipment.

The last operation to carry is that of assigning the material; in the case tape there is a construction steel like the 39NiCrMo3, with the properties shown in table 2.2.

Caratteristiche meccaniche / Mechanical properties					
Stato Condition	Saggio Ø mm. Specimen Ø mm.	Re min. N/mm ²	Rm N/mm ²	A min. %	KCU min. J
	16	785	980+1180	11	30
Bonificato	> 16	735	930+1130	11	30
Hardened and tempered	> 40	685	880+1080	12	30
	> 100	635	830+980	12	30
	> 160 ≤ 250	540	740+880	13	30

Table 2.3 Mechanical properties of 39NiCrMo3

The choice on this type of steel has good workability and excellent mechanical characteristics. The program needs to have Young's module, the Poisson module and

the density. These characteristics of the material are shown in figure 2.37.

Property Name	Value
Elastic Modulus =	210000.
Poisson Ratio =	0.30000001
Shear Modulus =	
Density =	7.8599996E-008
Thermal Expan. Coeff =	
Structural Damping Coeff =	
Reference Temperature =	

Figure 2.37 *Material parameters*

Repeating the procedure described above for each component of the equipment, the following numerical models have been obtained.

In the case of the slider, the model was created by inserting a further Multipoint Constraint with a 50 N force to simulate the weight of the hydraulic clamp and a joint along the sliding tracks inside the box (fig.2.38).

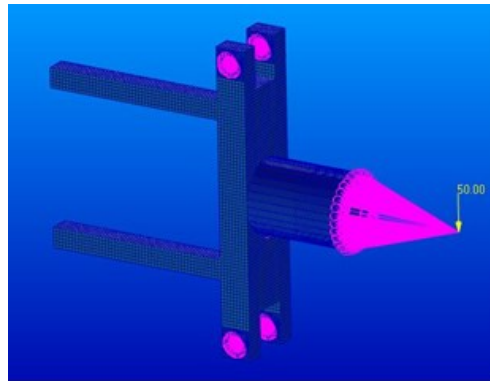


Figure 2.38 *Slider fem model*

For the support structures, two joints were fixed at the ends where the connection to the box is envisaged and the force is applied to the Multipoint Constraint to simulate the connection with the axis.

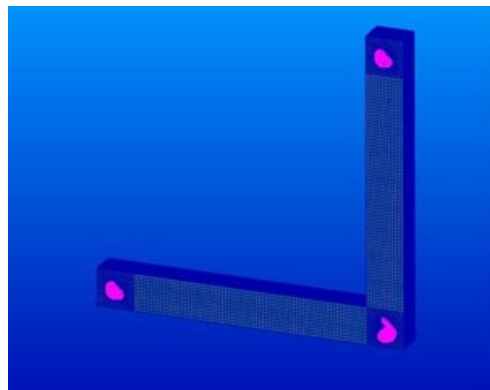


Figure 2.39 *Support structure fem model*

For the V-shaped crank, the only constraint is that of interlocking the central hole

where the bearing will be housed while the loads that have been applied to the centre of the holes along the crank arms.

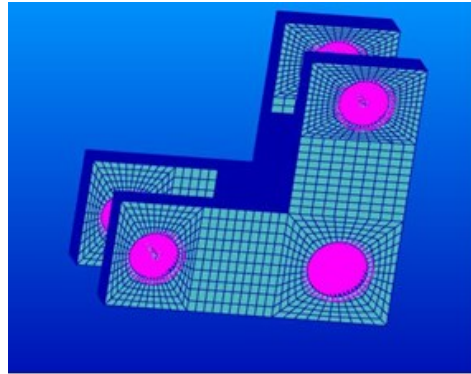


Figure 2.40 V-shaped crank fem model

In the case of the box, a joint constraint is placed in the lower part where it will be integrated with the lower crosspiece of the testing machine; while the load is applied with the methods previously illustrated.

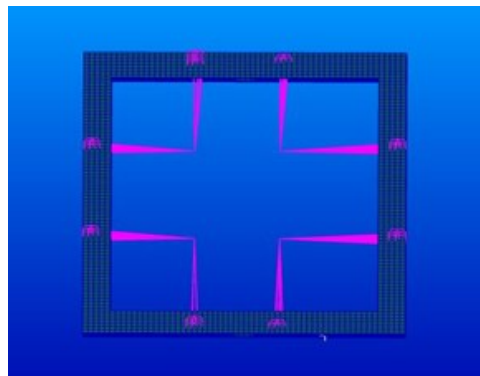


Figure 2.41 Box fem model

2.3.1. Linear static analysis

The type of analysis envisaged for the components is the Linear Static which in Nastran is named "Sol 101".

The parameters considered are the strain deriving from the applied loads axes, evaluated according to the Von Mises criterion.

In the case of the connecting rod, the strains and the stresses are within the parameters that can be considered a limit (see fig. 2.42 and 2.43).

In particular, it has been verified that in each component the maximum strains are always less than one-tenth of a millimetre and the maximum stresses are at the yield limit of the chosen material. The results have been reported using a 0.3 scale of factors for graphic reasons. So that strains and stresses can be appreciated.

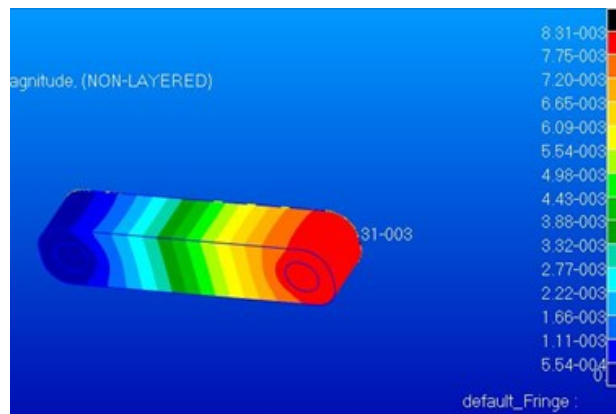


Figure 2.42 Connecting rod strains

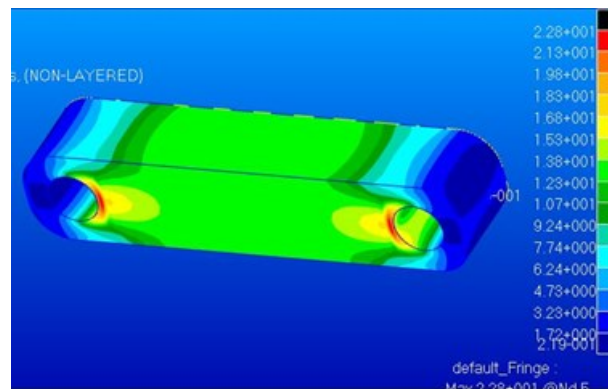


Figure 2.43 Connecting rod stresses

Figures 2.44 and 2.45 show the results related to the crank analysis. It is one of the components of great interest because its rotation allows the effective deviation of the input movement of the system.

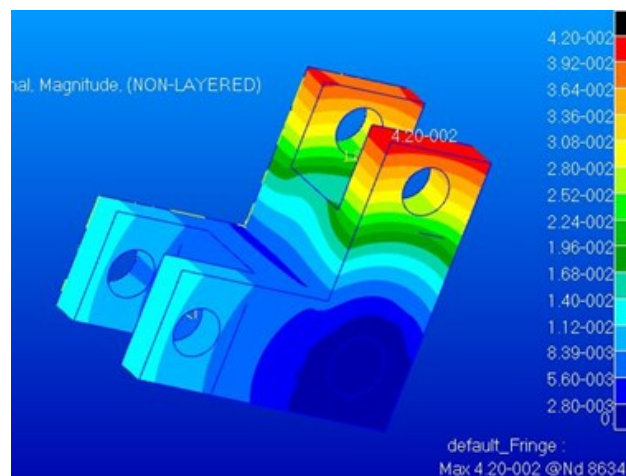


Figure 2.44 Crank strains

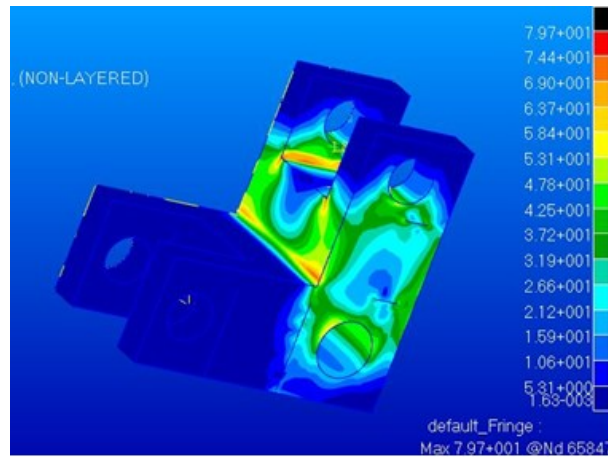


Figure 2.45 Crank stresses

The results of the analysis on the sliders and the support arms are shown below:

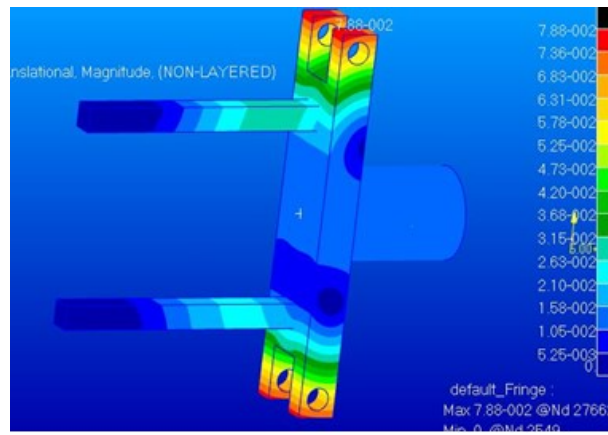


Figure 2.46 Slider strains

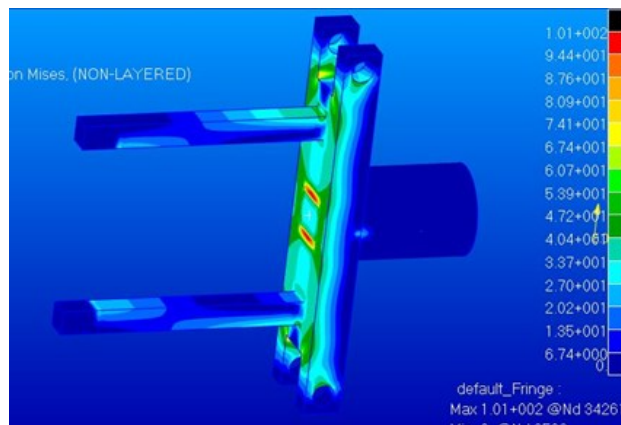


Figure 2.47 Slider stresses

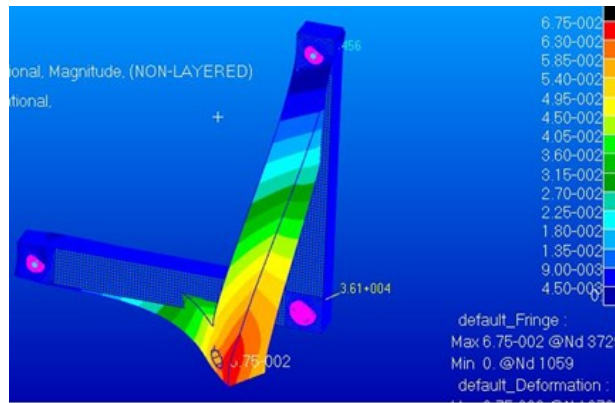


Figure 2.48 Support arm strains

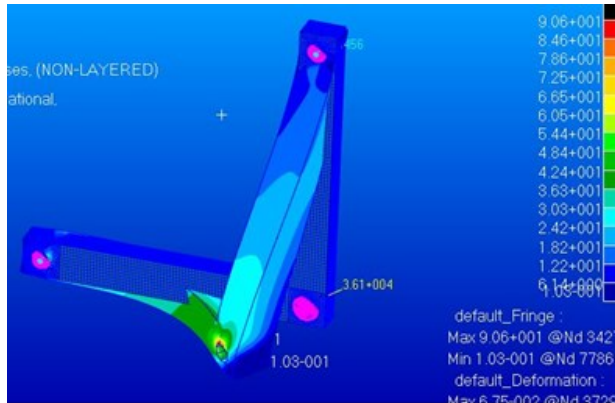


Figure 2.49 Support arm stresses

Another component of great interest is the axle on which the cranks rest on the bearings. In this case, the force that is exchanged has been represented not as a punctual load, but as "Total Load". A load that is distributed along the contact surface and it has been chosen to reproduce the action of the bearing.

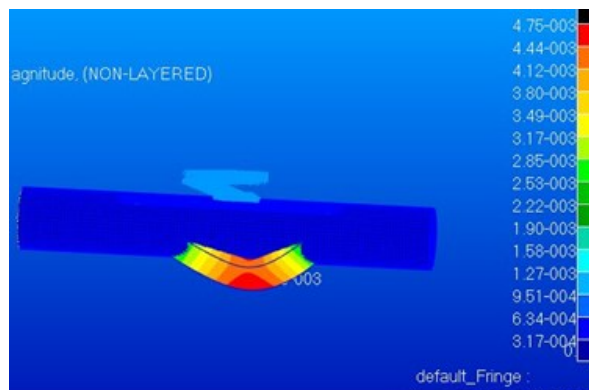


Figure 2.50 Axle strains

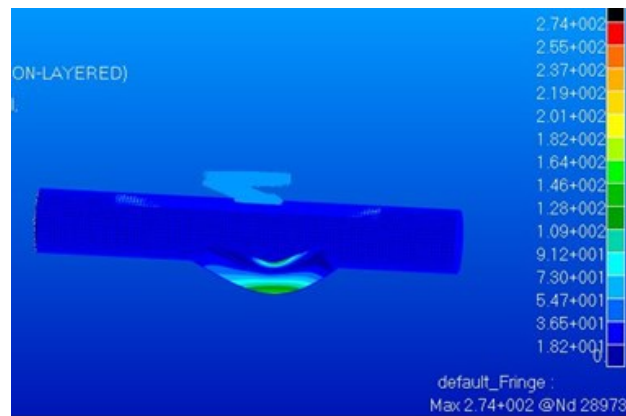


Figure 2.51 Axle stresses

In the case of the box, the first analysis with a 50 mm thickness has highlighted the strains. So, for this type of equipment it cannot be considered tolerable. Because of this it was decided to make increase the thickness of the component about 80 mm. According to the reported strain values analysis done again in the order of hundredths of a millimetre, the situation was acceptable, finally.

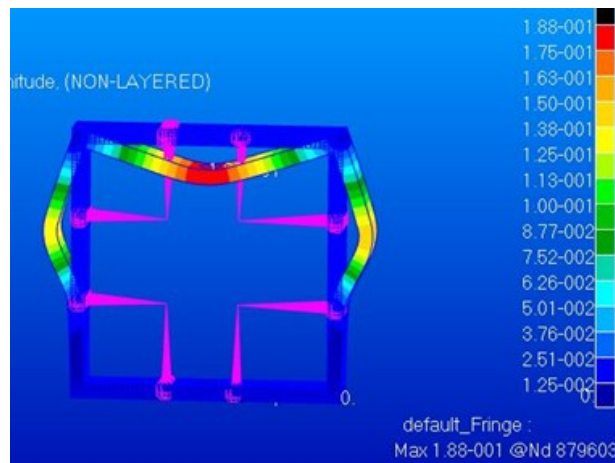


Figure 2.52 Box strains in case of thickness 50 mm

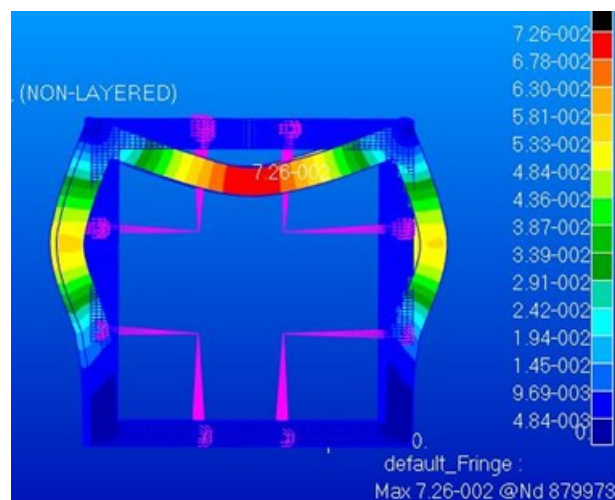


Figure 2.53 Box strains in case of thickness 80 mm

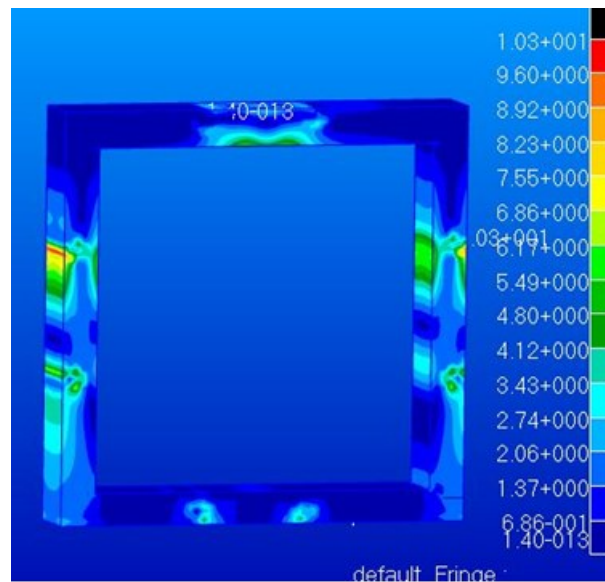


Figure 2.54 Box stresses in case of thickness 80 mm

As in the previous cases, the results of the analysis are comforting due to the correct size of each component.

This type of approach, based on the use of the Multipoint Constraint, has, within, a limit that must be mentioned. With this type of instrument, a rigid displacement of all dependent nodes is added to the independent one.

In fact, this hole does not rigidly follow the pin. The contact is only along a circumferential arc. Along which the exchanged action is distributed through a non-linear trend. It is deduced that during the contact the hole does not move deformed but tends to be oval. This load condition can be precautionary considered in relation to the estimate of the displacements, which represent the most important aspect because of rigidity. On the other hand, a greater degree of approximation is instead permitted thanks to the computation of the stresses that act. These virtues of the strength of the acting elements, are widely contained within the yield strength limits of the material.

2.3.2 Flex analysis in Adams/Nastran environment

The hypothesis on which the previous analysis was based was that of the perfect rigidity of the components under examination. But, a hypothesis of this type can only be considered true in part: the element of the equipment can be deformed by virtue of the material whose it is made and by amount of load to which it is subject during the movement. This eventuality can be appropriately evaluated by importing the results of the deformation analysis (Patran / Nastran) in Adams. This type of analysis is therefore required when the flexibility of the bodies can influence the kinematics of the mechanism we are talking about or when the precision required is particularly high. The logic

followed in this type of procedure is provided for the reintroduction within the Adams environment, and in particular, in the model. It was previously created with Nastran. Its name is the "MNF" file (Modal Neutral File).

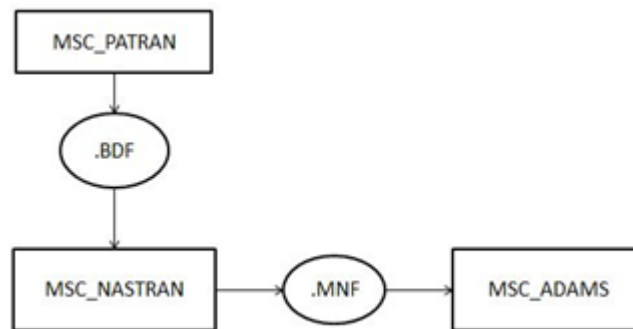


Figure 2.55 Rationale behind the deformability analysis

This type of file is the key element to put in the two software in communication and is the result of an appropriate modal analysis that is prepared in Patran and performed in Nastran SOL 103. With this type of analysis, it is, therefore, possible to evaluate the actual deformation of the several components, all inserted within the frame considered rigid. In this way, we can evaluate the error that could be made in the measurement of the strain of a sample with the test. The first step is to create a bdf file containing the information that the solver needs to perform the modal analysis. To do this you can take advantage from the models previously created for static analysis with SOL 101. However, they will be modified according to this new solution. First, the so-called DOFs must be created, that is, the degrees of freedom that are assigned to the dependent nodes of each MPC created. This is an algorithm implemented in the current versions of Patran that allows reducing the number of vibrating modes to reproduce the model of the movements of the flexible body. These elements not only have the function of creating the connection nodes of the flexible element with the rigid bodies of the whole system, but they constitute the essential element for generating the constrained vibrating means according to the Grag-Bamptons method.

The analysis requires to set a modal analysis (solution number 103). Before doing the analysis it is necessary to set correctly the parameters which will then allow the communication between the two programs. This can be done within the "Solution Parameters" submenu by entering the appropriate section called "Adams Preparation" in which the units of measurement must be aligned to that done in Adams. The program is asked to generate the output file. MNF.

By carrying out these simple operations, it is possible to correctly launch a modal analysis that will generate a file containing the discretized model with the relative vibrating modes.

After opening the program and loading the model previously created in the Adams environment, you can replace the rigid component with a flexible one within the model.

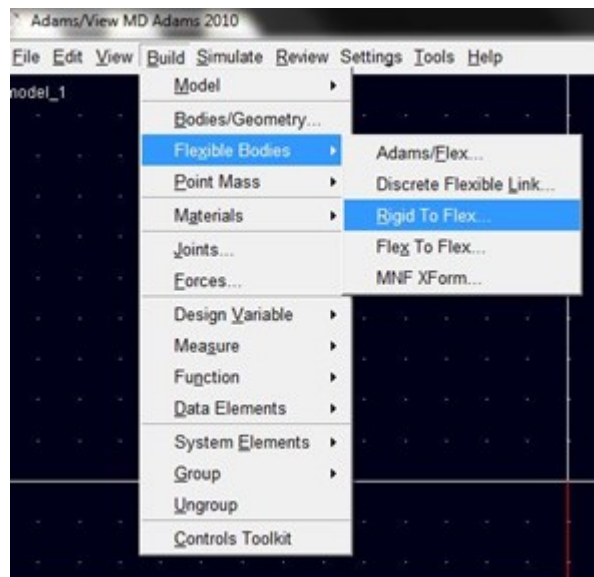


Figure 2.56 Importation of a flex component in Adams

The new flexible part, imported into the environment Adams, provides its own menu which can be directed into different ways of vibrating, and if necessary, allows you to eliminate elements that cannot compete with the strain.

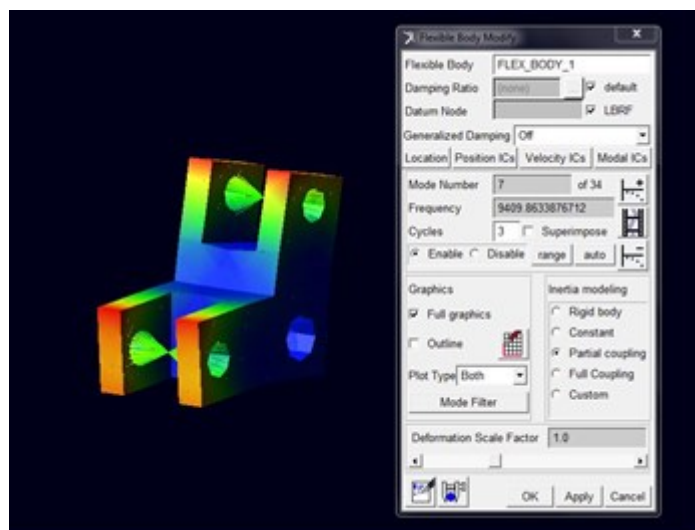


Figure 2.57 Setting of flex component properties

The flexible body, once introduced into the system, inherits not only the position but also the constraints assigned to the corresponding rigid bodies. The components that have been considered deformable inside the equipment are:

- Connecting rods
- Sliders
- Support arms
- V-shaped cranks
- Axles

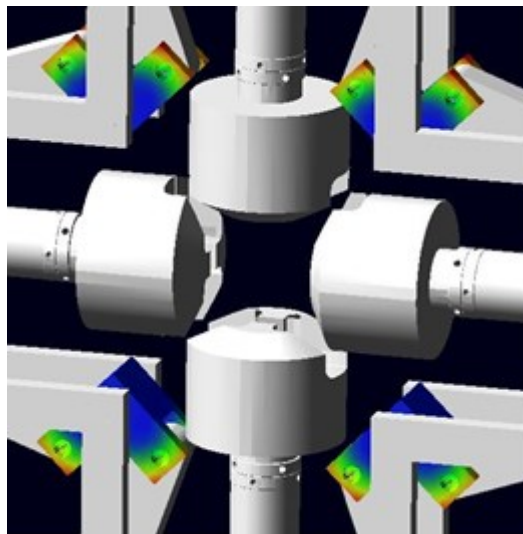


Figure 2.58 Detail of flexible cranks

This procedure can be repeated for all the components present in the equipment to evaluate the impact on the displacement of the hydraulic clamps of the deformation of the components.

Once all the deformable components have been inserted inside the equipment, it is possible to do the analysis and evaluate how the deformation of the bodies has influenced the displacement of the hydraulic clamps.

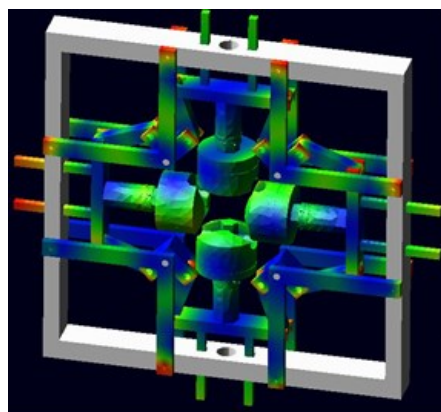


Figure 2.59 Equipment with all flexible components during the analysis

In order to evaluate the actual displacement of each hydraulic clamp, it was necessary to insert within the model of the appropriate "Markers", one integrated with the hydraulic clamp and one integrated with the Ground, positioned at the same point at the moment. In this way, it is possible to evaluate how, during the simulation, the integrated mark with the slider moves away from that integrated with the Ground. Therefore, the actual displacement of the hydraulic clamp, is integrated with the slider, now. The results obtained from the analysis can be evaluated in Fig 5.43 and clearly show how the deformation of the bodies has had an influence on the displacement of the hydraulic clamps integrated with the slider.

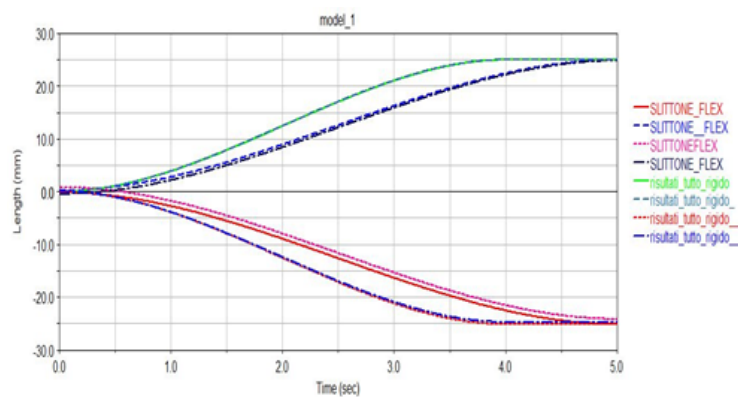


Figure 2.60 Comparison of the law of motions in both cases: rigid and flexible components

These results, also, show how the law of the displacements of the hydraulic clamps is changed over the time, as in the case of the completely rigid equipment. In a steady state, the maximum imposed about the 25 mm displacement has reached the average error. Evaluating it on the 4 hydraulic clamps, the result is 0.0363 mm.

	Rigid case max stroke [mm]	Flex case max stroke [mm]	Difference
Slider 1	25	24,976	0,024
Slider 2	-25	-25,014	0,014
Slider 3	25	24,9578	0,0422
Slider 4	-25	-25,065	0,065
Average			0,0363

Table 2.3 Comparison between rigid and flex analysis results

This means that, according to the ideal case, the position of the centre of the specimen will have the maximum value of 0.0363 mm and it is an acceptable value. So, the test was successful.

References

[1] “647 Side-Loading Hydraulic Wedge Grips” Product information, MTS System Corporation.

[2] “601.11 Spiral Washers” Product information, MTS System Corporation.

[3] MSC Adams user manual 2012.1.1

[4] SKF rolling bearings catalogue

[5] MSC Patran user manual

Chapter 3

Study of specimen shape for biaxial tests on composite and polymer materials

3.1 Optimization of shape for composite materials

One of the aims of this work was to achieve an improvement in the shape of the specimen in order to more clearly define the region subjected to a biaxial load, as that is the type of load to which many aeronautical structures are subject.

The optimization of this shape was made with the help of fem simulations.

In the first simulations, carried out in Ansys, it was considered a material consisting of an epoxy resin matrix and carbon fibers and was considered a stacking sequence shown in figure 3.1 (-45 °, + 45 °, + 45 °, -45 °).

The thickness used for the specimen is 0.6 mm.

About the boundary conditions, having to generate a type of biaxial load, a modeling was carried out in which two sides are loaded with a force of 500 N (this value is the applicable limit in the following experiments).

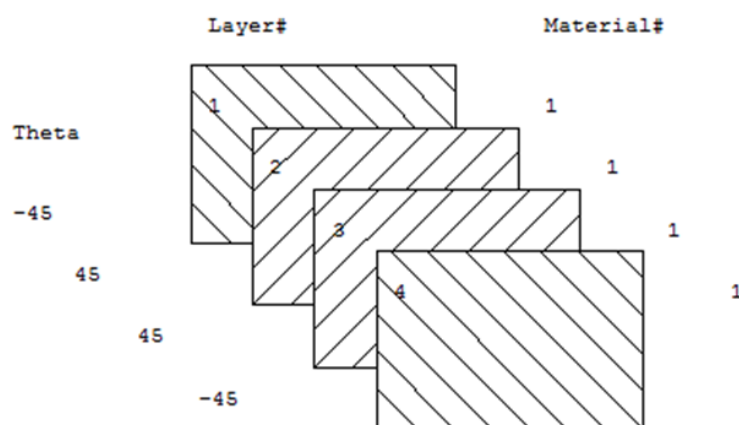


Figure 3.1 Stacking sequence

Many geometries have been investigated: in figure 3.2 only three are reported for brevity.

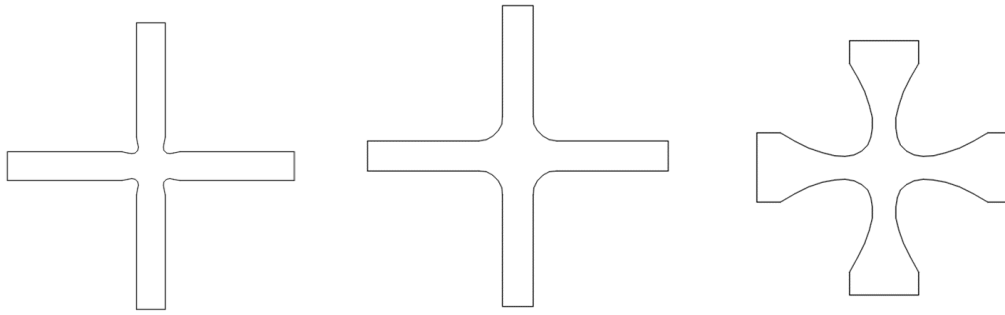


Figure 3.2 Investigated shapes

The first and the second shapes derive from the studies of Smits et al. [1], the third by Guelho et al. [2]. The third was chosen but with some modifications. In figure 3.3 there are the original dimensions investigated by Guelho.

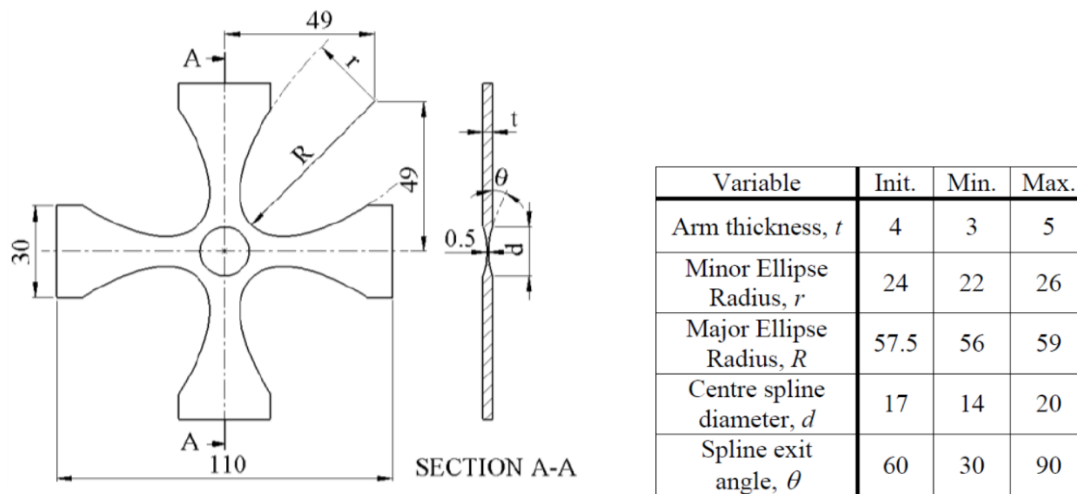


Figure 3.3 Guelho et al. specimen shape and dimensions [2]

For this work, it has considered this form of specimen maintaining the constant thickness over the whole specimen and imposing, to the variable dimensions indicated by Guelho, the lower values shown in the table.

The new specimen with his dimensions is shown in figure 3.4.

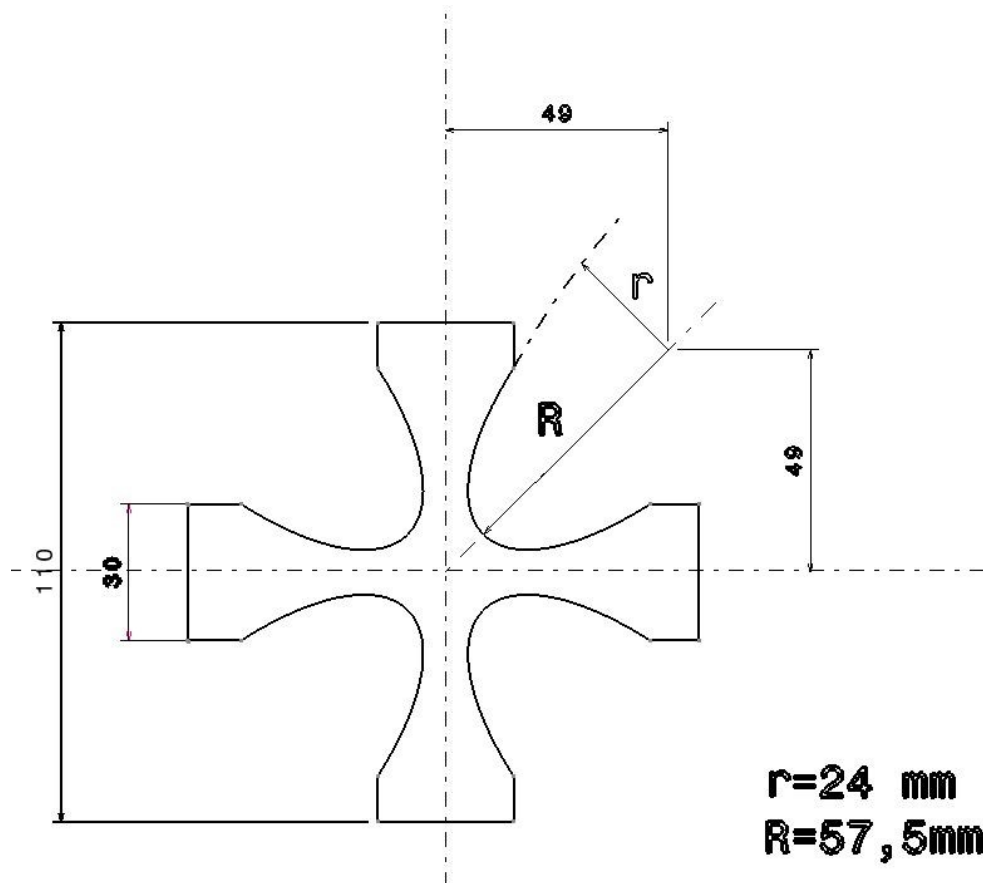
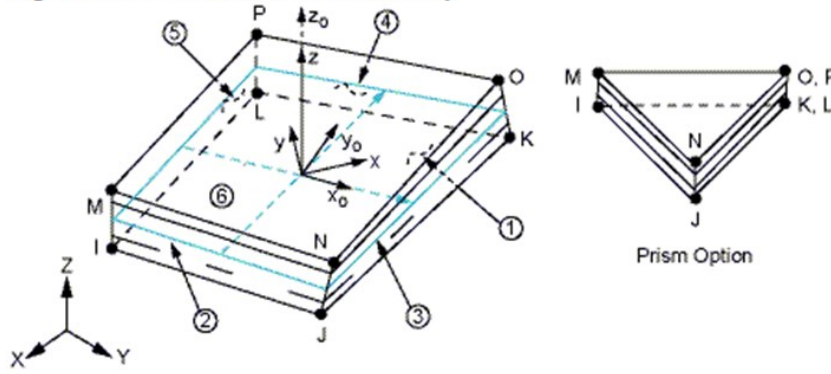


Figure 3.4 Modified shape

Referring to the studies previously analyzed, it was noted that all investigated shapes present fittings that allowed the reduction of a concentration of stresses in the corners of the specimen itself. This prevents cracks and breakages in the connecting part between the specimen arms and the biaxial load zone.

Given the geometry of the specimens, it was decided to manually construct the mesh. Moreover, the type of element used is SOLID SHELL [3], shown in figure 3.5. It is a three-dimensional finished element with 8 nodes, suitable for simulating structures with different thicknesses (from thin to moderately thick). It is particularly suitable for modeling composite laminates, as the formulation of this element is based on the Mindlin-Reissner theory. Each node has three degrees of freedom: the three translations in x, y and z directions.

Figure 190.1 SOLSH190 Geometry



x_0 = Element x-axis if ESYS is not supplied.

x = Element x-axis if ESYS is supplied.

Figure 3.5 Solid shell element [3]

For simplicity, only the results of the fem analysis on the third type of specimen of figure 3.2 are reported, which in the end is the one that showed a better behavior. The figure 3.6 shows the mesh built on the specimen, consisting of 15728 finished elements.

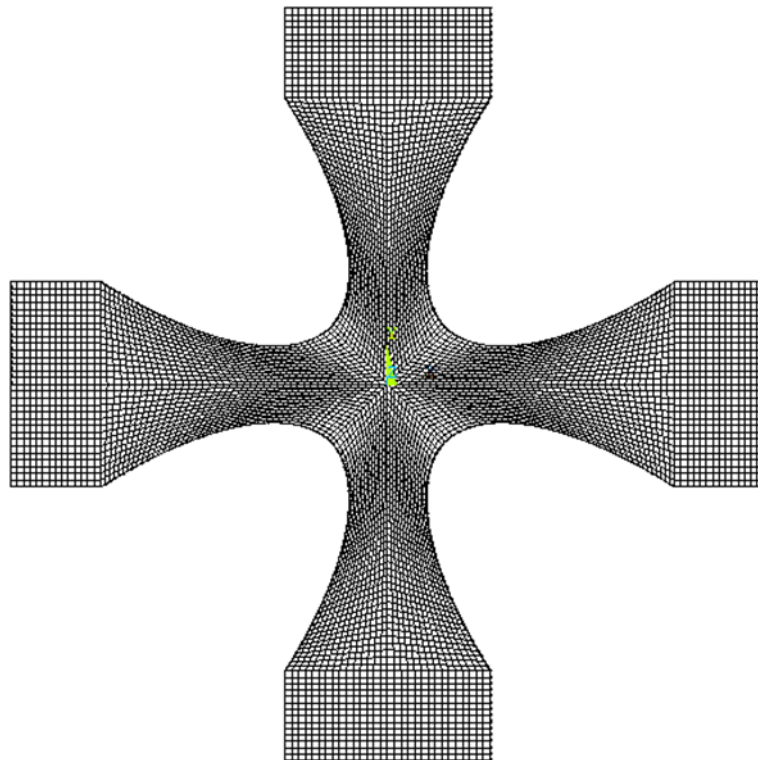


Figure 3.6 Solid shell mesh

About the load conditions, perfect clamping was hypothesized, and consequently, the modeling on the fem software was made using the MPC (Multi Point Constraint) option. The unloaded ends were constrained by interlocking. The constraint and load conditions are shown in figure 3.7.

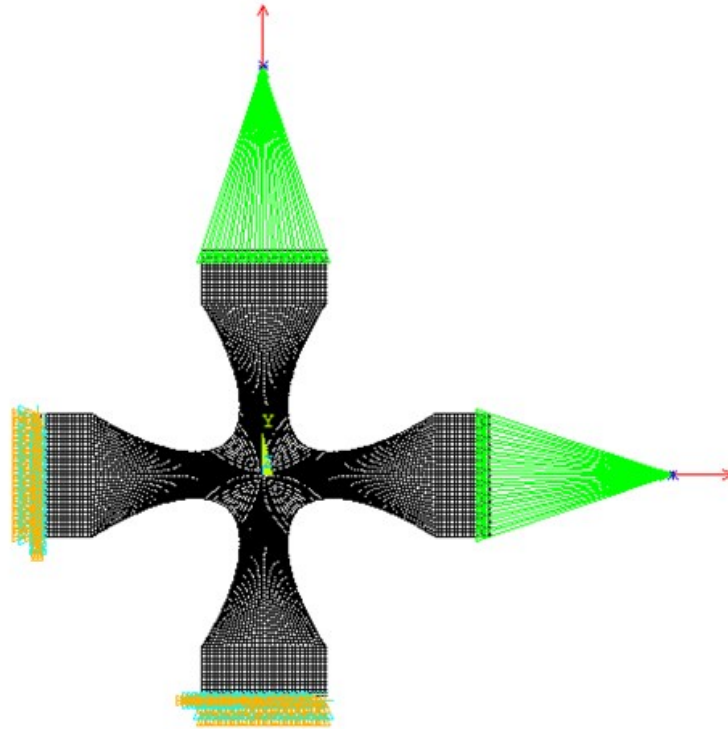


Figure 3.7 Boundary conditions

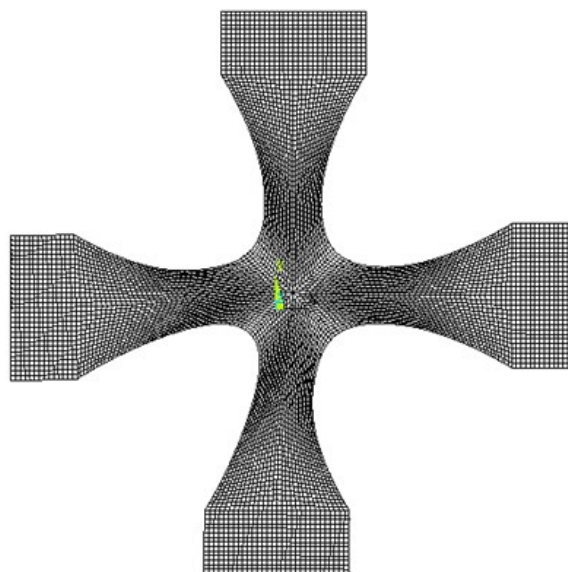


Figure 3.8 Deformed of the fem model

The figure 3.9 shows the distribution of the main strains.

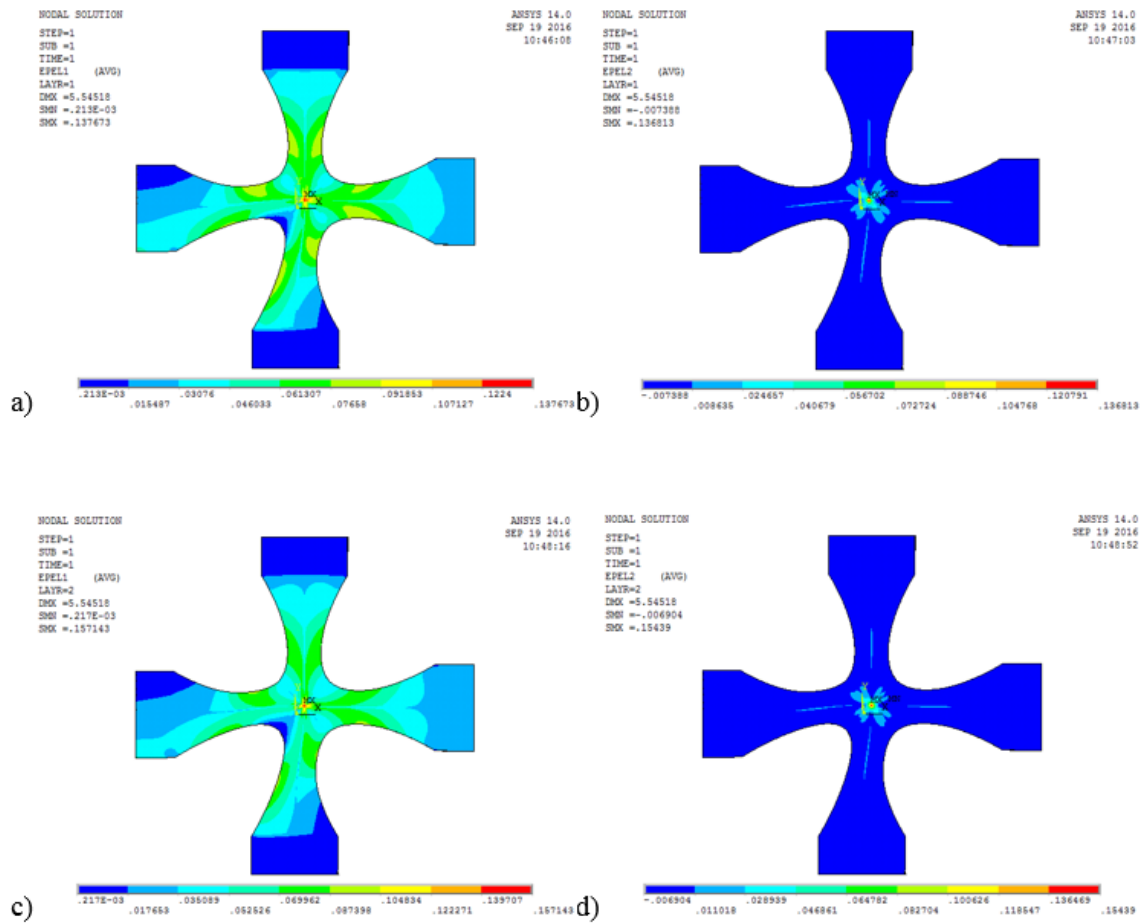


Figure 3.9 Main strains a) I and b) II for layer1; main strains c) I and d) II for the layer2

As regards the distribution of stresses, given the stacking sequence shown in figure 3.1, it was considered useful to construct a reference system rotated by 45° with respect to the global reference system (abscissa and ordinate respectively horizontal and vertical with respect to the graphic window).

This system was called CSYS11. The aim is to match the x and y-direction with the fibers direction, for each considered layer, obtaining more easily interpretable graphs.

The figure 3.10 shows the stresses along x and y in the CSYS11 reference system for the specimen. Given the symmetry of the specimen, only the results relative to layers 1 and 2 are shown, indicated in the legend to the left of the graph.

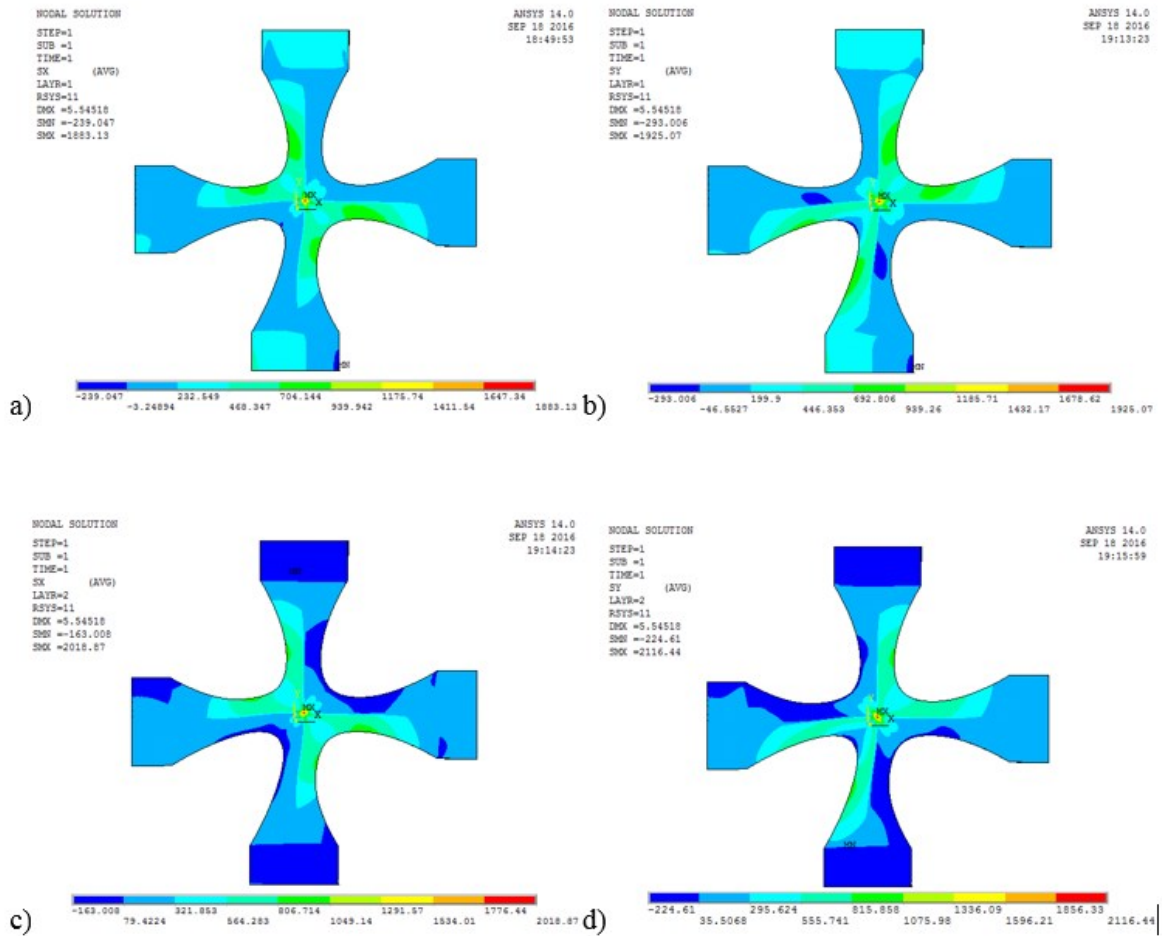


Figure 3.10 Stresses in the direction a) x and b) y in the CSYS11 reference system for Layer1; Stresses in direction c) x and d) y in the CSYS11 reference system for Layer2

From these results it is clear that this shape of the specimen is more suitable in case it is desired to investigate the characteristics of the strength of the material, since the priming of the break should occur in the central area of the biaxial load section, subjected to higher stresses. Moreover, the figure3.10 shows that stresses are minimal in regions far from the central one.

Later the same sample geometry was modeled on Patran software, for pre and post processing, and Nastran software for analysis.

As far as the boundary conditions is concerned, in order to generate a type of biaxial load, it was carried out through two sides loaded with a 463 N force (this value is the limit applicable in the following experiments) and it was hypothesized to be a perfect grasp modelled by two joints along the other two sides. The load is also set by the Master system and by Slave nodes (Multi Point Constraint) that allow the application of the same on a single node the consequent transmission to the whole side of the specimen. For the simulation, it was decided to model the geometry with

2D shell elements [2]. This allowed to have a lower computational burden for the software and to obtain the results for every single ply.

The geometric model has a 110mm x 110mm total dimension, a [0/90]S symmetrical stacking sequence. The considered material is a composite laminate of carbon fiber and epoxy resin. The solution executed is the linear Sol 101 [3].

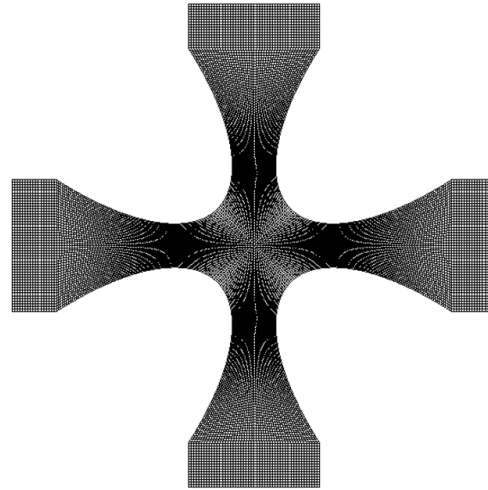


Figure 3.11 2D shell mesh

In order to obtain a symmetrical distribution of the loads, the load is applied to all the arms of the specimen, constraining the latter to be only in its central point.

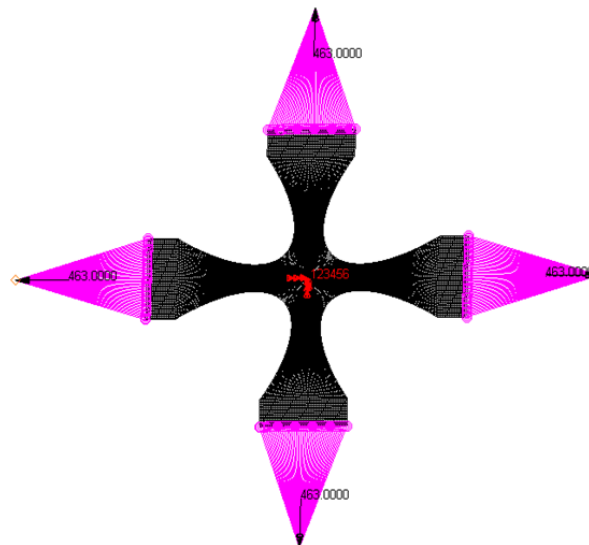


Figure 3.12 Boundary conditions and loads

The resulting distribution of the von Mises strains is shown in fig. 3.13 for the ply a 90°.

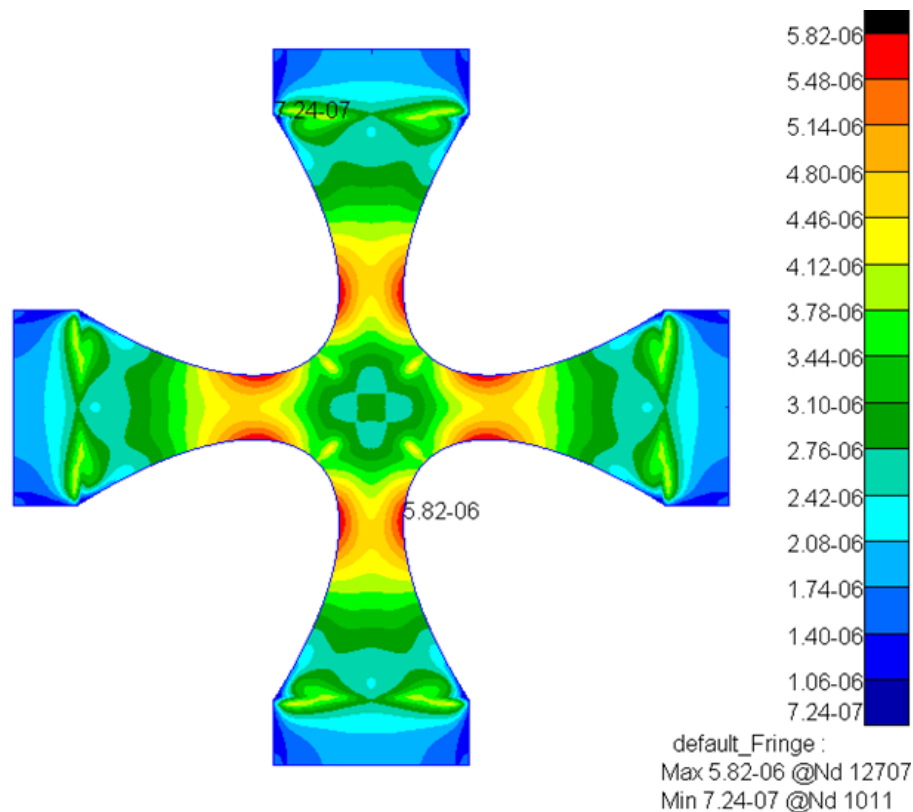


Figure 3.13 Von Mises strains

The result is the same for the 0° ply because the laminate is symmetrical. The presence of a central area with uniform strains is evident.

3.2 Optimization of the shape for polymeric materials

In the case of polymeric materials, from the studies of Helfenstein, Hollenstein and Mazza [4], it appears that the type of specimen that tends to maximize the biaxial loading zone is that which has a cruciform shape and in which there are some notches.

They also defined a link between the increase of notches on the specimen arms and the relative increase into the biaxial loading area.

For the optimization of the test form for biaxial tests about polymeric materials, it started from that of Helfenstein et al., modifying some things.

While the Helfenstein specimen has five notches on each arm, the form proposed in this thesis has six notches, as shown in figure 3.14.

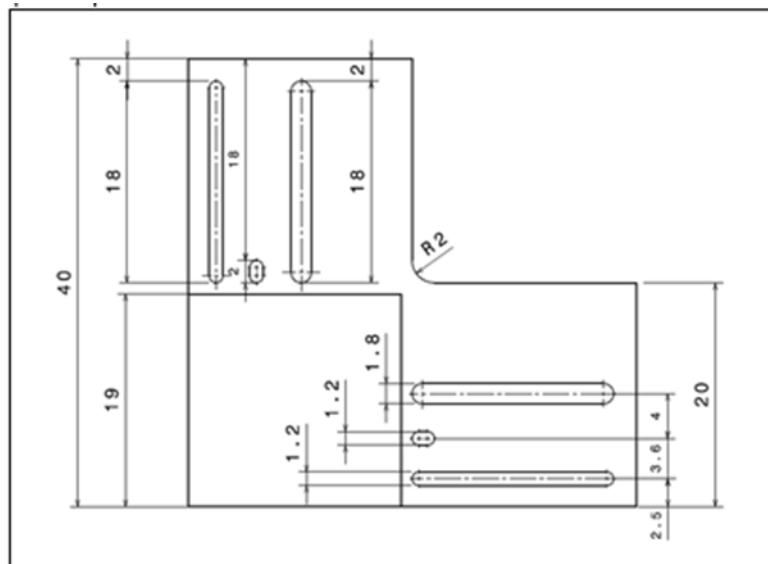


Figure 3.14 New shape proposed for polymeric materials

This solution not only allows the biaxial load area to be totally maximized, but, also, to prevent any breakage between the specimen arms.

Two fem simulations were performed with two types of polymeric material [5]. The first was made of SG-20 Sikasil, a silicone adhesive, with high structural strength, which exhibits hyper-elastic behaviour; the second one was instead made of Versilok, a two-component acrylic adhesive with an elastoplastic behaviour. These specimens were made with a 3mm thickness and modelled with chexa-like elements. These are shown in fig. 3.15 [3].

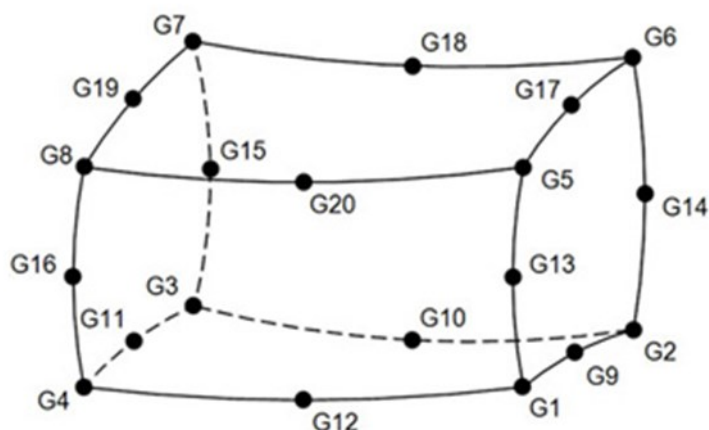


Figure 3.15 Chexa element

The boundary conditions of these specimens foresee a variation in the load conditions. This is imposed by a different speed. The specimens, in fact, were

loaded imposing a displacement at the free edges along the two main load directions whose values are about 5 mm/min and are jammed along the other two edges. The symmetry of the problem was also studied to pay attention on only a quarter of the sample and to reduce the computational costs of the operation. The solution implemented is the implicit non-linear Sol 600.

The 3.16 and 3.17 figures show the results of the fem analysis for the two materials considered.

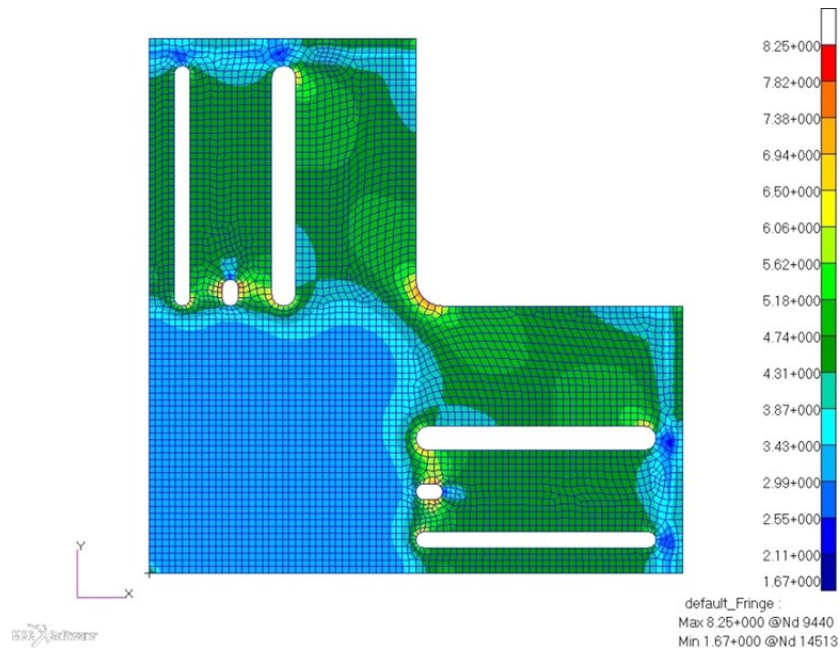


Figure 3.16 Main stresses on Versilok specimen

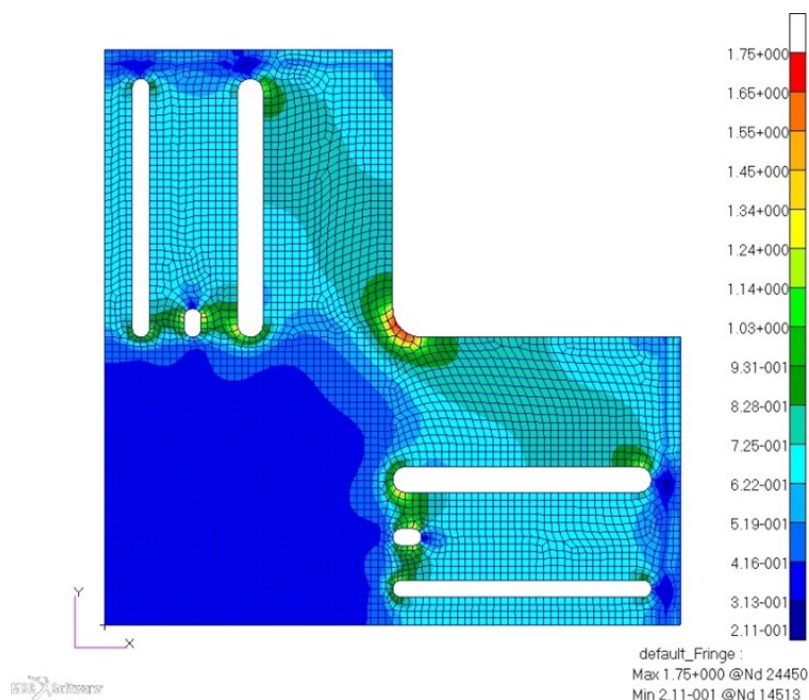


Figure 3.17 Main stresses on Sikasil specimen

The geometry with the notches of variable size maximizes the movement of the load to the measured section and allows to increase the dimensions of the latter.

References

- [1] A. Smits, D. Van Hemelrijck, T.P. Philippidisand, A. Cardon, Design of a cruciform specimen for biaxial testing of fiber reinforced composite laminates, Composites Science and Technology 66(2006)964-975
- [2] I. Guelho, L. Reis, M. Freitas, B. Li, J.F.A. Madeira, R.A. Cláudio, Optimization of cruciform specimen for low capacity biaxial testing machine, (2013)
- [3] Ansys user manual
- [4] MSC Patran user manual
- [5] MSC Nastran user manual
- [6] Helfenstein J, Hollenstein M, Mazza E (2009). Investigation on the optimal specimen design for planar-biaxial materials testing of soft materials. Proc. 6th Eur. Conf. Cost. Models for Rubber, 371-376.
- [7] Msc, "Experimental Elastomer Analysis", MAR 103, 2005

Chapter 4

Experimental activity

4.1 Introduction

The experimental activity has the main purpose to validate the biaxial test using the equipment and the specimens studied, through the comparison with fem results. The experimental tests, in a limited number, were made within the Tabasco project, promoted by the DAC (Campania Aeronautical District).

Tabasco is the Italian acronym of "Low Cost Production Technologies and Processes for Composite Structures for Advanced Aircraft of the General Aviation".

4.2 Materials and method

4.2.1 Materials

As part of the Tabasco project, the material considered for the construction of aircraft is a compound laminate in carbon fiber and epoxy resin. This is a laminate composed of 2 pleis of pre-waterlog 0/90 ° fabric, obtained with technological "vacuum bag". The specimens has a (0/90) stacking sequence and 0.5 mm thick. They were made from panels by performing a laser cut.

The characteristics of the fibers made of fabric are shown in fig. 4.1.

In order to compare the experimental results with those of the fem analysis, we understand that monoaxial tests were performed to produce the mechanical characteristics of the laminate material. Three tests were performed following the ASTM D638 standard [1] with a universal machine for tensile test MTS RT50.

T700S DATA SHEET

Highest strength, standard modulus fiber available with excellent processing characteristics for filament winding and prepreg. This never twisted fiber is used in high tensile applications like pressure vessels, recreational, and industrial.

FIBER PROPERTIES

		English	Metric	Test Method
Tensile Strength		711 ksi	4,900 MPa	TY-030B-01
Tensile Modulus		33.4 Msi	230 GPa	TY-030B-01
Strain		2.1 %	2.1 %	TY-030B-01
Density		0.065 lbs/in ³	1.80 g/cm ³	TY-030B-02
Filament Diameter		2.8E-04 in.	7 μm	
Yield	6K	3,724 ft/lbs	400 g/1000m	TY-030B-03
	12K	1,862 ft/lbs	800 g/1000m	TY-030B-03
	24K	903 ft/lbs	1,650 g/1000m	TY-030B-03
Sizing Type & Amount	50C		1.0 %	TY-030B-05
	60E		0.3 %	TY-030B-05
	FOE		0.7 %	TY-030B-05
Twist		Never twisted		

Figure 4.1 Fibre Data Sheet

The results of monoaxial tests on this type of material, acquired through three different methods, are shown in fig. 4.2.

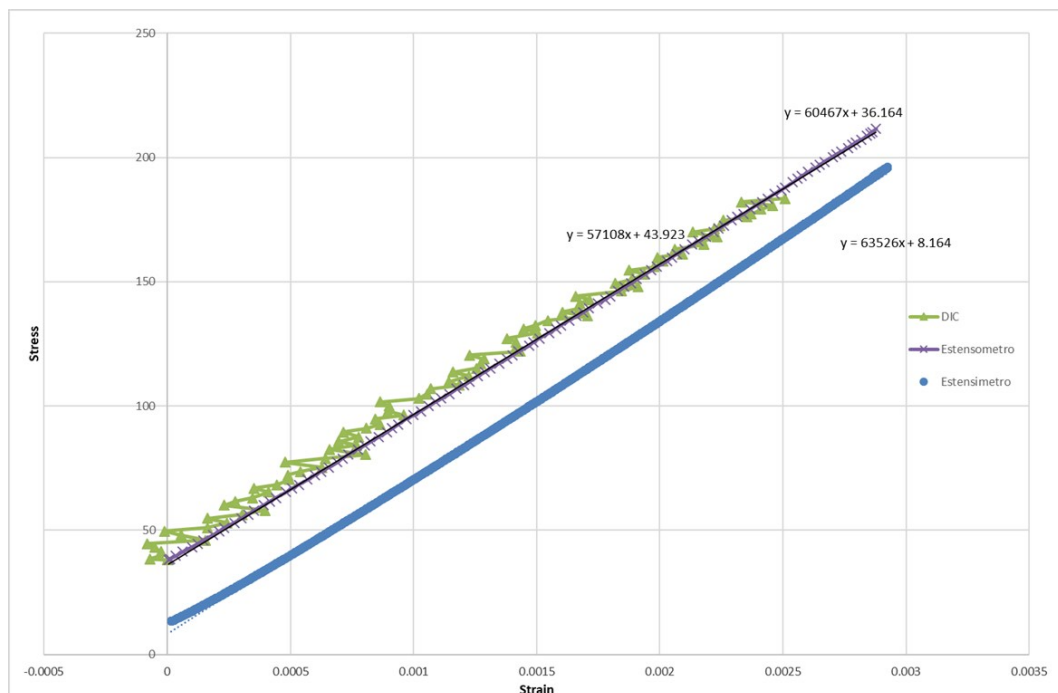


Figure 4.2 σ - ε curve

The elastic modules obtained to create the laminate material are: with DIC $E = 57100$ MPa, with extensometer $E = 60467$ MPa, with strain gage $E = 63526$ MPa.

Starting from these results, the value of the elastic module for the carbon fiber of the specimen has been defined: it is the same than the $120'000$ MPA used for all the following fem simulations.

The material considered in the tests with 2 pleis specimen did not show great success. It was considered a material consisting of two pleis and with a $0/90^\circ$ stacking sequence. The specimen is therefore not symmetrical.

For this reason another starting material was considered, in order to continue the experimental activity in the future: a symmetrical laminate consisting of four pleis with a $[\pm 45^\circ]$ stacking sequence as well as that considered in the study of the optimization of the specimen shape illustrated in chapter 3.

4.2.2 Test setup

Starting from the study carried out on the equipment described in the second chapter, after some modifications, the equipment was built, finally. As can be seen from figure 4.3, the modification has been made on the shape of the sliders.

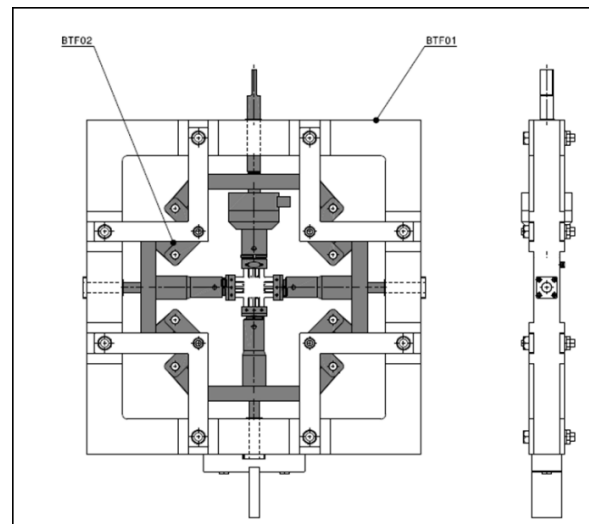


Figure 4.3 CAD model of definitive equipment

It must be remembered that the equipment consists of a fixed part included into the uniaxial test machine and in a mobile part connected to the mobile crosshead of the testing machine. The maximum length of the four slides is about 32mm and is due to the rotation of the cranks. The ratios of the crank mechanisms are equal to each other, and equally distributed along the incoming load to allow a biaxial test. The interface with the specimen has been realized with four mechanical clamps; the couplings between the connecting rods and the cranks. These have been realized with roller bearings, while the cylindrical guide slides inside with linear ball bearings.

Figure 4.4 shows the equipment created on the test machine.



Figure 4.4 New equipment for biaxial tests

This equipment was designed for specimen tests that require a less than 32mm stroke, with a 6mm maximum thickness and a 50mm maximum width.

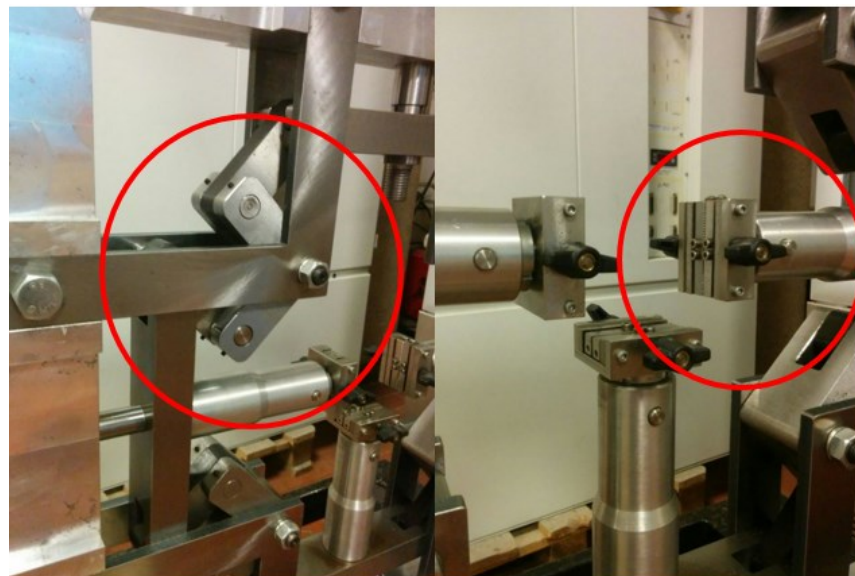


Figure 4.534 Details of cranks and clamps

The load transferred to each branch of the specimen is measured with a 5kN Kistler load cell, which was appropriately calibrated.

The camera used for the digital image correlation is a 36.3 megapixel Nikon D810, able to collect images at the rate of 5 frames per second. The correlation

between the images is done with the VIC2D software [2].

The material test machine used for biaxial tests is a MTS 810.

4.2.3 Specimen preparation for DIC

According to the DIC (Digital Image Correlation) and exploiting the correlation between the algorithms and the Fourier's transformations, through an optical method, has been provided a map of the strain state of the specimen.

From the knowledge of some parameters, the images recorded by the camera are compared, pixel by pixel, using the correlation of algorithms.

One of the basic steps is the preparation of the specimen that consists of painting this last one with a layer of paint of negligible thickness that does not change its mechanical characteristics. The speckle pattern was applied with a spray technique. A layer of opaque white varnish was applied, first of all, in order to have a homogeneous base on which a black opaque speckle pattern was made (see fig. 4.6 and 4.7) [3].

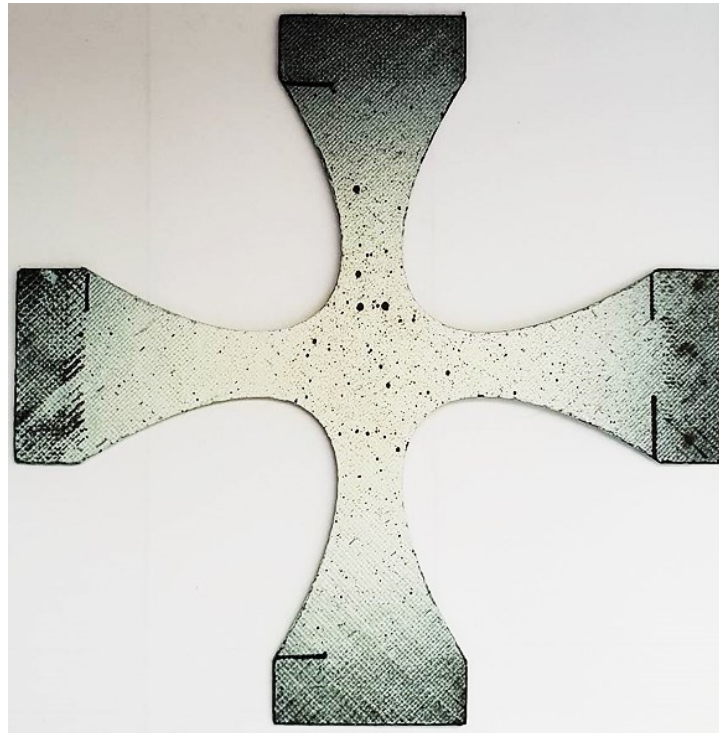


Figure 4.6 35 Speckle pattern on specimen

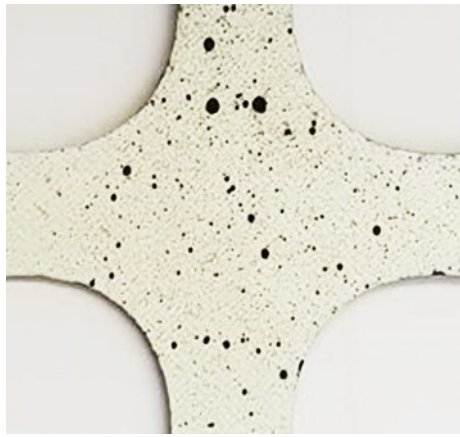


Figure 4.7 Detail of speckle pattern in the biaxial zone

Two lenses have been used, respectively 4x and 1x, which joined together to obtain a 5x focal zoom. Then the way of using this type of lens was found, and it was therefore necessary to position the camera as close as possible to the specimen (see fig. 4.8).

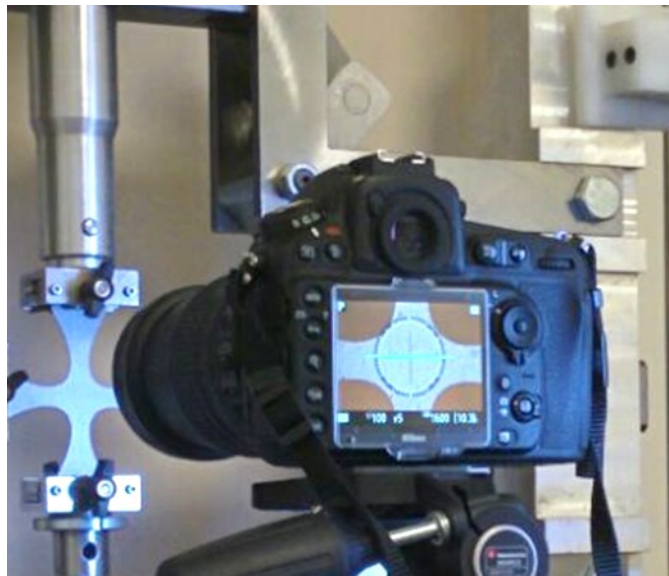


Figure 4.8 Camera positioning

4.2.4 Biaxial tests and digital correlation of images

Before starting the tests it was necessary to lubricate the equipment over and over again to minimize internal friction. This is an important phase to ensure that the applied load goes all over the specimen and is not absorbed in large part by the equipment itself.



Figure 4.936 Biaxial test performing

Once five biaxial tests have been performed, the images of the specimens are acquired in all the tests. So, the illustrated tests deal with the specimens at 0/90° stacking sequence

A 2 mm / min speedy test value was set on the test machine. The test was blocked when the force value reached 2000 N (or 500 N on each arm).

The software VIC2D, through correlation of algorithms, allows the control of the length of the specimen, analyzing, image by image, the variation of the distance between the two points defined in the initial calibration (see fig. 4.10).

The operation has used the speckle pattern put in on the specimen.

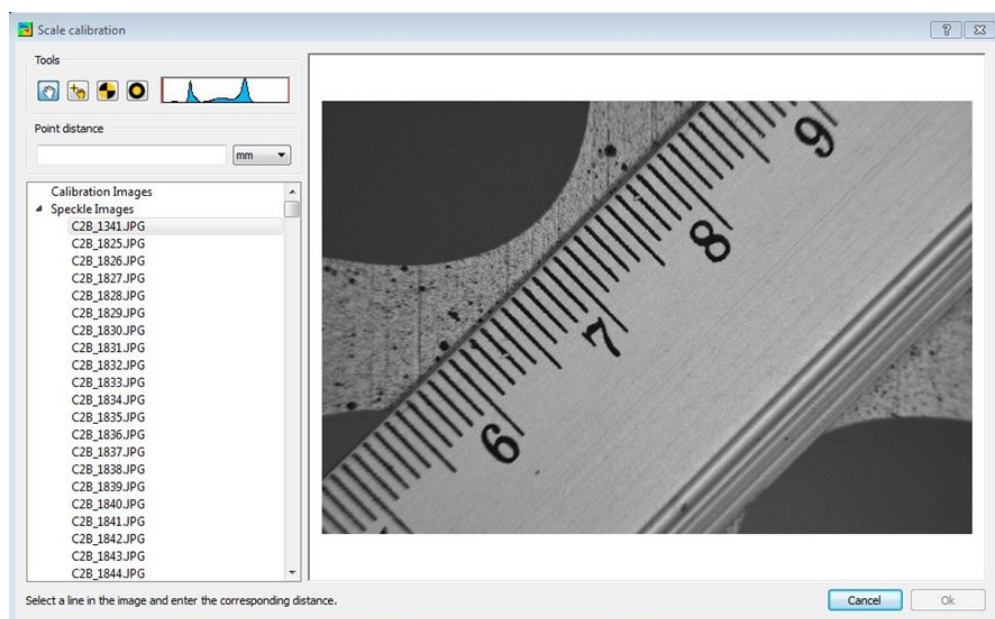


Figure 4.1037 Image calibration

The next step defines an area of interest (AOI) (see fig. 4.11), which allows to narrow the field of analysis on a single portion of the specimen, in order to

avoid, analyzing unnecessary parts of the images created during the test, blurred areas or an undefined pattern in the analysis. It is important to obtain a symmetrical AOI to subsequently have a distribution of the deformations which, also, are symmetrical.

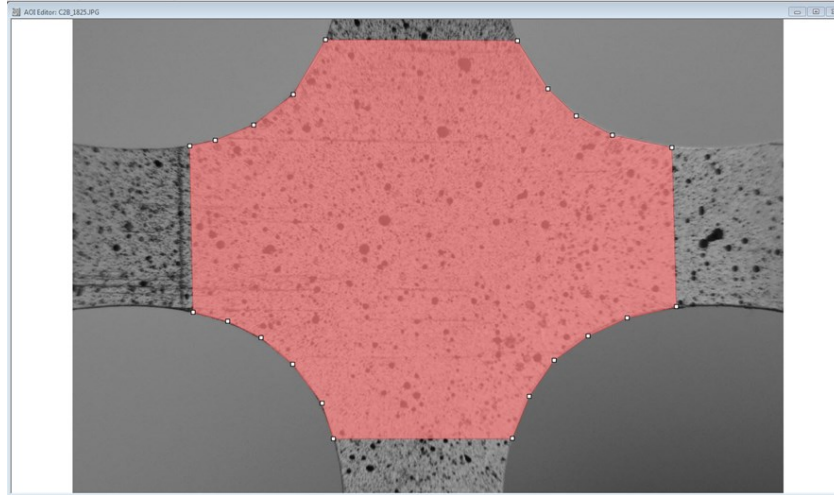


Figure 4.1138 Area of interest

In order to perform the correlation it is important to define the "Subset" and "Step" quantities. The first definitions about dimensions of the sub-images, or the number of sub-images are created in the area of interest. The value of Step, instead, considers the calculation steps, making the calculation more precise, but also heavier, therefore, longer, as soon as it decreases. In the figure 4.12 the chosen values are shown.



Figure 4.1239 DIC analysis settings

4.3 Results and fem validation

The average of the results of biaxial tests was compared with the results of the fem analysis (carried out with Patran/Nastran software) in terms of strain. Subsequently it was considered a reference point on the specimen. The same point was then identified on the model fem and its evolution during the test was observed.

The analysis is focused on the 0° ply because it is the one that has been treated with the speckle pattern and analyzed with the VIC-2D. It is compared therefore with the 0° ply in the fem analysis. The fact that the specimen is not symmetrically balanced influences the graphic results and therefore, the two plies will produce different graphic results. The biaxial loading area has a very homogeneous distribution of the strains in both cases, except for the central area which, obviously, on Patran, is constrained to obtain a symmetric distribution of the strains. The two strain distributions are shown in the figure 4.13 and 4.14.

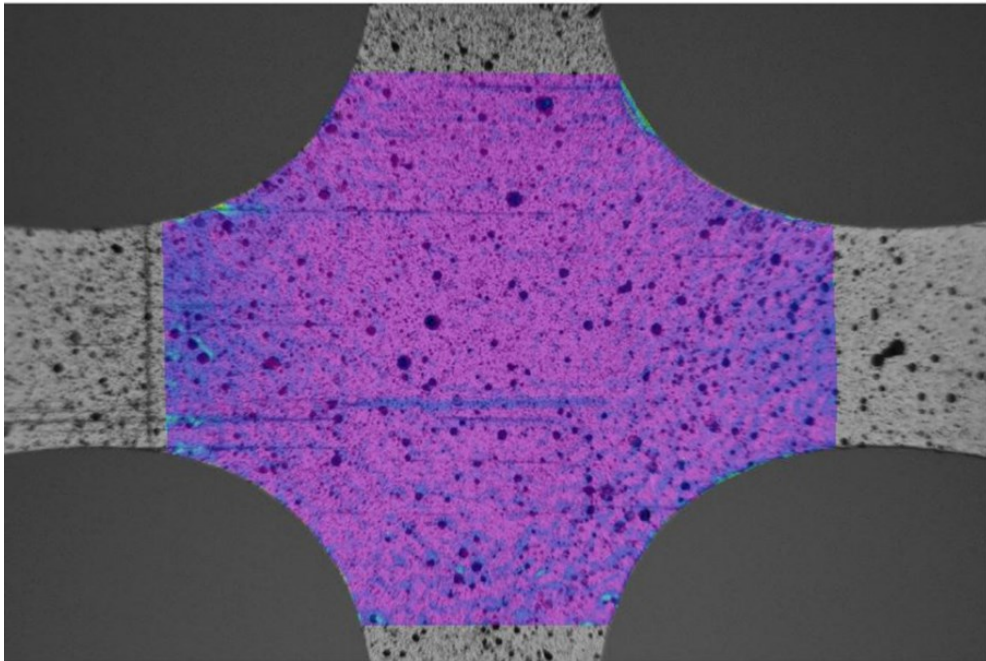


Figure 4.13 Distribution of maximum strain in the main direction with DIC

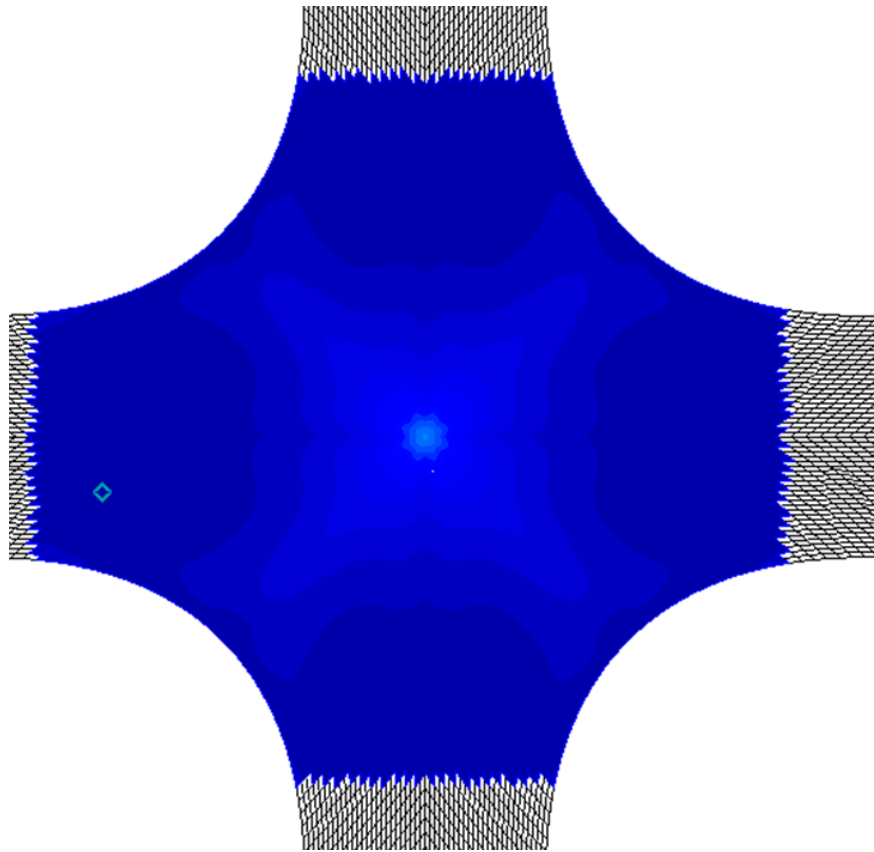


Figure 4.14 Distribution of maximum strain in the main direction with fem

A more precise analysis of the individual values was made on a single point of the specimen analyzed with the VIC-2D software and compared with the corresponding element of Patran.

Specifically, the reference element is the 18577 placed at 44.3 mm from the right edge of the specimen and at 52.3 mm from the upper edge of the specimen.

The values of the latter will turn out to be 0.00087464 and 0.00095179 regarding the strain of Von Mises on the ply at 0° in the directions y and x respectively and 0.0011495 for the maximum strain in the main direction.

In the figure 4.15 are shown these values for the finite element identified.

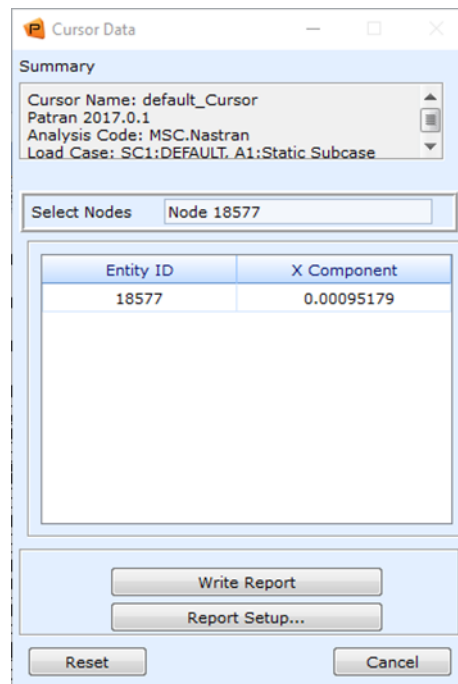
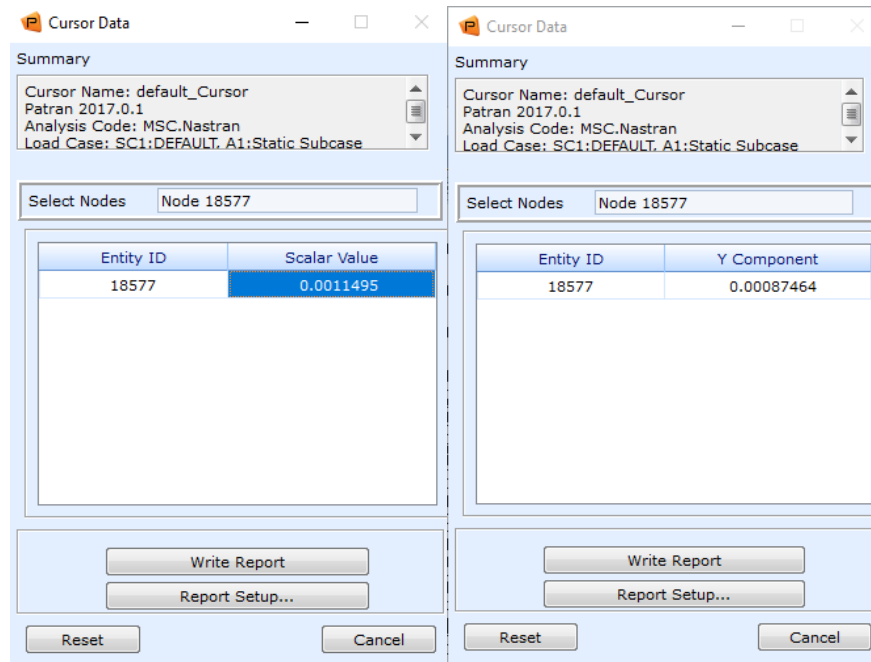


Figure 4.15 Values for identified element on Patran model

In the figure 4.16 it is shown the same point identified on the specimen. It is also shown the maximum strain distribution in the main direction, resulting from the DIC analysis.

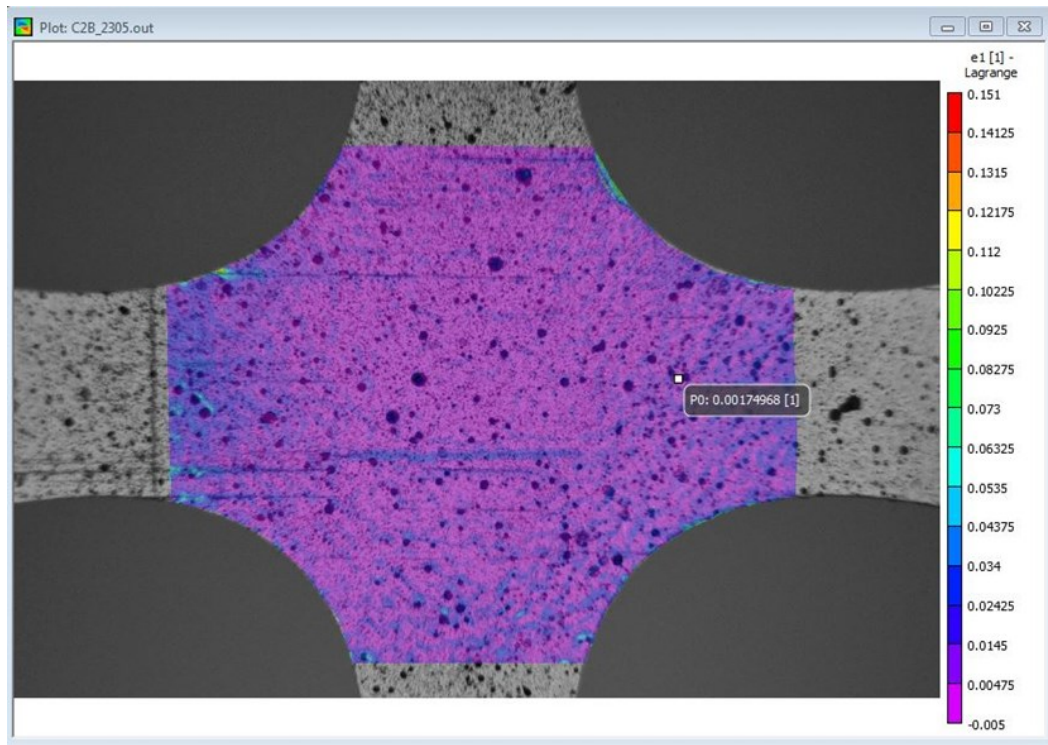


Figure 4.16 Maximum strain distribution in the main direction

In the figure 4.17 and 4.18 it is shown the Von Mises strains in y and x directions.

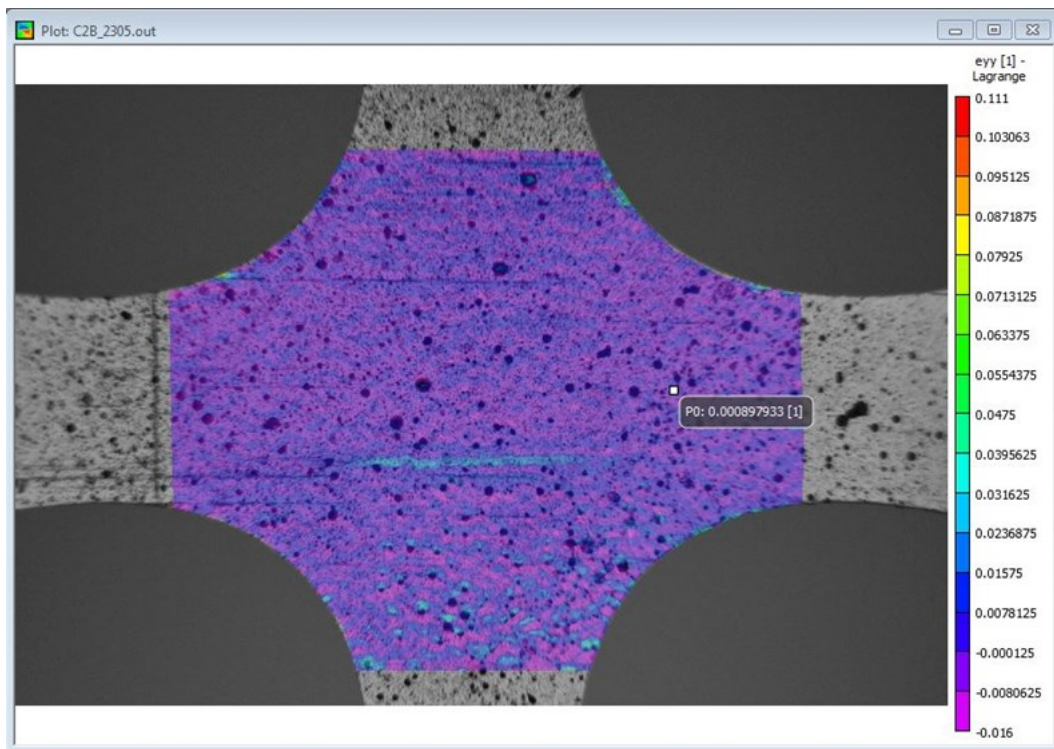


Figure 4.17 Strain in y direction

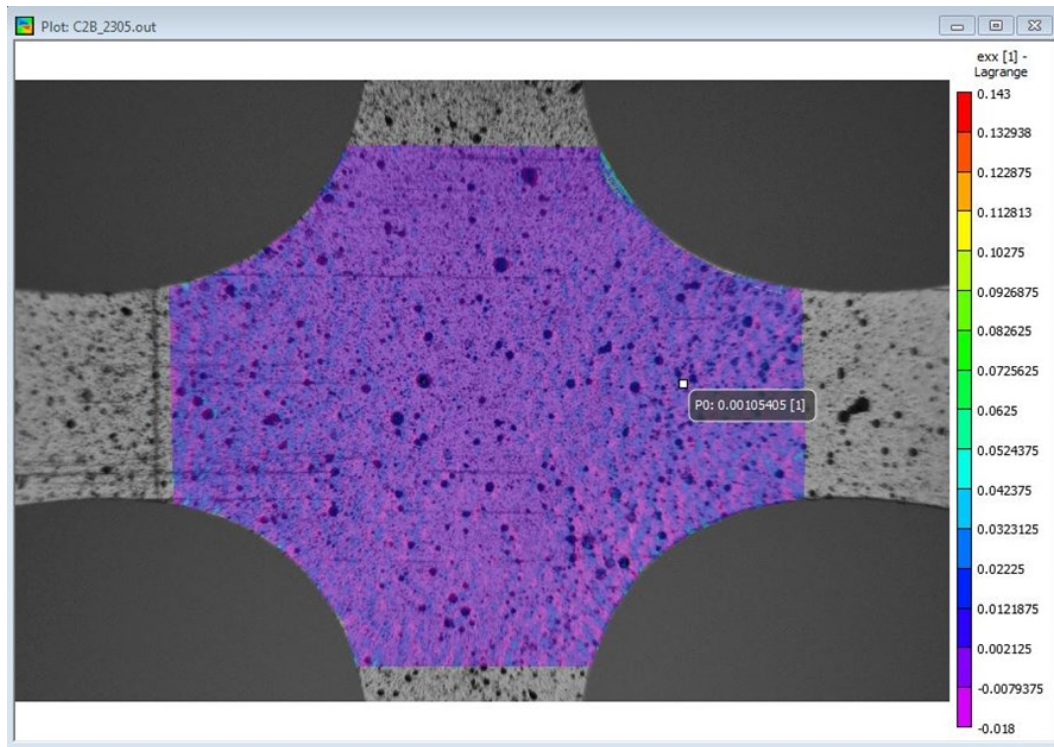


Figure 4.18 Strain in x direction

At the end, a summary table can be created on the values analyzed in the point.

	VIC-2D	PATRAN
Maximum strain in the main direction	0.00174968	0.0011495
Strain in y direction	0.000897933	0.00087464
Strain in the x-direction	0.00105405	0.00095179

Table 4.4 Comparison between DIC and fem values

4.4 Conclusions

The experimental activity allowed to verify the operation of the experimental equipment, for the execution of biaxial traction tests. The tests have highlighted the possibility of making tests on the materials, tests that would be reliable, but that anyway changes must be made to the equipment to increase its reliability before undertaking extensive experimental campaigns on materials. Indeed this work focused on setting up the equipment.

The tests were carried out using a new digital image through an acquisition system and a related analysis software in order to determine the deformed maps.

The specimens were extracted from available panels as part of the TABASCO project of the DAC and were prepared according to the indications provided for the use of the DIC.

The comparisons between the experimental and numerical data have made it possible to check that the equipment is applied to the load on the four arms correctly and it has also been verified how the area, in which the deformation stays constant, is becoming wide.

However, it was noted that the value of the applied load increases as much as the equipment showed an abnormal behaviour. So, the two transversal sliders were too strongly and therefore not acceptable.

The problem is due to the high presence of junctions which load the internal friction equipment. This causes a lack of symmetry in the movement of the branches, between the fixed-mobile structures near the connecting areas. This, as before mentioned, generates limitations in the test when high forces are reached. This particular situation doesn't characterize the material during the break and limits itself to about 4 minutes maximum duration test and about 500 N per arm. If the load keep increasing, it would tested the steel of the test rig only, instead of the specimen one.



Figure 4.19 Slider inclination

The horizontal arms tend to flex under their own weight (see Fig. 4.20)

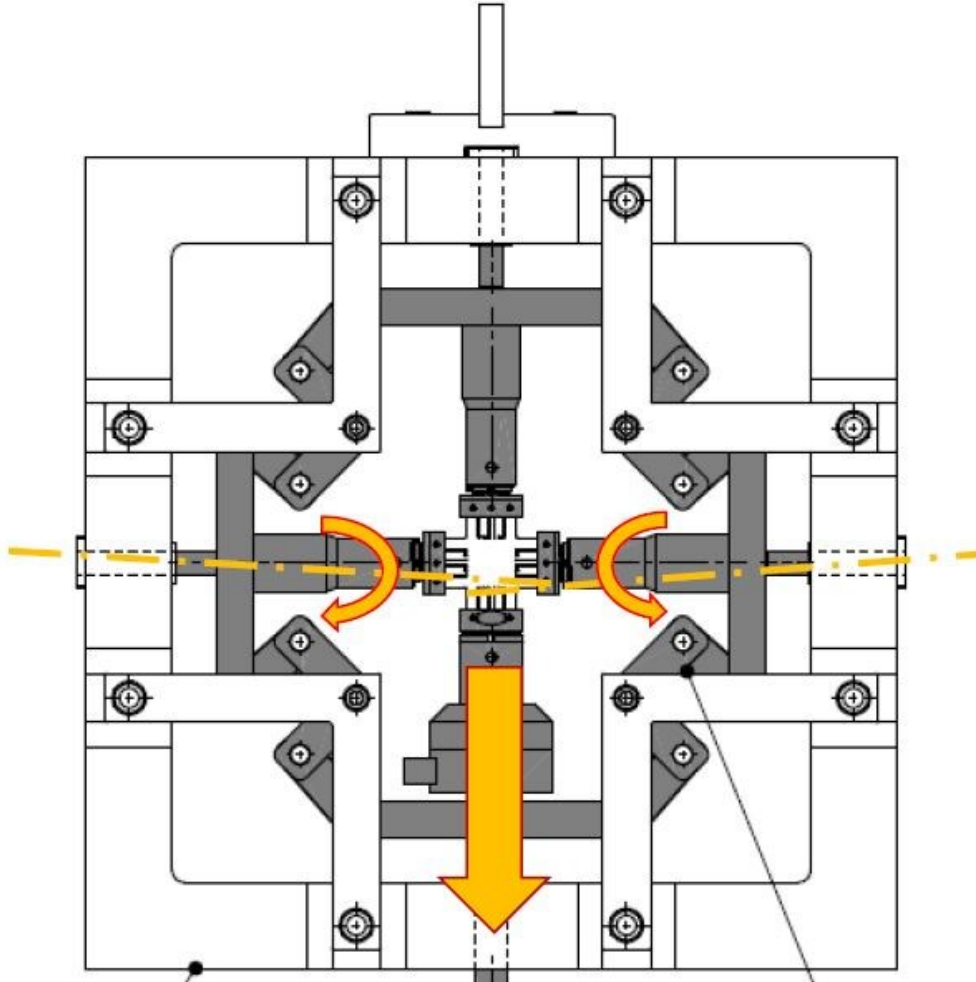


Figure 4.20 Flexion of the arms

It is now possible to suggest future modifications to the equipment.

The first change to be made will be the creation of larger diameter guides for the two horizontal arms; in addition, the shaft that runs in the guide must be replaced by a drawn and chromed shaft coupled with two Teflon-type sliding bearings.

The cranks must be lightened especially in the areas where they could come in contact with the support arms. In figures 4.21 and 4.22 it is possible to see in detail the areas in which the cranks will be lightened.

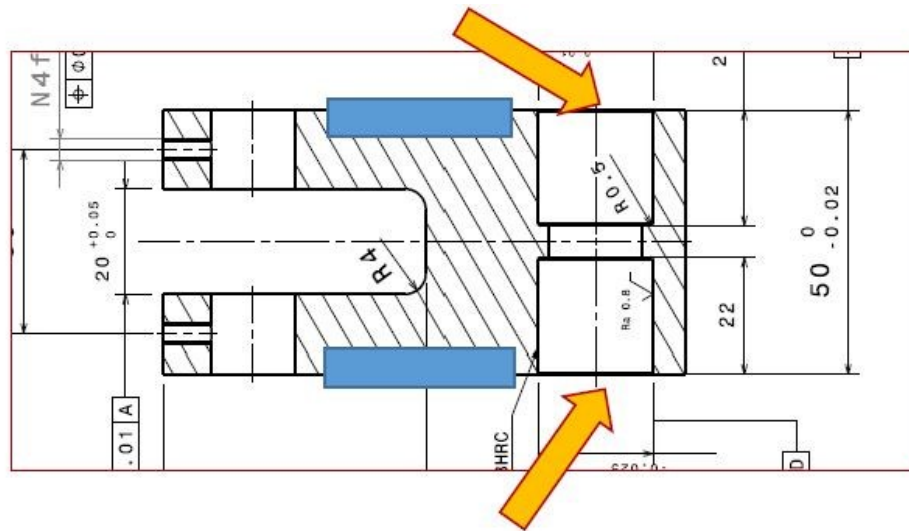


Figure 4.21 Detail of cranks

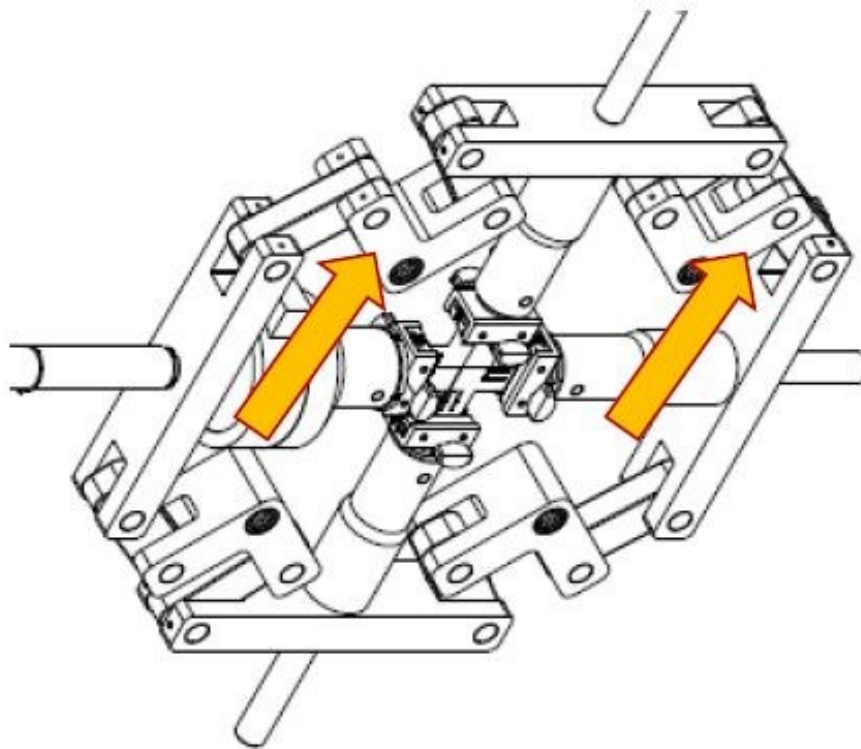


Figure 4.22 Areas of possible crank contact

Another problem is that the lower jaw must win the weight of the moving part of the mechanism and recover the games before the test.

The solution to this problem could be the insertion of some tension springs which

would support the weight of the mobile part of the equipment. The position of the springs is shown in red in fig. 4.23.

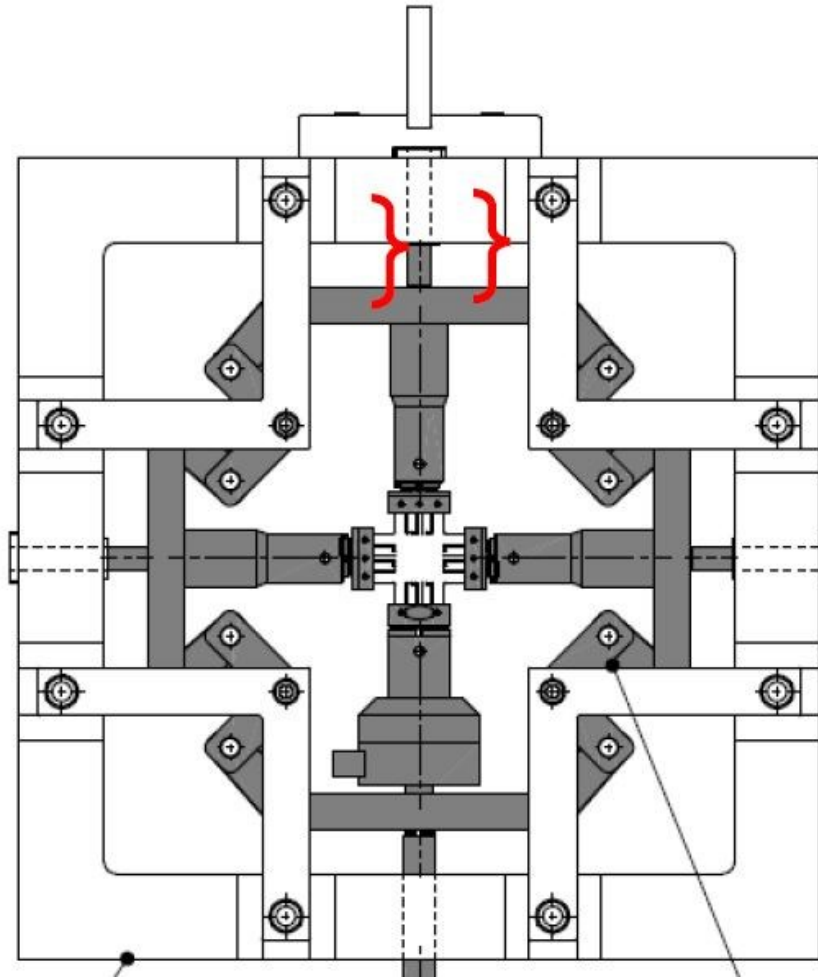


Figure 4.23 Position of the springs

Each L-rib (support arms) will be replaced with two parallel plates, one on each side. These support arms will be laser-shaped and drilled in a CNC in a single operation to ensure correct positioning of the rotation axes. The draft of the new plates is shown in the figure 4.24.

References

[1] ASTM D638 standard

[2] VIC2D_2009_Manual

[3] R. Cintròn, V. Saouma, Strain measurements with digital image correlation, 2008, Jr. Network for Earthquake Engineering Simulation of Colorado University